



Universidade do Minho
Escola de Engenharia

Fábio Alexandre Amorim Melo

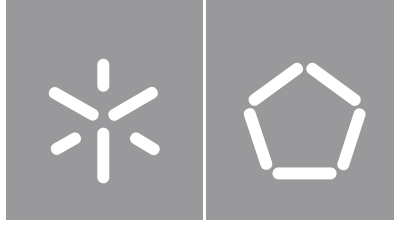
Doubly-fed Induction Generator Wind Turbine System

**Doubly-fed Induction Generator
Wind Turbine System**

Fábio Melo

UMinho | 2019

dezembro de 2019



Universidade do Minho
Escola de Engenharia

Fábio Alexandre Amorim Melo

**Doubly-fed Induction Generator
Wind Turbine System**

Dissertação de Mestrado
Eletrónica Industrial e Computadores

Trabalho efetuado sob a orientação do
**Professor Doutor Manuel João Sepúlveda Mesquita
de Freitas**

DIREITOS DE AUTOR E CONDIÇÕES DE UTILIZAÇÃO DO TRABALHO POR TERCEIROS

Este é um trabalho académico que pode ser utilizado por terceiros desde que respeitadas as regras e boas práticas intencionalmente aceites, no que concerne aos direitos de autor e direitos conexos.

Assim, o presente trabalho pode ser utilizado nos termos previstos na licença abaixo indicada.

Caso o utilizador necessite de permissão para poder fazer uso do trabalho em condições não previstas no licenciamento indicado, deverá contactar o autor, através do RepositóriUM da Universidade do Minho.

Licença concedida aos utilizadores deste trabalho



Atribuição-NãoComercial
CC BY-NC

<https://creativecommons.org/licenses/by-nc/4.0/>

Acknowledgements

First of all, i would like to thank my mentor, Professor Doctor Manuel João Sepúlveda Mesquita de Freitas, for his guidance, availability, advice and support throughout the making of this dissertation.

I thank all of the staff of the Industrial Electronics Department for their sympathy, help and availability showcased.

I thank all of my friends that, through one way or another, always supported me throughout the several moments in the making of this dissertation, and also for all the motivation provided.

I would like to thank also my sister, Rita Melo, my father, José Melo, my grandmother, Custódia Amorim, and thank specially my mother, Emília Melo, and also to my late grandfather, António Melo, for all the patience and support, even in the most difficult moments. I thank also all of the sacrifices they did for me in order to provide me with the opportunity to study higher education as well as providing me with everything I needed throughout my life. For all the affection, help and love, a very sincere and big thank you.

STATEMENT OF INTEGRITY

I hereby declare having conducted this academic work with integrity. I confirm that I have not used plagiarism or any form of undue use of information or falsification of results along the process leading to its elaboration.

I further declare that I have fully acknowledged the Code of Ethical Conduct of the University of Minho.

Resumo

A produção de energia Elétrica com recurso a combustíveis fósseis contribui para o aumento das emissões dos gases de efeito de estufa, mais especificamente de CO₂, para a atmosfera. Nas últimas décadas tem havido maiores preocupações ambientais no que diz respeito ao estado atual da produção de energia elétrica, o que tem aumentado o investimento nas energias renováveis, na esperança de se obter uma energia mais sustentável, sem a emissão dos gases de efeito de estufa. Uma dessas energias renováveis, é a energia eólica, que tem enorme potencial em Portugal, e que tem tomado cada vez mais um papel ativo maior no mundo.

O conceito de produção de energia eólica com um gerador de velocidade variável tem recebido muita atenção devido ao facto de os métodos de controlo utilizados terem que ser melhorados e mais eficientes. Assim sendo, nesta dissertação é desenvolvido um sistema de controlo para um gerador indutivo duplamente alimentado (DFIG), por forma a extrair o máximo de potência possível. Para que tal seja possível, é utilizado um conversor *back-to-back* composto por dois conversores, um conversor AC-DC (Corrente Alternada – Corrente Contínua), denominado retificador, e um por um conversor DC-AC (Corrente Contínua – Corrente Alternada), denominado inversor, e por um condensador *DC-link* ligado entre ambos. Estes conversores são controlados através de um circuito de controlo, e inseridos num sistema gerador de turbina eólica (WTGS). O sistema é testado em contexto de simulação em computador para provar o conceito.

Para realizar esta dissertação, é necessário um estudo teórico de cada componente do WTGS, em especial do gerador DFIG e do seu modelo matemático, para possibilitar o desenvolvimento do sinal de controlo e de todo o circuito de interface.

Palavras-chave: Energia Eólica, Turbina Eólica, Sistema Gerador de Turbina Eólica, Conversor *Back-To-Back*, Gerador Indutivo Duplamente Alimentado.

Abstract

The production of electrical energy resorting to fossil fuels contributes to the increase in the emissions of greenhouse gases, more specifically CO₂ for the atmosphere. In the last decades, there have been increasing environmental concerns regarding the current status of the electrical energy production, which has increased the investment in the renewable energies, in hopes for a more sustainable energy, without the emission of greenhouse gases. One of these renewable energies, is wind energy, which has enormous potential in Portugal, and that has been getting a bigger active role in the world.

The concept of wind energy production with a variable speed generator has gotten a lot of attention due to the fact that the control methods used need to be improved and more efficient. As such, this project is focused on the development of a control system for a doubly-fed induction generator (DFIG), so that it is possible to extract the maximum power possible. To make this possible, it is used a back-to-back converter composed of two converters, a AC-DC converter (Alternating Current – Direct Current), called rectifier, and a DC-AC converter (Direct Current – Alternating Current), called inverter, and a DC-link capacitor connected in between them. These converters are controlled by means of a control circuit, and are inserted in a wind turbine generator system (WTGS). The system is tested in computer simulation environment to prove the concept.

To develop this project, it is necessary a study of each component of the WTGS, specially the DFIG and its mathematical model, to make possible the development of the control system as well as all of the interface circuits.

Keywords: Wind Energy, Wind Turbine, Wind Turbine Generator System, Back-To-Back Converter, Doubly-Fed Inductive Generator.

Index

Acknowledgements	ii
Resumo.....	iv
Abstract.....	v
Figure Index.....	viii
List of Tables	xi
List of Initialisms.....	xii
List of Symbols	xiii
Chapter 1 – Introduction.....	1
1.1. Problem Overview	2
1.2. Motivation.....	6
1.3. Objectives.....	6
1.4. Project Structure	7
Chapter 2 – Wind Energy.....	9
2.1. Wind Energy Technology.....	10
2.1.1. State of Art.....	10
2.1.2. Advantages and disadvantages of wind energy	13
2.2. A Wind Turbine Generator System	14
2.2.1. System analysis and wind turbine modelling	15
2.2.2. Wind Turbine Generator System components.....	18
Chapter 3 – System interface and its components.....	22
3.1. Typical system interface	23
3.2. System components	23
3.2.1. Doubly-fed induction generator	24
3.2.2. Power electronics.....	28

3.3. Hardware components used for the control of the system	32
3.3.1. Microcontroller – Arduino	33
3.3.2. Optocoupler HCPL-3120	33
3.4. Mathematical transformations required for modelling of the system.....	34
3.4.1. Clarke transformation ($\alpha\beta\gamma$ transformation)	34
3.4.2. Park Transformation ($dq0$ transformation).....	36
3.4.3. Inverse Park and Clarke Transformations.....	37
3.5. Modelling of the system.....	37
3.5.1. Modelling for the RSC.....	38
3.5.2. Modelling for the DC-link section.....	41
3.5.3. Modelling for the GSC	42
3.6. Control algorithms.....	43
3.6.1. Control algorithm of the RSC	44
3.6.2. Control algorithm of the GSC	46
Chapter 4 – Simulations using Computer Programs	48
4.1. Simulation of machine working principles.....	49
4.2. Simulation and analysis of the steady state of the machine	61
4.3. Simulation of the machine with the wind turbine model.....	65
4.4. Simulation of the implemented system	68
Chapter 5 – Laboratory experiment.....	76
Chapter 6 – Conclusions and future work.....	80
Appendix A	82
Appendix B.....	84
References	88

Figure Index

Figure 1 – a) Share in installed power capacity in 2005. b) Share in installed power capacity in 2017 (Source [7]).....	3
Figure 2 - Cumulative power capacity between 2000 and 2016 in mainland Portugal (Source [8])	4
Figure 3 - Wind potential in mainland Portugal (Source: [9]).....	5
Figure 4 – Vertical-axis windmill (Adapted [10])	10
Figure 5 – Three-bladed wind turbine in Viana do Castelo.....	12
Figure 6 – Installed Power and Diameter evolution of wind turbines over latest years (Adapted [11])	12
Figure 7 – Wind stream imaginary boundary (Adapted [11])	15
Figure 8 – Wind turbine MPPT control (Adapted [15]).....	18
Figure 9 - Architecture of a wind turbine (Adapted [16])	19
Figure 10 – Different installation designs for a wind propeller turbine (Adapted [11]).....	20
Figure 11 - Stall in an aerofoil (Adapted [11])	21
Figure 12 - Basic configuration of a wind energy production system (Adapted [19]).....	23
Figure 13 - Principle of DFIG (Adapted [19])	25
Figure 14 - Three-phase rotating magnetic field (Adapted [21])	26
Figure 15 - Schematic of the interaction of the rotor speed and the frequency of the rotating magnetic fields created in the rotor windings (Adapted [22]).....	27
Figure 16 - MOSFET diagram.....	28
Figure 17 - MOSFET with the snubber circuit.....	29
Figure 18 - Simple representation of a back-to-back converter in a WTGS.....	30
Figure 19 – Three-phase rectifier output waveforms	30
Figure 20 – Typical three-phase rectifier with DC-link capacitor.....	31
Figure 21 – Ideal single-phase MOSFET inverter simulation	31
Figure 22 - Typical three-phase inverter using MOSFETs.....	31
Figure 23 - Voltage and current windings of a transformer (Adapted [24])	32
Figure 24 - Arduino Mega2560 ([25]).....	33
Figure 25 - Optocoupler HCPL-3120 schematic ([26])	34

Figure 26 - All reference frames combined (Adapted [27])	35
Figure 27 - Normal three-phase reference frame alongside the $\alpha\beta$ and the dq reference frames (Adapted [27])	35
Figure 28 – Clarke transformation (Adapted [27]).....	36
Figure 29 – Park transformation (Adapted [27])	36
Figure 30 - Representation of concepts of the asynchronous machine (Adapted [29]).....	38
Figure 31 - Model of the asynchronous machine in dq coordinates referred to the stator (Adapted [27]).....	41
Figure 32 - Display of the DC-link system in the back-to-back converter (Adapted [15]).....	42
Figure 33 - Model of the grid in dq coordinates (Adapted [15]).....	43
Figure 34 - Simple control schematic of a WTGS	44
Figure 35 - Schematic of the RSC control algorithm (Adapted [29])	45
Figure 36 - Schematic of the GSC control algorithm (Adapted [15]).....	47
Figure 37 - System developed in MATLAB Simulink for testing the machine working principles .	49
Figure 38 - Control circuit of the RSC	53
Figure 39 – Control block of the calculation of the theta angle of the rotor	54
Figure 40 – Clarke transformation control block	54
Figure 41 – Park transformation control block.....	54
Figure 42 - Inverse Park transformation control block	55
Figure 43 - Inverse Clarke transformation control block.....	55
Figure 44 – Standard PI control block used in system	55
Figure 45 - Control block of active and reactive powers decoupling of the RSC	56
Figure 46 - Machine measured variables	56
Figure 47 – Machine operating as a motor at sub-synchronous speed	57
Figure 48 - Machine operating as a generator at sub-synchronous speed	58
Figure 49 - Machine operating as a motor at synchronous speed	58
Figure 50 - Machine operating as a generator at synchronous speed.....	59
Figure 51 - Machine operating as a motor at hyper-synchronous speed.....	60
Figure 52 - Machine operating as a generator at hyper-synchronous speed	60
Figure 53 - Steady State Analysis of the system	61
Figure 54 - Analysis of sub-synchronous operating point in steady state	63
Figure 55 - Analysis of hyper-synchronous operating point in steady state	64

Figure 56 - Wind Turbine block.....	65
Figure 57 - Graphic of estimated wind power based on both the tip-speed ratio and the wind speed	66
Figure 58 - MPPT control block	67
Figure 59 – Wind speed input and expected power to be obtained	67
Figure 60 - Test of the MPPT block.....	68
Figure 61 - Control block of active and reactive powers decoupling of the GSC	70
Figure 62 - Power electronics of the WTGS	71
Figure 63 - Control circuit of the GSC	72
Figure 64 - GSC simulation results for 9 metres per second of wind speed.....	73
Figure 65 - RSC simulation results for 9 metres per second of wind speed.....	74
Figure 66 - Flow chart of the control design for the microcontroller	77
Figure 67 - Partial circuit design in veroboard	78
Figure 68 - Circuit design.....	79

List of Tables

Table 1 - Simulink program data parameters 50

Table 2 - Gains used for the RSC system..... 51

Table 3 - Parameters added to the system..... 69

Table 4 - Gains used for the GSC control 69

Table 5 - Equations to estimate both stator and rotor values during simulations 82

Table 6 - Other relevant equations for the simulation analysis 83

List of Initialisms

Nomenclature	Meaning
AC	Alternating Current
CO ₂	Carbon Dioxide
DC	Direct Current
DFIG	Doubly-Fed Inductive Generator
GSC	Grid Side Converter
MPPT	Maximum Power Point Tracking
PWM	Pulse Width Modulation
RSC	Rotor Side Converter
TSR	Tip Speed Ratio
WTGS	Wind Turbine Generator System

List of Symbols

Symbol	Meaning	Unit
E_k	Kinetic Energy	Joule (J)
m	Mass	Kilogram (kg)
v	Speed	Metres per second (m/s)
ρ	Air Density	Kilogram per cubic metre (kg/m ³)
V	Volume	Cubic metres (m ³)
A	Cross-sectional area	Square metres (m ²)
P	Power	Watt (W)
T	Torque	Newton metres (N.m)
ω	Angular Velocity	Radians per second (rad/s)
n	Rotational speed	Revolutions per minute (rpm)
r	Radius	Metres (m)
f	Frequency	Hertz (Hz)
U/u	Voltage	Volt (V)
I/i	Current	Ampere (A)
R	Resistance	Ohm (Ω)
L	Inductance	Henry (H)
C	Capacitance	Faraday (F)
Φ	Flux Linkage	Weber (Wb)
θ	Represents the rotation angle	Degrees ($^\circ$)

Symbol	Meaning
v_w	Wind speed
P_t	Wind turbine power
C_p	Turbine power coefficient given by the tip-speed ratio, λ , and the pitch angle, β
β	Pitch angle of the blade

C_{pmax}	Maximum turbine power coefficient given by the tip-speed ratio, λ , and the pitch angle, β (value supplied by the wind turbine manufacturer)
λ	Tip-speed ratio
C_t	Coefficient of the wind turbine
T_{em}	Electromagnetic torque of the machine
ω_t	Angular velocity of the wind turbine
n_{rotor}	Rotor speed
n_s	Synchronous speed
$n_{nominal}$	Nominal speed of the machine
f_{stator}	Frequency of the stator or supply
f_{rotor}	Frequency of the AC currents fed into the doubly-fed induction generator rotor windings
N_p	Number of poles of the machine
s	Slip of the machine
$P_{resistor}$	Power of the snubber resistor
C_s	Capacitance of the snubber capacitor
U_d	Voltage of the snubber diode
$R_{snubber}$	Resistance of the snubber resistor
I_{rr}	Power supply current
I_o	Saturation current
U_{gs}	MOSFET Gate-Source voltage
U_{th}	MOSFET Threshold voltage
U_a, U_b, U_c	Represent the three-phase voltage quantities in the abc coordinates
i_a, i_b, i_c	Represent the three-phase current quantities in the abc coordinates
$\phi_{as}, \phi_{bs}, \phi_{cs}$	Flux linkage of the stator per phase
$\phi_{ar}, \phi_{br}, \phi_{cr}$	Flux linkage of the rotor per phase
i_α, i_β	Represent the stationary orthogonal reference frame quantities
i_γ	Represents the homopolar component of the system
i_d, i_q	Represent the rotating reference frame quantities
U_{as}, U_{bs}, U_{cs}	Phase voltages of the stator in the abc coordinates
U_{ar}, U_{br}, U_{cr}	Phase voltages of the rotor in the abc coordinates
$U_{abs}, U_{bcs}, U_{cas}$	Line voltages of the stator in the abc coordinates

$U_{abr}, U_{bcr}, U_{car}$	Line voltages of the rotor in the abc coordinates
i_{as}, i_{bs}, i_{cs}	Phase currents of the stator in the abc coordinates
i_{ar}, i_{br}, i_{cr}	Phase currents of the rotor in the abc coordinates
$U_{\alpha s}, U_{\beta s}$	Components α and β of the stator voltages in $\alpha\beta$ coordinates
$U_{\alpha r}, U_{\beta r}$	Components α and β of the rotor voltages in $\alpha\beta$ coordinates
U_{ds}, U_{qs}	Components d and q of the stator voltages in dq coordinates
U_{dr}, U_{qr}	Components d and q of the rotor voltages in dq coordinates
$i_{\alpha s}, i_{\beta s}$	Component α and β of the stator currents in $\alpha\beta$ coordinates
$i_{\alpha r}, i_{\beta r}$	Component α and β of the rotor currents in $\alpha\beta$ coordinates
i_{ds}, i_{qs}	Component d and q of the stator currents in dq coordinates
i_{dr}, i_{qr}	Component d and q of the rotor currents in dq coordinates
ϕ_{ds}, ϕ_{qs}	Component d and q of the flux linkage of the stator in dq coordinates
ϕ_{dr}, ϕ_{qr}	Component d and q of the flux linkage of the rotor in dq coordinates
R_s	Equivalent resistance of the stator per phase in a delta connection
L_s	Equivalent inductance of the stator per phase in a delta connection
R_r	Equivalent resistance of the rotor per phase in a delta connection
L_r	Equivalent inductance of the rotor per phase in delta connection
L_m	Equivalent magnetizing inductance per phase referred to the stator
L_m^t	Transpose of the matrix given by the magnetizing inductance viewed from the stator
ω_s	Angular speed of the stator
ω_r	Angular speed of the rotor
ω_{shaft}	Angular speed of the shaft
$\theta_s(t)$	Angular position of the currents and voltages of the stator
$\theta_r(t)$	Angular position of the currents and voltages of the rotor
$\theta_m(t)$	Mechanical angular position of the rotor shaft
n_{rs}	Turn ratio between the number of rotor and stator windings
i'_{dr}, i'_{qr}	Component d and q of the rotor currents in dq coordinates referred to the stator
u'_{dr}, u'_{qr}	Component d and q of the rotor voltages in dq coordinates referred to the stator
ϕ'_{dr}, ϕ'_{qr}	Component d and q of the flux linkage in dq coordinates referred to the stator
R'	Equivalent resistance of the rotor per phase in dq coordinates referred to the stator

L'_r	Equivalent inductance of the rotor per phase in dq coordinates referred to the stator
i_{dcr}	DC-link current from the RSC side
i_{dcg}	DC-link current from the GSC side
U_{dc}	DC-link capacitor voltage
C_{dc}	DC-link capacitance
i_{dc}	DC-link capacitor current
U_{aG}, U_{bG}, U_{cG}	Phase voltages of the GSC in the abc coordinates
i_{aG}, i_{bG}, i_{cG}	Phase currents of the GSC in the abc coordinates
R_f	Resistor in the grid side filter
L_f	Inductance in the grid side filter
U_{df}, U_{qf}	Components d and q of the grid filter voltages in dq coordinates
i_{dG}, i_{qG}	Components d and q of the GSC currents in dq coordinates
ω_s	Synchronous angular speed

Chapter 1 – Introduction

Nowadays, electrical energy has a vital role in the daily routine of a common person, and, with the evolution of technology, and all of the methods used, it is more likely that electrical energy will become something imperative in the basic daily life needs of a regular person that has access to it.

In the current chapter, the different forms of energy production will be mentioned, such as the non-renewable energies on which the world is still very dependent on, as well as the renewable energies, which have started to get a bigger role in the latest years, especially when it comes to electrical energy production. The huge usage of non-renewable energies, mostly fossil fuels, has been causing big environmental, social and economic changes all around the world. Due to the current process of climate change, as well as all the scientific analysis and reports on the non-renewable energy sources usage and the alarming impacts felt in several areas around the world already, have led to the international community having increasing concerns in the search of reliable alternatives, such as the renewable energies, over the last couple of years.

Due to the availability of the wind and the financial incentives given by the government to attract a lot of investors (which can be, for example, lower energy bills or subsidies provided by governmental programs), as well as the technological advances made in the area to make the systems more effective and affordable, a short overview of the current situation of wind energy in Europe is done in this chapter, with special focus around the situation in Portugal, in order to understand the potential of the country when it comes to type of energy production. Having almost half of its border with sea, Portugal possesses a high wind potential, which has also attracted a lot of investments in the most recent years towards making wind energy one of the primary energy source production of the country, while at the same time, making it less dependent on the non-renewable energy sources, specially from the fossil fuels derivatives.

Following the study mentioned, this chapter will also describe the several motivations responsible for the choice of the topic for this project, alongside its several objectives, as well as the chapter structure of this current report, which will be explained in detail.

1.1. Problem Overview

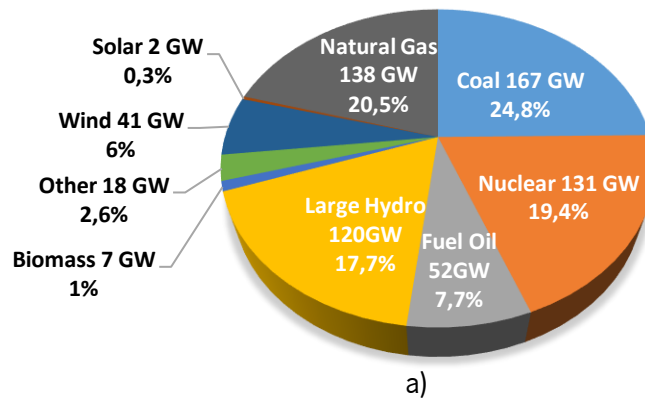
From millenniums ago until today, there has always been research for different types of energy sources, and even more today due to the increasing awareness of environmental issues regarding the current energy production market. The search for these energy sources is always in order to try to maximize production while at the same time reducing both costs and environmental impacts to the minimum. With the needs for energy going up every year, due to the growing industrialization in every country, more and more economic resources are being invested by each country in exploring the potential of the diverse resources available in the planet. [1]

During the last decades, the growth of the consumption of electrical energy was accompanied by the increased use of non-renewable energy sources, like coal and oil derivatives, which lead to increased environmental concerns by the world community. The use of these non-renewable energy sources has a negative impact in the environment, mainly because of the usage of coal and oil derivatives in combustion reactions, as they release considerable amounts of gases for the atmosphere, such as CO₂, which in large amounts brings considerable impact to the ozone layer. The existing ozone layer in the stratosphere allows for filtering of the ultraviolet rays, and during the last years it has been significantly affected because of the CO₂ emissions. [2]

Moving into the different energy sources used nowadays, from the non-renewable energy sources, there is electrical energy production using mainly coal, fuel oil, natural gas, and nuclear power, while from the renewable energy sources, there is mainly wind power, solar power, large hydro power and biomass power. It is possible to observe in figure 1 two graphs, a) and b), which represent the installed power capacity of each energy type and its share within the countries of the European Union (which includes Austria, Belgium, Bulgaria, Croatia, Cyprus, Czech Republic, Denmark, Estonia, Finland, France, Germany, Greece, Hungary, Ireland, Italy, Latvia, Lithuania, Luxembourg, Malta, Netherlands, Poland, Portugal, Romania, Slovakia, Slovenia, Spain, Sweden and United Kingdom) in the year of 2005 and also the year of 2017.

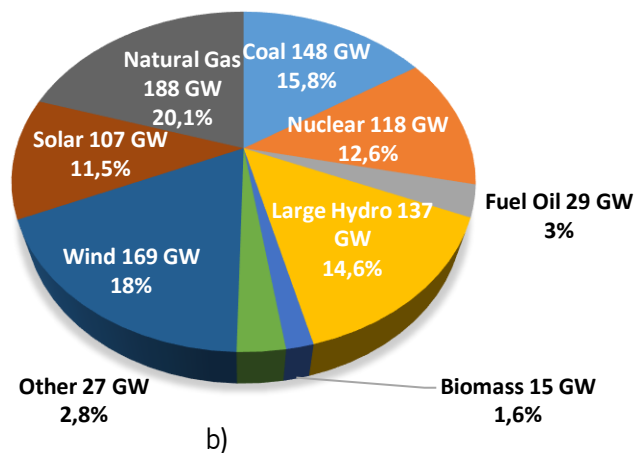
Due to the demand for electrical energy rising up in the latest years as a consequence of the fast-growing industrialization of all countries, as it is possible to understand comparing both figures, the total installed power capacity is growing. And, keeping in mind the limited amount of the non-renewable energy sources, the need for new reliable alternatives must be found to satisfy the growing energy needs of these countries.

2005



a)

2017



b)

Figure 1 – a) Share in installed power capacity in 2005. b) Share in installed power capacity in 2017 (Source [7])

In Europe, the need for alternative sources of energy production lead to more investments being made in the renewable energies [3][4]. These have gotten a lot of attention from countries and investors, specifically wind energy, due to the fact of being very reliable and environment friendly energy sources. Despite the need of a big investment at the start for building several WTGS, this is all driven mainly by the need of a cleaner energy. Being Wind considered a renewable energy source, it is needed a study to determine the best places to take advantage of the existing wind potential.

Having Portugal little to none fossil fuel energy sources, the country itself needs to find a way to produce electric energy using renewable energies, so that it does not rely only on the imports of fossil fuel derivatives. In the latest years, there has been a big investment in renewable energy sources around the country [5][6], as shown in figure 2, being the investment in wind energy one of the biggest.

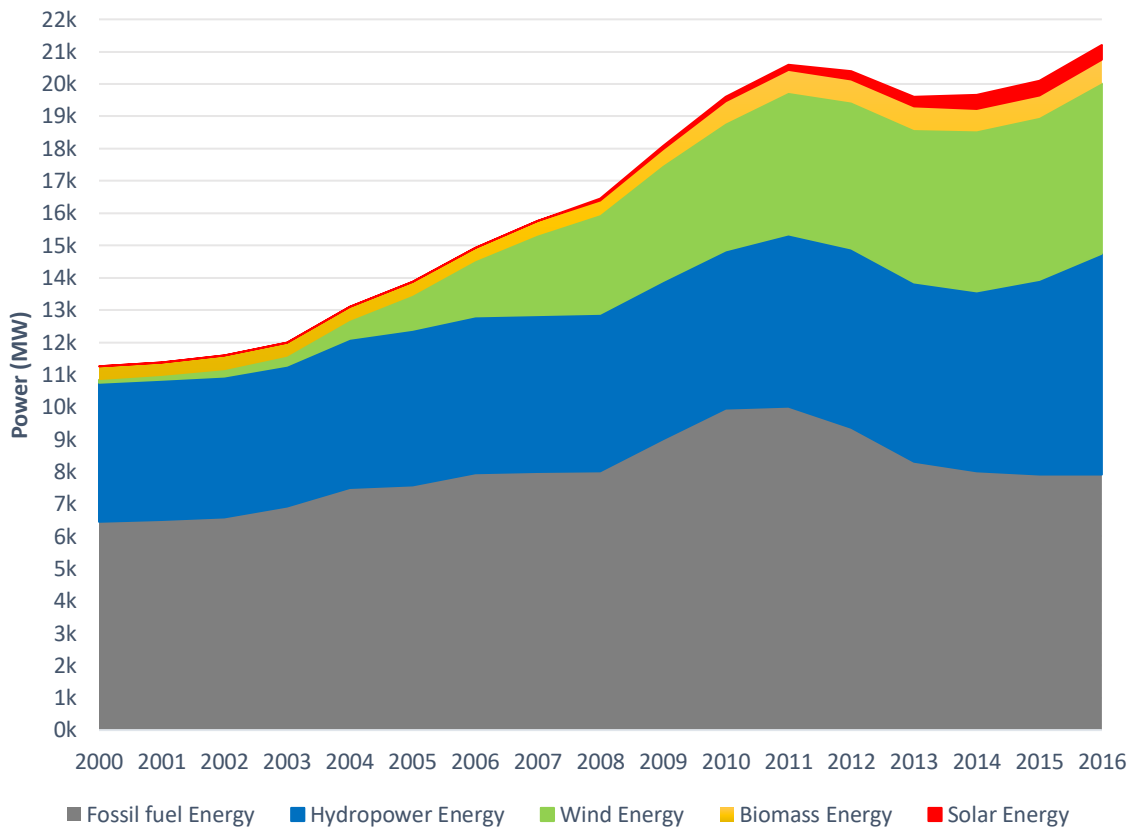


Figure 2 - Cumulative power capacity between 2000 and 2016 in mainland Portugal (Source [8])

Portugal has its own natural resources in its own way. In figure 3, it is possible to observe the average wind speed in the mainland, and, having the country a huge wind potential, it is very important to understand where it will be more effective the production of energy from wind power, keeping in mind that altitude and being near the coastline are two of the most relevant factors when doing an analysis to a certain area.

To sum up, wind energy has had a very fast growth in the latest years, turning it into one of the biggest renewable energy sources, not only in Portugal but also in other European countries, as it is represented in figures 1. Non-renewable energy sources have started to decrease in terms of percentage of the total amount of power capacity possessed, as countries and investors slowly become aware that newer technologies are being discovered every day that allow for more power production and cost efficiency when it comes to renewable energies, and also that the limited amount of fossil fuels on the planet will not last for long. But still, this transition process will still take some decades to be fully implemented, as educating the world population about the matter is amongst one of the biggest problems in the subject matter.

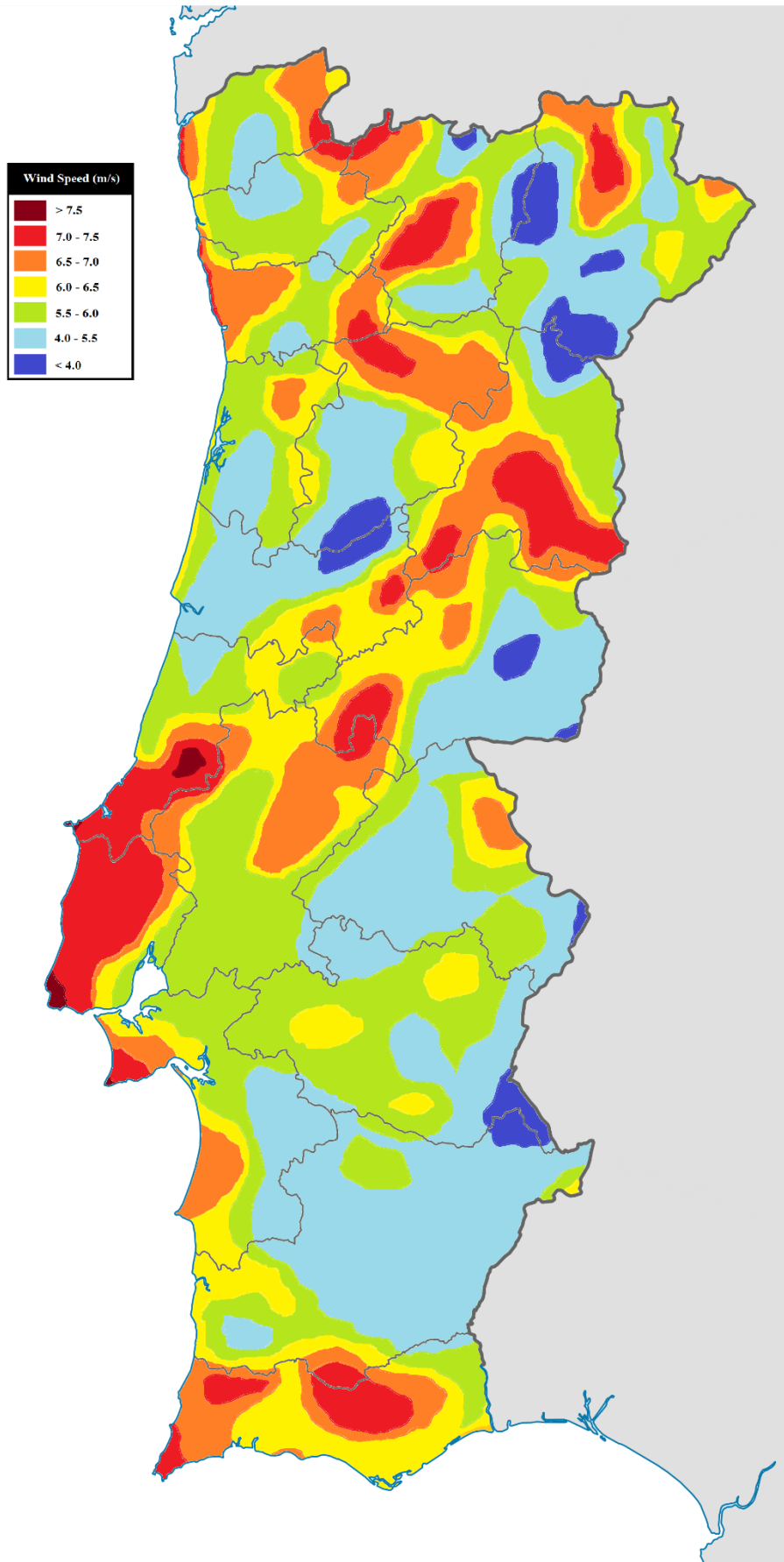


Figure 3 - Wind potential in mainland Portugal (Source: [9])

1.2. Motivation

One of the biggest motivations is having in mind the current status of the energy market, which is dominated by the use of non-renewable energy sources, more specifically the energy produced from fossil fuel derivatives, and it makes the need for a more clean and renewable energy bigger by the year. [7]

The big economic and environmental advantages of using the wind energy and utilizing the huge wind potential in Portugal are to be fully explored. In order to do so, it is imperative the use of power electronics circuits alongside complex control systems to fully take advantage of this energy. There are several ways of elaborating a WTGS, and these will eventually get improved with time, increasing the efficiency and the performance of the systems developed. On top of that, people are starting to become more aware about the situation surrounding renewable and non-renewable energies, thus making a very interesting topic and one of the most debated within the country in the most recent years.

Lastly, taking into consideration obviously all the specifications of the power electronics and the control system needed to elaborate this WTGS, the fact that this project has never been developed in the university department proved to be a good challenge overall.

1.3. Objectives

The main objective of this project is to develop the interface structure of a WTGS, using a DFIG, in order to produce the maximum amount of power. This interface is composed of a back-to-back converter, which consists of two converters, the RSC and the GSC, connected to one another by means of a DC-link capacitor, and this enables the power to flow in both ways, having in mind the working concept of this generator. For a better ongoing of this project, its main stages consist in the following:

- Research and study of a DFIG inserted in a WTGS;
- Development of a back-to-back power electronic converter;
- Development of a control algorithm for both the RSC as well as the GSC that integrate the back-to-back power electronic converter, so that it allows the maximum power extraction from the system developed;

- Simulations of the developed power electronics and control algorithm using MATLAB Simulink program;
- An attempt at a simple proof of concept by means of an experimental testing.

And also, this project can be of use in what comes to a better understanding of how to develop the interface circuits and the control algorithm that incorporate the system, and to offer aid to others that wish to go on to develop a WTGS of their own in the university department in the future.

1.4. Project Structure

The present project is divided in six chapters, each of which is subdivided accordingly to the respective content in each one of them. With this in mind, the project structure is as follows:

- In the first chapter a small introduction is done, as well identifying the problem this project plans to solve, alongside the motivations, the objectives and the structure of this project;
- The second chapter contains brief history of the evolution of the technologies used in wind energy over the years, as well as advantages and disadvantages of the use of this energy. In this chapter is also an analysis of the physics of a WTGS as well as its integrating parts illustrated;
- The third chapter presents the system interface as well as a general overview of each respective component, with special emphasis on an extensive analysis and understanding of the working principles of the generator used in this project as well as the control algorithm used and the power electronics associated to the system to make it function properly.
- The fourth chapter consists on several simulations to study the behaviour of the system. Each respective part of the system tested will be previewed in Simulink. Every simulation is done in order to better understand the working principles of the system analysed in the third chapter so that a proof of concept of this project can be done in laboratory environment.
- The fifth chapter starts explaining exactly how the attempted proof of concept in laboratory environment was projected, showing also every step taken into consideration for the practical testing. It also contains an analysis made about this proof of concept.

- The last chapter, the sixth chapter, will feature the conclusions about this project as well as possible future work.

Chapter 2 – Wind Energy

The present chapter contains an analysis of the energy inserted in the topic of this project, the wind energy. Throughout the years, it existed many different ways of using this energy, having most of them evolved through time to become more effective and more reliable. Each way of producing this energy has several advantages and disadvantages that had to be taken into consideration at all times, especially when considering the budget available for the financing of these projects. With this being said, the first part of this chapter contains an overview of the evolution of the way that people harness the power of the wind, dating back from the early years since this energy was first used until it developed into what today is called as a WTGS. Alongside this will be the several advantages and disadvantages of harnessing and using this type of energy by means of a WTGS.

The second part of this chapter consists of a system analysis made to the WTGS in terms of the physics behind it, as well as an understanding of its modelling, which will be very important in the on-going of this project since the control algorithm developed incorporates all of the theory as well as the several mathematical equations.

2.1. Wind Energy Technology

Depending how strong the wind is, certain things can be moved when the wind blows, like the blades of a turbine for example. So, energy exists in the wind, and the ways of using or transforming that same energy for personal use or for helping with the energetic needs of a civilization needs has evolved throughout time.

2.1.1. State of Art

Since early recorded history, people have harnessed the energy of the wind, mostly for their own purposes. From thousands of years back, wind has been used for several needs. It was used by windmills, mostly for grinding grain or pumping waters, and it was used as well in the sailing ships as their main source of energy. Horizontal and vertical windmills were already in existence, having an important role in the rural economy of most countries (some of these windmills are even still working today, for example in Iran, as their design is shown in figure 4).

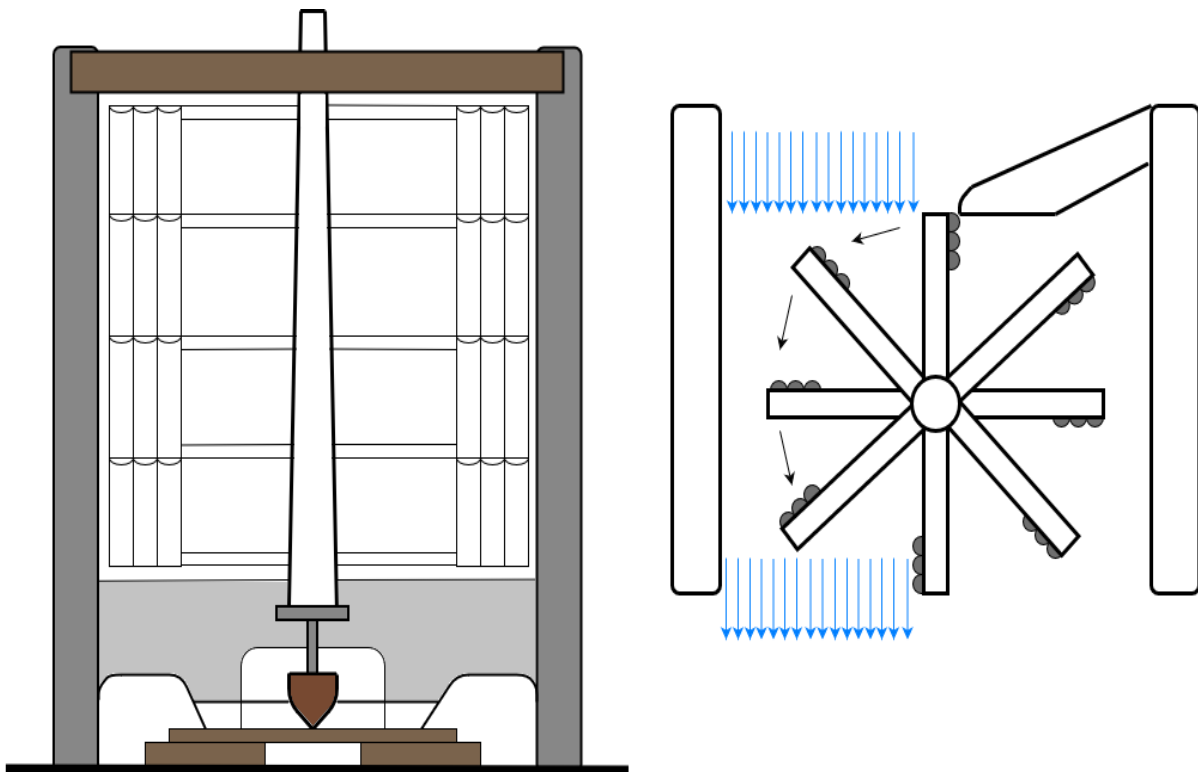


Figure 4 – Vertical-axis windmill (Adapted [10])

Eventually, new ideas and ways of using the energy of the wind would spread around the world. With time, people started to use windmills extensively for food production. The use of this types of windmills would eventually fall into disuse with the use of fossil-fuelled engines that were later invented.

In the late nineteenth century, windmills were being used to pump water for farms and ranches, and later to generate electricity for homes and industry. The investment in the technology made by several countries was growing over the years. The improvements were getting better, however, the growth and advance of the technology was put a bit aside due to the availability of cheap oil and low energy prices, up until the 1970s when most developed countries became aware of the oil shortages and understood a change was needed in the energy production market. It created an interest in possible alternative energy sources, paving the way for the re-entry of the wind turbine to generate electricity. A lot of countries started to have government-funded projects, where it was being conducted a large-scale research on wind turbines, leading to several experiments. These experiments had significant impact in the outgrowing of the industry, and its results pioneered many of the multi-megawatt turbine technologies in use today.

In 1957 a Danish engineer named Johannes Juul built a wind turbine, and the basics he used from his research and development were very important in the establishment of a wind turbine concept which consisted in a three-bladed, stall-regulated rotor at a fixed speed, with an induction machine drive train. This very simple model had a big success, with most of the other countries adapting their models to this prototype, having displayed in figure 5 a turbine used today based on this concept.

With the advance of technology, more interest was being added to the investigation and research of a possible variable-speed, as well as a blade pitch control of this type of wind turbines. Despite wind power not generating as much electricity as fossil-fuels, and thus not being an immediate substitute for petroleum in most applications (especially transport), all of the fear and concerns about the shortages only stacked to the urgency to expand wind power, alongside other renewable energies. Earlier oil crises had already caused many utility and industrial users of petroleum to shift to coal or natural gas, and wind power had already showed great potential for replacing natural gas in electricity generation on a cost basis with the technological advances made in the last years. These advances can be understood with the size evolution of wind turbines displayed in figure 6.



Figure 5 – Three-bladed wind turbine in Viana do Castelo

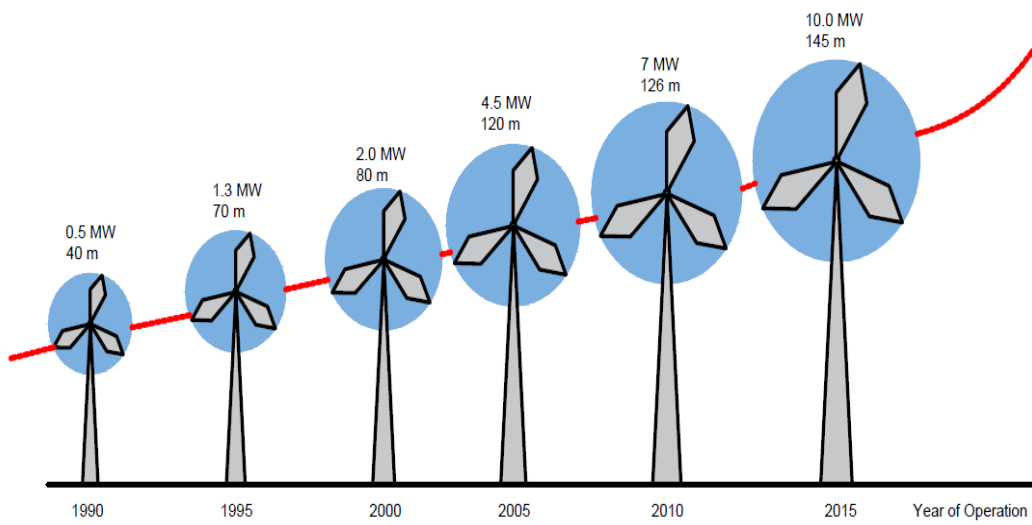


Figure 6 – Installed Power and Diameter evolution of wind turbines over latest years (Adapted [11])

Nowadays, the main reason, for the use of wind turbines to generate electrical power is to lower the CO₂ emissions as much as possible to help limit climate change. Even with that in mind, there is still a lot of discrepancy between the investments made by different countries, and there are a lot of important factors having their respective impact in the investment of every country. Those factors include firstly the wind potential of the respective country as well as their financial support for the investment, and secondly bureaucratic issues like permissions for construction or local impact in populations, having even some investments being done in offshore sites to avoid this factor. [11][12][13]

2.1.2. Advantages and disadvantages of wind energy

As everything in the world today, all the pros and cons must be overviewed so that a proper judgement can be made in what comes to knowing if something is worth or not to invest on. Due to the fact that this field is already being explored for a lot of years already, it is known that wind energy has a lot of advantages, such as:

- The wind being a free, natural and unlimited resource, that with modern technology can be used to generate electrical energy efficiently;
- A WTGS does not produce any greenhouse gas or other pollutants;
- The energy produced in these systems comes at a very low price in the market, mainly due to the facts that the price does not include the fuel price (because there is no fuel cost like coal or oil being used in these systems, only wind) and also government incentives and policies;
- This type of energy is sustainable. Wind comes from the heating of the atmosphere from solar radiation, and it is generated by convection processes due to different air temperature in the atmosphere. So as long as there is sun as well as air surrounding the planet, there will always be wind;
- Remote areas that do not have access to electricity can use wind turbines to produce their own supply;
- Due to the advance of the technologies used, the wind turbines are available in a range of sizes, which means a vast range of people and businesses can use them for their

own purposes, from supplying only one house of one person and its own needs, to supplying entire cities.

However, wind energy also has its own flaws. Basically, there is a lot of complications towards the whole process of building and establishing the wind turbine systems. The disadvantages consist mostly on:

- The fact that the strength of the wind is not constant. This means that wind turbines do not produce the same amount of electricity all the time. There will be times where they will not produce any electricity at all;
- Wind turbines are noisy, so they should be located within certain distance from populated areas. Also, it brings a negative impact on the wildlife of the area (especially for birds) and affects the landscape view;
- The manufacture of the parts that compose a wind turbine produces some pollution;
- Despite all of the long-term benefits, it still requires a huge investment at the start, as not only the wind turbine system is needed but also establishing the infrastructure and the transmission lines, allowing it to be connected with the grid;
- Large amounts of wind turbines are needed in order to be able to produce the same amount of energy as produced in a single powerplant that uses another type of fuel;
- Big studies and analysis must be done beforehand to the terrain where it is desired to install a wind turbine, to see if the wind turbine can be reliable in energy production and also to assure that it doesn't bring negative impacts to the surrounding areas and also to the environment.

In the end, every advantage and disadvantage mentioned in the list must be taken into consideration when planning an investment in wind energy and in wind turbine sites, so that when going forward with projects to build several wind turbine systems it can be a good and proper investment for the future. [11]

2.2. A Wind Turbine Generator System

A Wind Turbine Generator System (WTGS) is a system composed of a wind turbine with certain generator and power electronics associated to it, and it has the goal of transforming the kinetic energy available in the wind into electrical energy ready for use in the grid.

2.2.1. System analysis and wind turbine modelling

Kinetic energy exists in any moving object, and if that object stops, the energy will be gone. The wind, which consists in the movement of air, also has kinetic energy. Using the proper units for measuring the mass and the speed of the moving object, its kinetic energy can be calculated as displayed in (1).

$$E_k = \frac{1}{2}mv_w^2 \quad (1)$$

When it comes to a moving fluid (gas or liquid), energy can be found in the same way as described before, but there are two important things to keep in mind when it comes to a fluid in motion. Firstly, the mass of a fluid in motion is defined by its volume, because there is no solid object with a defined mass to be considered. And secondly, it is to keep in mind that, for a moving fluid, the whole volume moves.

Considering the wind as a moving fluid without boundary, an imaginary boundary will be generated by it and by the objects it passes through (assuming it is round for simplicity effects, it can be seen in figure 7. At first, it is shown the wind stream moving in a straight line until it comes across an object, in this case the wind turbine. The turbine obstructs the flow of the wind, so the particles start moving outwards as they approach the turbine, and shortly after passing the obstacle they resume their parallel flow at some point.

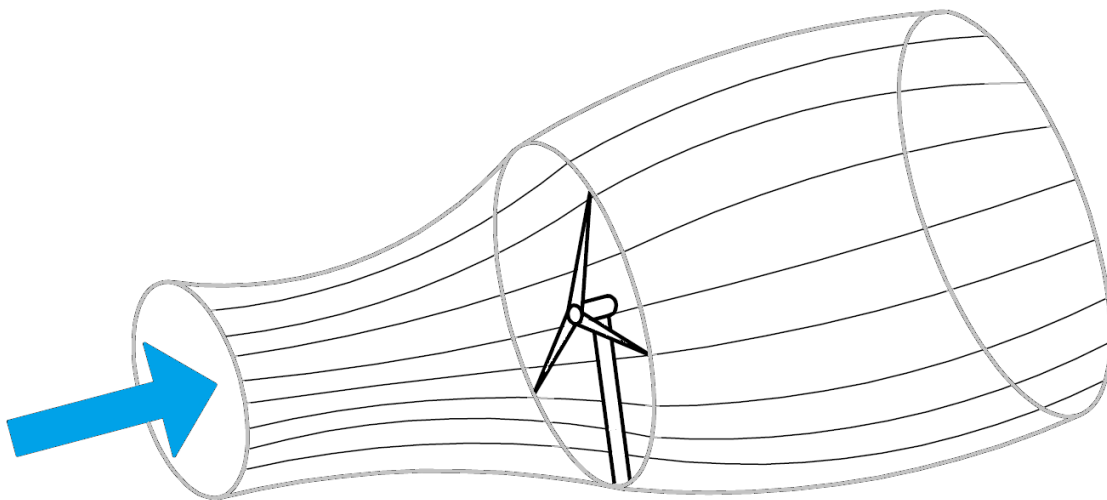


Figure 7 – Wind stream imaginary boundary (Adapted [11])

All things considered, in the case of a moving fluid, it is more useful to determine the power within the wind rather than its energy, because it depends on the length of the stream which can vary a lot. With this taken into consideration, it is possible to substitute the mass from (1) by (2).

$$m = \rho V \quad (2)$$

Also, considering the shape of the wind stream as a typical pipe or tunnel section, meaning that A is equal to πr^2 , it is possible to determine the amount of air volume moved per second with (3).

$$\text{Volume per second} = Av_w \quad (3)$$

Using both equations (2) and (3) to substitute variables in (1), it is possible to calculate the amount of power in a moving fluid through (4).

$$P_w = \frac{1}{2} \rho A v_w^3 \quad (4)$$

Analysing this last equation, and having in mind how the air density behaves, there will be more power in the wind available for the turbine with cold weather, since it comes with a higher air density. The same can be said when it comes to winter and summer seasons, as well as when comparing day and night, but despite these facts, the difference in power due to temperature changes is not too much.

Even with everything said up until now, all of the power that the wind carries cannot be totally absorbed by the wind turbine. Only a portion of it can be absorbed, and a lot of factors must be taken into consideration regarding the turbine being used. Factors such as the type of turbine used, its efficiency, the surroundings, the height and other conditions in the operation of a turbine all influence the amount of power that can be absorbed. So, in order to calculate the fraction of power that a wind turbine can harness from the wind, a power coefficient, C_p , must be considered to calculate the power obtained from the wind turbine as displayed in (5).

$$P_t = C_p P_w \quad (5)$$

With (4) and (5) in mind, the wind turbine power can be calculated in (6).

$$P_t = \frac{1}{2} C_p \rho A v_w^3 \quad (6)$$

Something important to also consider is the mechanical torque of the turbine, as well as the torque coefficient. They are displayed in equations (7) and (8), respectively.

$$P_t = T_{em} \omega_t \quad (7)$$

$$C_t = \frac{C_p}{\lambda} \quad (8)$$

The tip-speed ratio, λ , which is the ratio between the tangential speed of the tip of a blade and the actual speed of the wind, is defined in (9).

$$\lambda = \frac{\omega_t r}{v_w} \quad (9)$$

This power coefficient, C_p , is given in function of the tip-speed ratio, λ , and also on the pitch angle of the turbine blades, β . Its value depends also on other factors, and most turbines in the market have this value between 0.4 and 0.5 out of 1. Taking this into consideration, it is possible to calculate the value of the mechanical torque of the turbine displayed in (10) using (6), (7), (8) and (9).

$$T_{em} = \frac{1}{2} \rho \pi r^3 v_w^2 C_t \quad (10)$$

For control purposes in later chapters, this equation is changed as shown in (11). It is considered the optimal values for the variables C_p , C_t , λ and β in order to track the maximum power point (also known as MPPT algorithm).

$$T_{em} = \frac{1}{2} \rho \pi r^3 \frac{w_t^2 r^2 C_{p_{max}}}{\lambda_{opt}^2 \lambda_{opt}} = \frac{1}{2} \rho \pi \frac{r^5}{\lambda_{opt}^3} C_{p_{max}} w_t^2 = k_{opt} w_t^2 \quad (11)$$

The MPPT control block that will be implemented in later chapters is based on equation (11) is displayed in figure 8. [11][12][13][14][15]

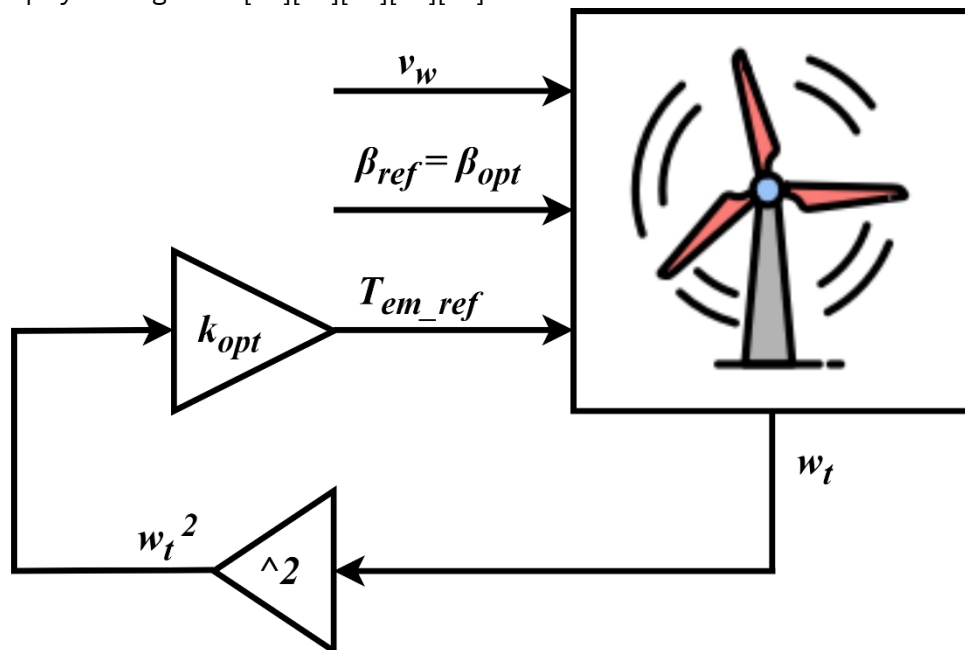


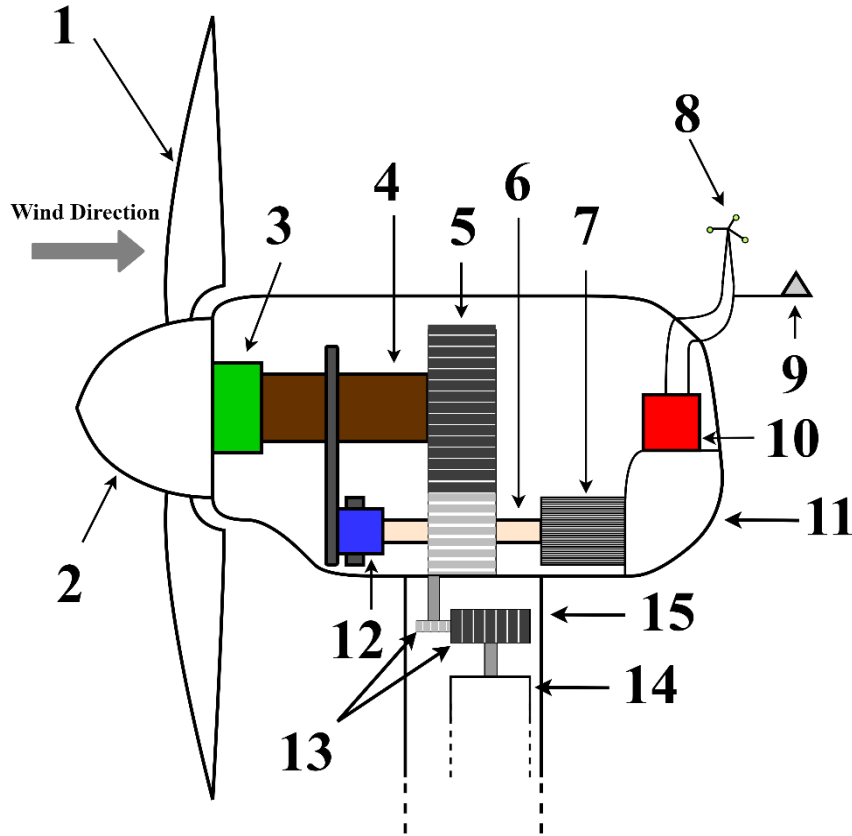
Figure 8 – Wind turbine MPPT control (Adapted [15])

2.2.2. Wind Turbine Generator System components

A WTGS is a system that converts kinetic energy firstly into mechanical energy, and then to electrical energy. There are two types of wind turbines used in a WTGS, turbines of horizontal axis and turbines of vertical axis. Horizontal axis turbines are the most used nowadays because of their better efficiency compared to the vertical ones, and, for the purpose of this project, that will be also the type of turbine that will be considered throughout the development.

The detailed architecture of a typical horizontal axis wind turbine is represented in figure 9, where it is also possible to observe each component that integrates the wind turbine as well as their respective function. The power electronics are next to the generator, and the power that is extracted is passed through a transformer to adapt do the grid conditions, so that then it can be transported and stored in a power substation before being put to use.

The most famous and used horizontal axis wind turbine is the propeller turbine. This turbine normally has three blades on top of a tower, and it is also very sensitive to wind changes. Two of its possible configurations are displayed in figure 10, whereas it can be facing wind upwards or downwards.



1	Rotor Blade	2	Rotor Hub	3	Pitch System	4	Low Speed Shaft
Rotates when the wind is blowing, spinning the rotor		Formed by both the Hub and the Blades		Pitches the blades into or out of the wind to control the rotor speed		Rotates when the blades are rotating	
5	Gearbox	6	High Speed Shaft	7	Generator	8	Anemometer
Connects the High Speed Shaft to the Low Speed Shaft		Drives the Generator		Produces AC electricity		Measure and transmits the wind speed data to the Controller	
9	Wind Vane	10	Controller	11	Nacelle	12	Brake
Helps the Yaw Drive to turn the turbine in the wind by measuring the wind direction		Starts the machine at low speeds (when it is enough to produce efficiently energy) and turns it off at higher speeds (to prevent possible damages)		Sits atop the turbine tower		Stops the rotor in special situations	
13	Yaw Drive	14	Yaw Motor	15	Tower		
Adjusts the turbine to be always facing the wind. Downwind turbines do not require yaw drive		Powers the Yaw Drive		Made from tubular steel or similar material. Supports the wind turbine structure and all its components			

Figure 9 - Architecture of a wind turbine (Adapted [16])

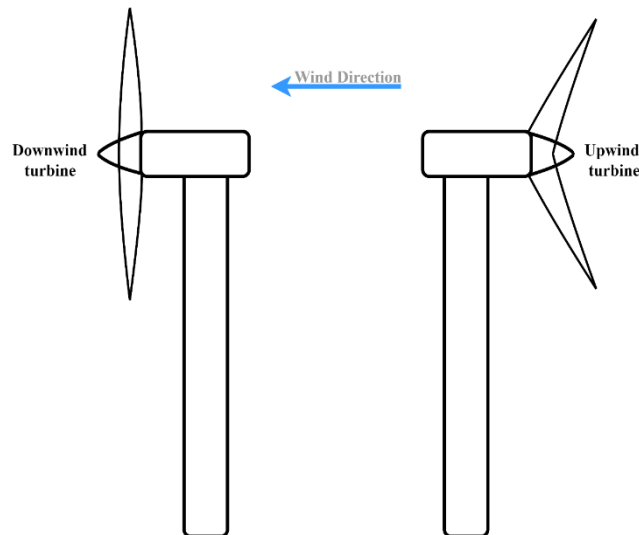


Figure 10 – Different installation designs for a wind propeller turbine (Adapted [11])

Being a bit more specific in the components of a wind turbine, the rotor part is responsible for transforming the kinetic energy within the wind to mechanical energy. The nominal power of a turbine is directly related to the diameter of its rotor, and its size can be adjusted to optimize turbines to work in specific conditions.

The height of the tower of the WTGS system is also important to have in mind because it allows the turbine to be facing more regular and strong wind, and by doing so improving its efficiency. The most common tower type used, are the steel tunnelled towers, because the safety they provide to workers who have to do regular maintenance is very important, as the structure allows for an internal staircase.

Wind turbines are projected to be optimized when it comes to producing energy, so they also come with some types of power control (which come in handy for example in situations where there are strong winds and they should help prevent the damages to the turbine from the excesses of energy), which are blade pitch control and stall control.

Blade pitch control is a mechanism that consists on rotating the blades on their longitudinal axis. It must be operated from inside the hub by an electric or a hydraulic actuator. The blades are adjusted simultaneously to the required value and by doing so changing the range of its power capture capacity to a range between their minimum and maximum possible (this changes the power coefficient value C_p). Adding this control mechanism to a wind turbine increases the number of components in it, and by doing so the cost goes up also. But the megawatt-sized turbines used today are equipped with this control mechanism.

There are two types of stall control, passive and active. The passive one focuses on a simple control system which consist on a turbine with fixed blades that are projected so that when the wind speed is high some turbulence will be generated, which will mean a loss of energy in the total amount available for harnessing but protecting the turbine from potential damages caused by overspeed. When it comes to the active stall control (normally for bigger sized turbines, with over 1 MW of power), the blades rotate on their respective axis. There is a controller which changes the attack angle of the blades (figure 11 is a representation of the variation of the attack angle of a turbine), so that whenever the generator is over its rated power, the controller forces the blades to change their angle and doing so forces an aerodynamic loss of the excess of wind energy. Comparing this to the passive stall control, active stall makes the control of the output of power more precise, and allows this type of turbines to work at their specified power no matter the wind speed.

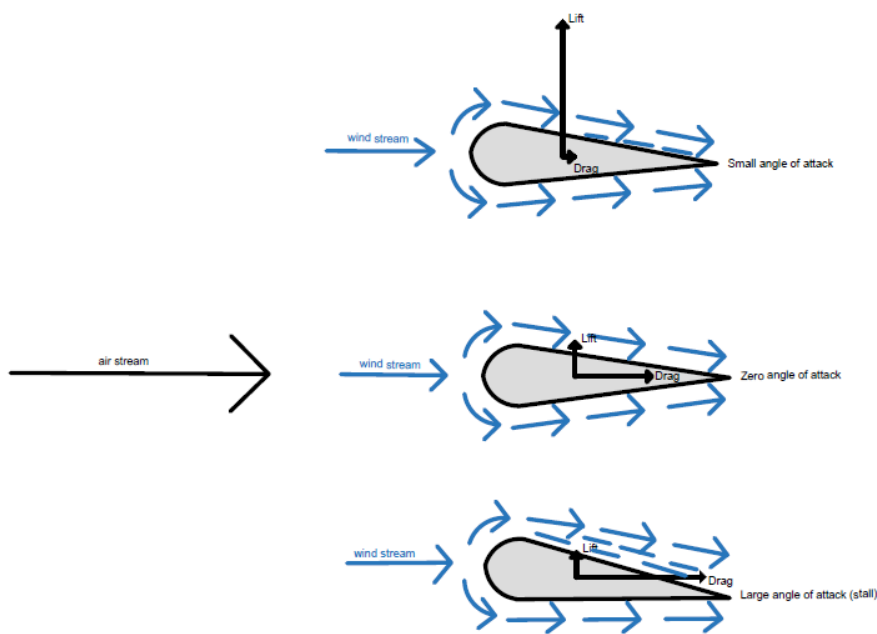


Figure 11 - Stall in an aerofoil (Adapted [11])

Every type of configuration done in a wind turbine depends also on the generator used in it. The generator is the component of the system that transforms mechanical energy into electrical energy. There are different types of generators used, such as a DC generator (very little used), a synchronous generator (alternator) and an asynchronous generator (induction generator). The generator used in this project will be analysed in the next chapter, as well as an overview of its context within the whole power electronics that the system will require. [11][12][13][14][17][18]

Chapter 3 – System interface and its components

Going further into the system analysis, this third chapter will present the system interface to be developed throughout this project as well as every component that integrates it.

One of the key components of this project, the DFIG, is fully analysed, from its working principles till its operation modes. Along this comes also an understanding of MOSFET, snubber, the back-to-back converter specifying both AC-DC and DC-AC converters, and lastly, the transformer.

The control part of this project is totally specified during this chapter. Firstly, the hardware components of the control system used to generate the control signal, Arduino and the Optocoupler HCPL-3120, are briefly overviewed. After it, all the modelling needed is done, in order to develop the control algorithms for the semiconductors in both the AC-DC and DC-AC converters, and with this comes as well the needed mathematical transformations, Clarke and Park. And lastly, the schematics of the control algorithms are presented and they are followed by a detailed description and analysis before moving onto the implementation part in simulation environment.

3.1. Typical system interface

In this section, the interface of the system will be previewed. Figure 12 shows a step-by-step configuration of a system that produces wind energy separating it in few categories.

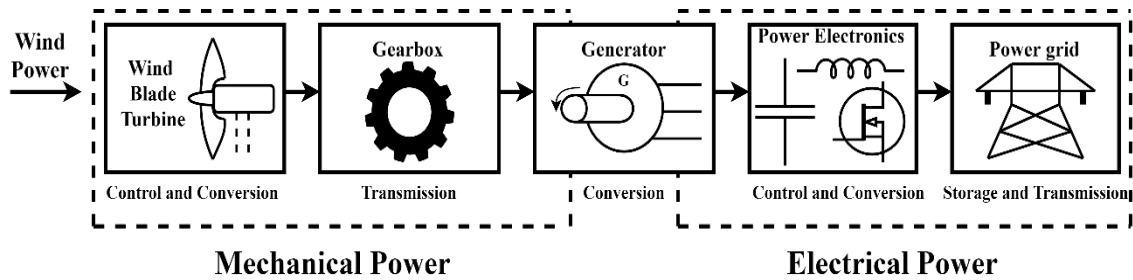


Figure 12 - Basic configuration of a wind energy production system (Adapted [19])

The mechanical part has a wind turbine and can include a gearbox. The turbine is responsible for extracting the kinetic energy from the wind and then transfer that energy through a mechanical shaft in the form of torque and the rotational speed thereof. It is possible to use a gearbox, and if so, a transformation ratio will be applied between the torque and the rotational speed, being the new values transferred to the generator. This generator will transform the mechanical energy into electrical energy in certain values of voltage at a certain frequency. On the other part of the system, the electrical power part has power electronics circuits that converts the electrical energy into the grid standards before transferring that energy to the grid itself, and also having to do power control so that it is possible to adjust the energy produced from the wind to the grid standards.

For the simulation purposes in this project, both the mechanical power part as well as the electrical power part of the system will be considered.

3.2. System components

As shown previously, a wind energy production system has several components, and the ones used in this project, the DFIG as well as all the electronic components of the control circuit, will be analysed.

3.2.1. Doubly-fed induction generator

A doubly-fed induction machine is an electric motor or an electric generator that has windings on both stationary and rotating parts, and where those windings transfer significant power between shaft and electrical system. Usually the stator winding is connected to the power grid through of a transformer, mainly for isolation purposes, while the rotor winding is fed from or to the grid by means of a back-to-back converter (composed of both AC-DC and DC-AC converters).

Although their principles of operation being known for decades, doubly-fed electric machines have only recently entered into common use due to the newest concepts of electrical power productions from wind power technologies. The ability to maintain the amplitude and frequency of their output voltage at a constant level, no matter the wind speed, is their biggest advantage when used in a WTGS, and with that comes also the ability to connect the machine to the power grid and have it always synchronized with the grid. Also, this type of machine, despite being similar to other AC machines, has the possibility to run at a slightly different speed from their synchronous speed, making it more reliable when it comes to the power production, and this also allows for the blades and the turbine to adjust to the wind speed as opposed to a synchronous machine where the turbine is locked at a fixed speed and where the mechanical components of the WTGS suffer more with constant wind speed while not being as effective in power production. On top of all of this, due to the fact that the stator is directly connected to the grid, only around 20-30 per cent of the total power go through the power electronics part of the circuit, which transitions into less loss of power and also cheaper and smaller converters modules used in the system.

The doubly-fed induction machine can work in four different modes: as a generator and as a motor in both sub-synchronous (below synchronous speed) and hyper-synchronous (above synchronous speed) speeds. Working as a generator in sub-synchronous speeds, the stator is generating the power but part of it must be fed back to the rotor, while at hyper-synchronous speed both the stator and the rotor are producing power to the grid. When the machine is operating as a motor, the torque has a positive value, whereas in the generator mode the machine needs torque as a mechanical input, so the torque has a negative value. There will be a better understanding of this last point later in this report.

Figure 13 represents the working principle of the Doubly-fed Inductive Generator, in which is possible to identify the rotor and the stator of the generator and how each of them connects to the Grid (without mentioning the use of the transformer).

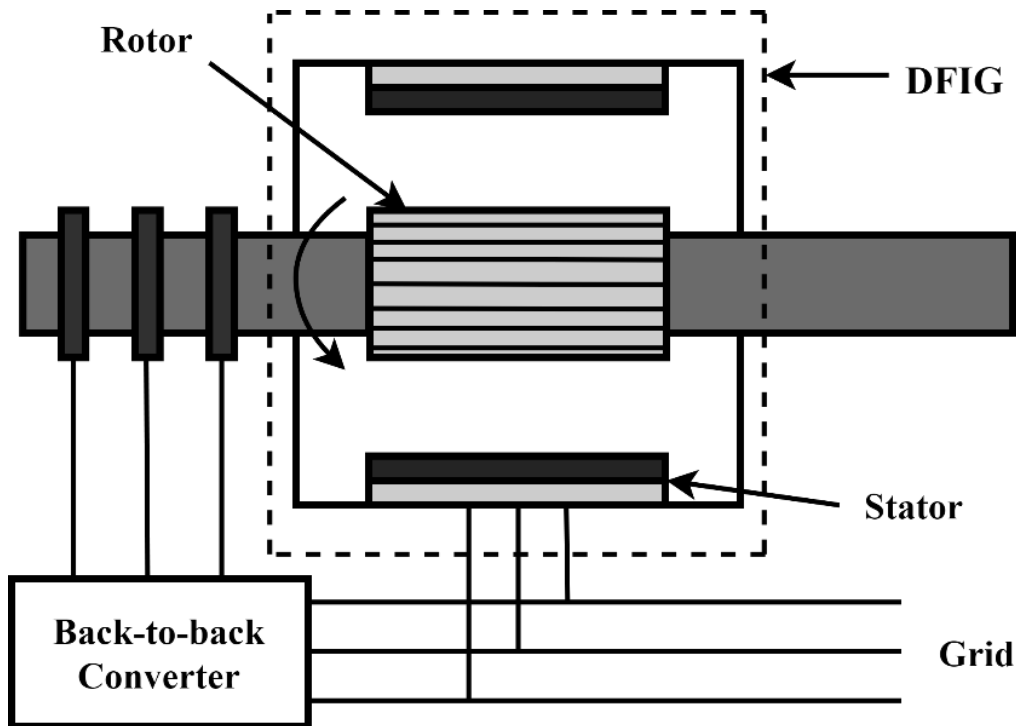


Figure 13 - Principle of DFIG (Adapted [19])

In order to determine the speed of the machine, the formula (12) is used.

$$n_s = \frac{120f_{stator}}{N_p} \quad (12)$$

Having this in mind, the basic concept of slip, which represents the difference between the synchronous speed of the magnetic field and the rotating speed of the shaft, is given by (13).

$$s = \frac{n_s - n_{nominal}}{n_s} \quad (13)$$

When it comes to a doubly-fed induction generator, the supply is given to both the stator and rotor windings. In a DFIG, the rotor produces a magnetic field whose speed is determined by the frequency of the AC current fed to the rotor winding. The frequency of the magnetic field passing through the stator depends on the mechanical speed of the rotor and also on the speed of the rotor magnetic field. The stator frequency, when both the rotor and its magnetic field rotate in the same direction, can be calculated as displayed in (14), and when and its magnetic field rotate in opposite directions, the formula becomes instead (15).

$$f_{stator} = \frac{n_{rotor}N_p}{120} + f_{rotor} \quad (14)$$

$$f_{stator} = \frac{n_{rotor}N_p}{120} - f_{rotor} \quad (15)$$

With everything said so far, it is possible to understand figure 14, which illustrates a three-phase rotating magnetic field.

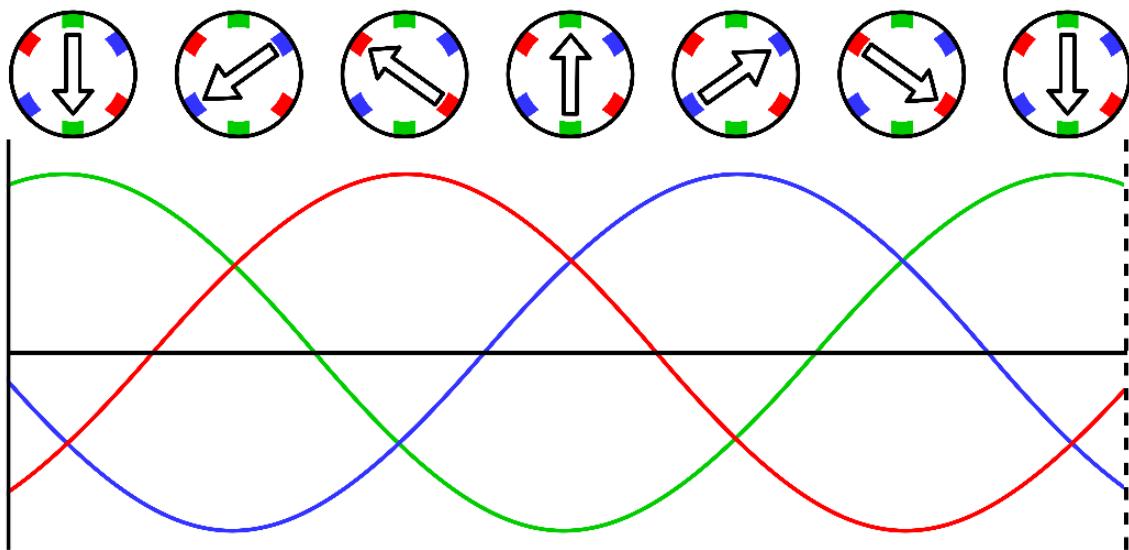


Figure 14 - Three-phase rotating magnetic field (Adapted [21])

One last thing to keep in mind is the inertial response of the generator, which is influenced by the sensitivity of its electromagnetic torque to changes in the frequency of the power system. This inertia is responsible for short-term energy storage, so that when a variation in the frequency of the system happens, it will either absorb excess energy or provide additional energy, as required. For the implementation of this system, this factor is taken into consideration when doing a wind speed variation, as the system will take its time to adapt based on the inertia of the machine. To finish this DFIG analysis, it is displayed figure 15, which represents the behaviour of the DFIG depending on the direction of the magnetic field of both stator and rotor. [16][22]

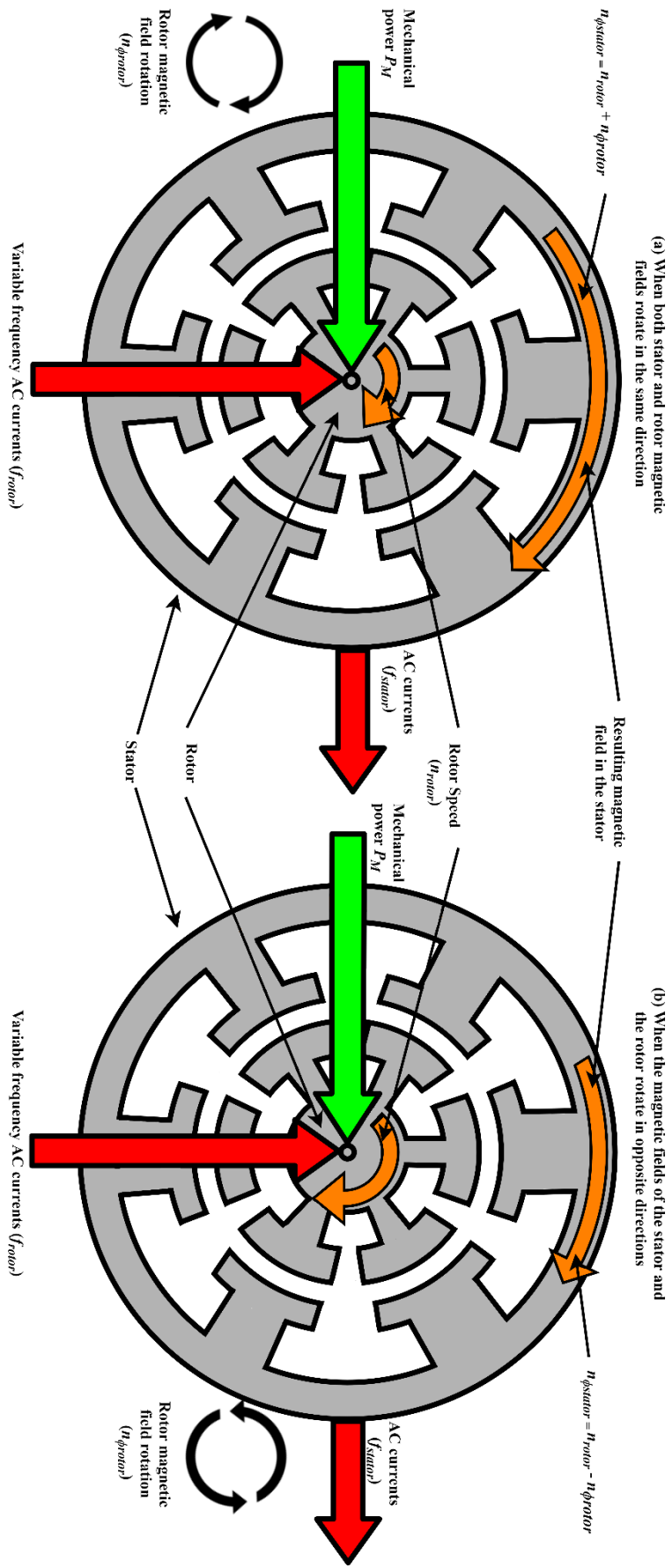


Figure 15 - Schematic of the interaction of the rotor speed and the frequency of the rotating magnetic fields created in the rotor windings (Adapted [22])

3.2.2. Power electronics

The power electronics used in this project include the back-to-back converter (composed of the AC/DC converter, the DC/AC converter as well as the DC-link capacitor), some passive filters, a transformer and the components of the control circuit.

The MOSFET, metal oxide semiconductor field effect transistor, is a semiconductor device that presents lower power losses when compared to other semiconductors, also higher switching speed and it is the most used semiconductor for low voltage circuits and applications because of its efficiency. Since this project will be done in low voltage, this semiconductor is the best option for using in both converters.

This semiconductor has four terminals, Source (S), Gate (G), Drain (D) and the last one can be called either Body (B) or Substrate (S). However, in this device, the body or substrate is often connected to the source terminal through a diode, making it a three-terminal device. Its symbol schematic is displayed in figure 16. Also, this device has an insulated gate, and its voltage determines the conductivity of the MOSFET. For this project, the MOSFET STF23NM50N will be used. [23]

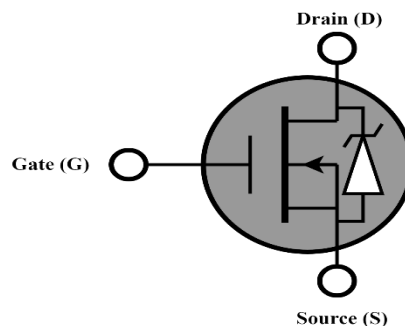


Figure 16 - MOSFET diagram

The MOSFET is included in a snubber, which is a device commonly used to suppress the exceed of the stresses that power electronic converters are exposed to. In this project, the MOSFETs will be exposed to certain stresses, so it is imperative the use of snubbers to protect from voltage and current peaks during the turn-off and turn-on transients of this semiconductors used for both the AC/DC and the DC/AC converters. The design of the snubber used together with the MOSFET in this project for the laboratory experiment is displayed in figure 17.

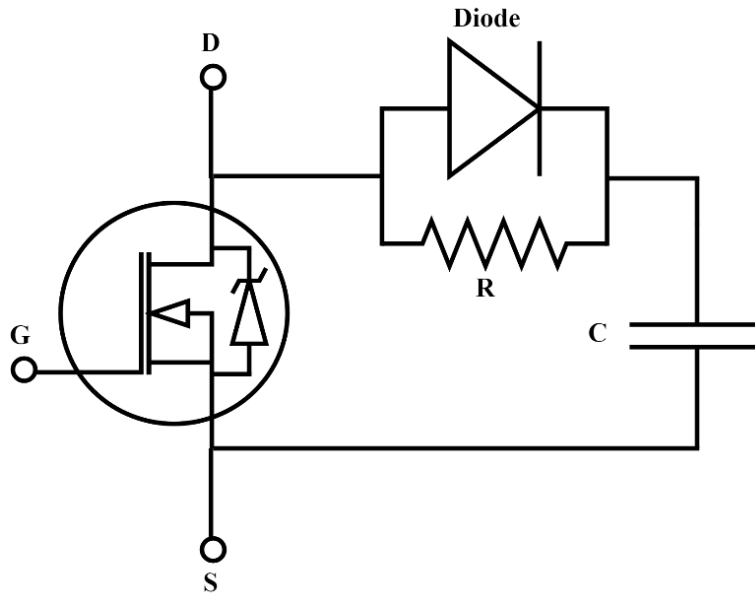


Figure 17 - MOSFET with the snubber circuit

The resistor displayed is a power resistor, and to dimension it is needed to follow equations (16), (17) and (18). The last of the three is an assumption based on practical experiments. [23]

$$P_{resistor} = \frac{C_s U_d}{2} \quad (16)$$

$$\frac{U_d}{R_{snubber}} < I_{rr} \quad (17)$$

$$\frac{U_d}{R_{snubber}} = 0.2I_o \quad (18)$$

The snubbers are an integral part of the back-to-back converter. This back-to-back converter is a bidirectional converter that integrates two converters, the RSC and the GSC, and separating both converts is the DC-link capacitor. This converter uses bidirectional switches, which enable power flow in both ways, and, depending on the power flow one of the converters becomes a three-phase rectifier while the other becomes a three-phase inverter. Figure 18 shows its representation within a WTGS highlighting the RSC and the GSC (without mentioning the use of the transformer).

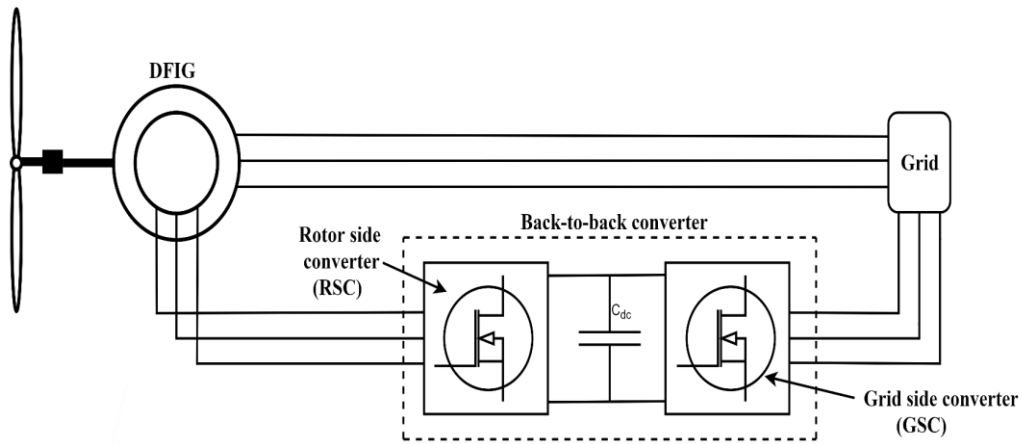


Figure 18 - Simple representation of a back-to-back converter in a WTGS

Taking into consideration how the back-to-back converter operates, it is necessary to understand how both a rectifier and an inverter operate. The rectifier (or AC-DC converter) is an electrical drive that converts the input voltage from alternating current (AC) to direct current (DC). But in order to have a more stable and filtered DC signal, it is necessary to insert a DC-link capacitor between this AC-DC converter and the DC-AC converter. The capacitor works with the AC-DC converter and acts as a storage of DC power and filters out some of the ripple of the DC voltage before the inverter. Figure 19 shows the output voltage of a three-phase full wave rectifier. The ideal capacitor would eliminate the value of the ripple, but in reality, there are no perfect capacitors. Figure 20 displays a typical three-phase rectifier using MOSFETs and with a DC-link capacitor.

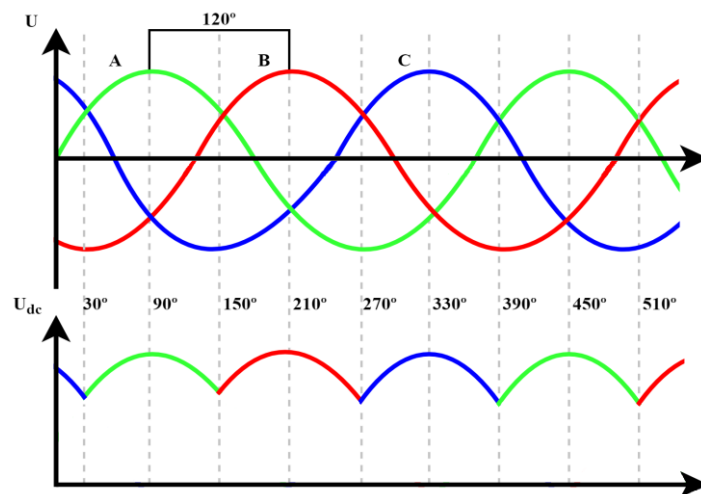


Figure 19 - Three-phase rectifier output waveforms

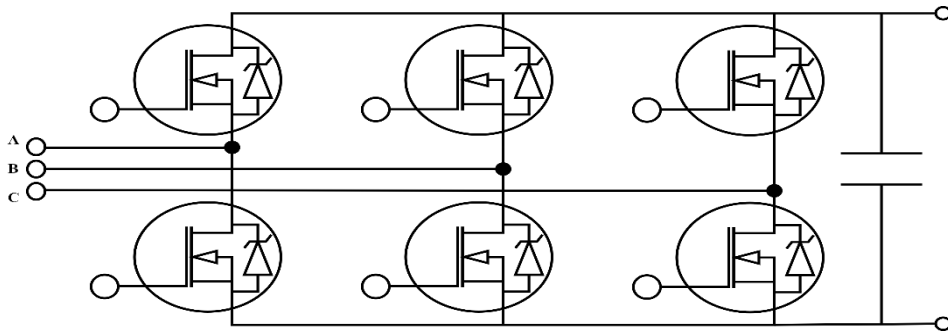


Figure 20 – Typical three-phase rectifier with DC-link capacitor

On the other hand, the inverter (or DC-AC converter), as the opposite of the previous converter previewed, is an electrical drive that converts the input voltage from direct current (DC) to alternating current (AC). Figure 21 illustrates an example of an output of a three-phase inverter (having each division 30 degrees, it can be observed the phase of 120 degrees from S1 to S3, from S3 to S2 and from S2 to S1), while Figure 22 displays a typical three-phase inverter using MOSFETs.

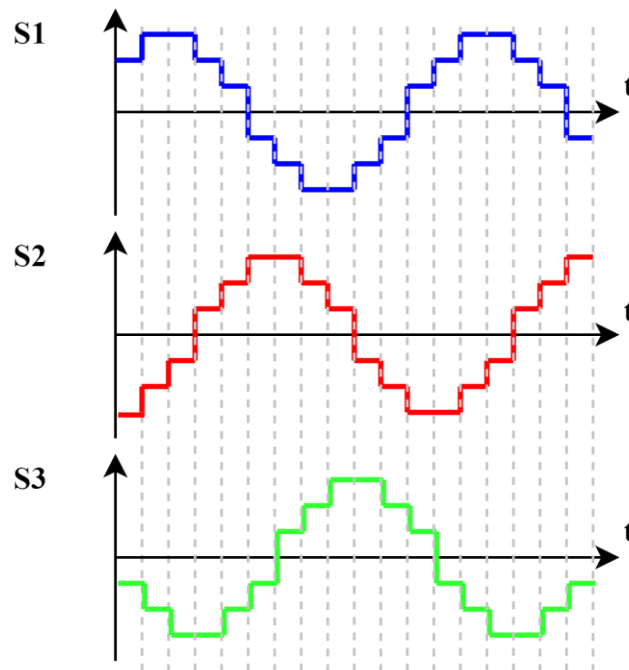


Figure 21 – Ideal single-phase MOSFET inverter simulation

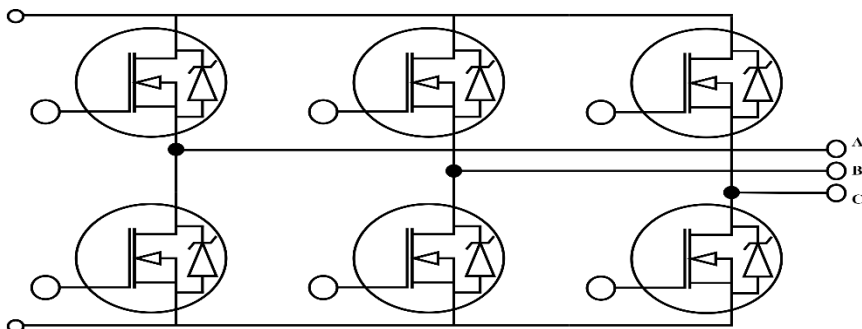


Figure 22 - Typical three-phase inverter using MOSFETs

To provide isolation between the back-to-back converter and the grid, a transformer is used due to its galvanic isolation provided. This electrical drive enables the transfer of electrical energy between circuits by electromagnetic induction. Galvanic isolation is a principle that prevents current flow between working circuits of an electric system. It is mostly used for safety reasons, but it can also be used to prevent ground loops, when circuits that communicate between themselves possess their respective grounds at a different potential from one another. Figure 23 represents a simple display of a transformer. For the purpose of this project, a transformer will be used to isolate the grid from the power electronics circuit. [24]

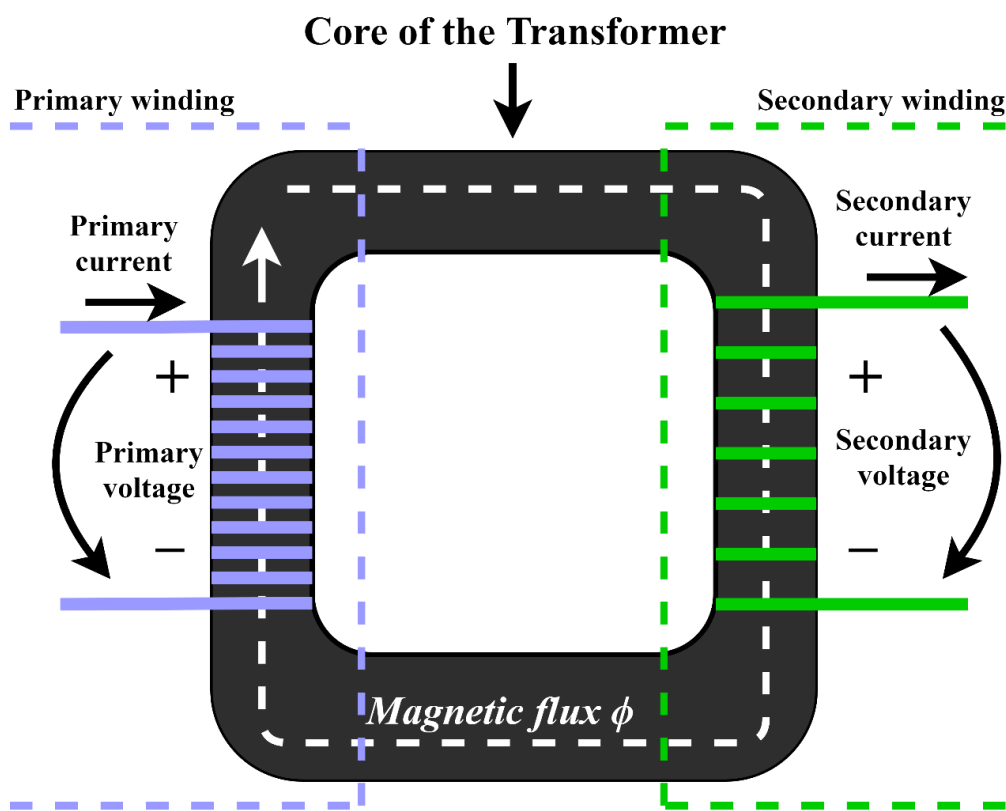


Figure 23 - Voltage and current windings of a transformer (Adapted [24])

3.3. Hardware components used for the control of the system

The hardware components used in the control of the system include the microcontroller used in the project, as well as the optocoupler used along it.

3.3.1. Microcontroller – Arduino

For the making of this project, the microcontroller used is the Arduino Mega2560, represented in figure 24. This microcontroller has several advantages, such as the possibility of using in different operating systems, the very simple and clear programming environment, and most importantly the software is published as open source tools.

This board is a microprocessor based on the ATmega1280, and it consists in 54 digital input/output pins, in which 14 can be used as PWM outputs, 16 analog inputs, 4 USARTs (Universal Synchronous/Asynchronous Receiver/Transmitter), a 16 MHz crystal, an ICSP (In-Circuit Serial Programming), USB (Universal Serial Bus) connection, etc. For this project, it is used three PWM outputs as well as one ADC pin. [25]



Figure 24 - Arduino Mega2560 ([25])

3.3.2. Optocoupler HCPL-3120

The Optocoupler operates by emission and reception of light, which allows to isolate the control part of the system from the power electronics part. Since the interface between them is made through a beam of light, there is no physical contact between both parts of the system. In this project, it is important the use of this component to make the voltage U_{gs} always higher than the voltage U_{Th} , and, as in the upper branch MOSFETs the voltage of the source is not known, Optocouplers are connected to the MOSFETs gates to ensure that the voltage of the gate is always higher than the source voltage and to prevent eventual short circuit. Figure 25 represents the internal schematic of the Optocoupler used in this project. [26]

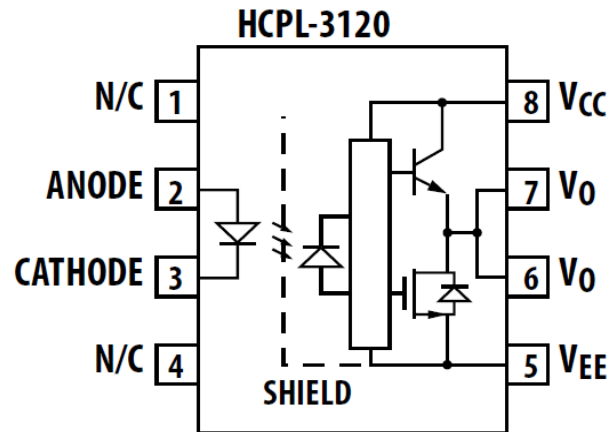


Figure 25 - Optocoupler HCPL-3120 schematic ([26])

3.4. Mathematical transformations required for modelling of the system

In this current section, it will be presented the mathematical transformations required for the modelling of the system. For modelling the DFIG, it is needed to fully understand some mathematical transformations as well as its working principles previously explained in this report.

The behaviour of these type of AC three-phase machine is normally described by their voltage, current and inductance equations. The coefficients of the different equations that describe them vary throughout time (except when the rotor is stationary) and that leads to a very complex modelling of the system, since the flux linkages as well as both voltages and currents change continuously. To simplify this complex analysis, mathematical transformations are used to reduce the complexity of these differential equations. For the purpose of this project, both the Clarke and Park transformations will be analysed and used in the modelling of this machine, and it will be very useful for the generation of the reference used in the control signal. These explanations are based in [27][28].

3.4.1. Clarke transformation ($\alpha\beta\gamma$ transformation)

The Clarke transformation converts balanced three-phase quantities represented by a three-phase reference frame into balanced two-phase quadrature quantities represented by a two-phase reference frame, while the Park transformation converts vectors in a balanced two-phase

orthogonal stationary system into an orthogonal rotating reference frame. All of the three reference frames are displayed in the figure 26, and their combination is displayed in figure 27.

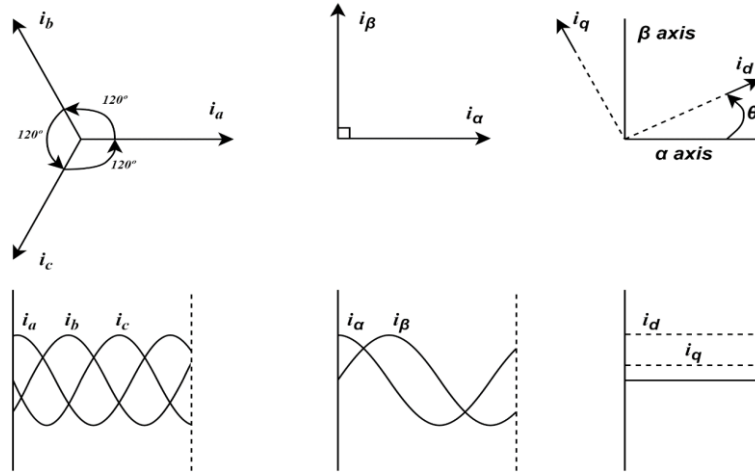


Figure 27 - Normal three-phase reference frame alongside the $\alpha\beta$ and the dq reference frames (Adapted [27])

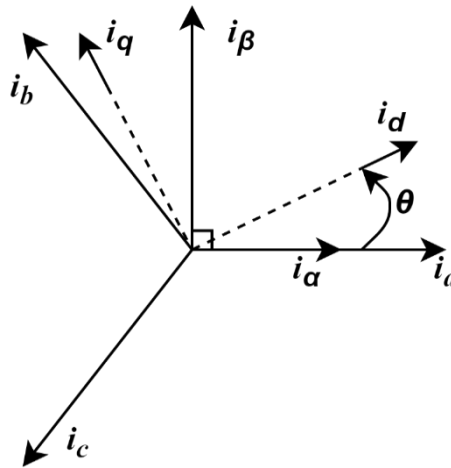


Figure 26 - All reference frames combined (Adapted [27])

As mentioned before with the Clarke transformation, the three-phase quantities are translated from the three-phase reference frame to the two-axis orthogonal stationary reference frame, and are represented as (19).

$$\begin{cases} i_\alpha = \frac{2}{3}i_a - \frac{1}{3}(i_b + i_c) & (19.a) \\ i_\beta = \frac{2}{\sqrt{3}}(i_b - i_c) = \frac{2}{3}\sqrt{3}(i_b - i_c) & (19.b) \\ i_\gamma = \frac{2}{3}(i_a + i_b + i_c) & (19.c) \end{cases}$$

The two-phase variables of this transformation are denoted as α and β and figure 28 displays the transformation to obtain their correspondent orthogonal stationary reference frame.

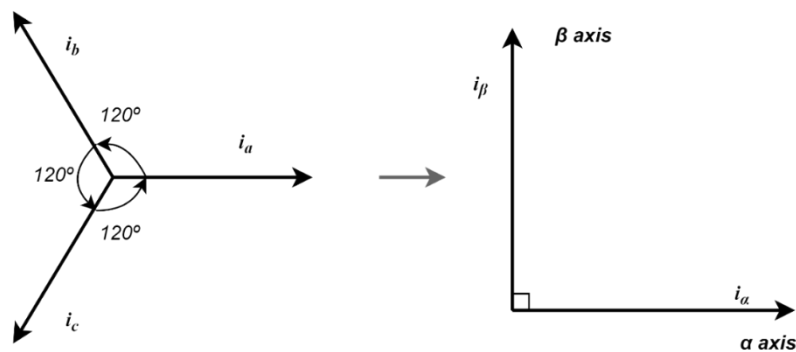


Figure 28 – Clarke transformation (Adapted [27])

For the purpose of this project, it is considered that the machine used has its internal connections between the rotor and the stator made by 3 wires, meaning it has no neutral phase. This translates to the homopolar component (γ) not being considered in the modelling of the machine.

3.4.2. Park Transformation (***dq0*** transformation)

As mentioned in the Clarke transformation, the Park transformation can be applied changing it from a $\alpha\beta\gamma$ system to a $dq0$ system, where 0 component is the same as in the $\alpha\beta\gamma$, which is irrelevant for the purpose of this project. The two-axis orthogonal stationary reference frame quantities, α and β , are transformed into rotating reference frame quantities, d and q , using Park transformation, as displayed in figure 29.

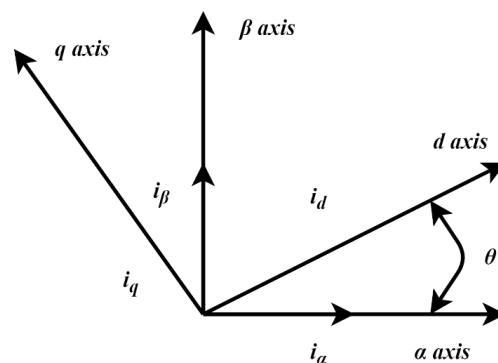


Figure 29 – Park transformation (Adapted [27])

After applying the Park transformation process, the equations (20) are obtained.

$$\begin{cases} i_d = i_\alpha * \cos \theta + i_\beta * \sin \theta & (20.a) \\ i_q = i_\beta * \cos \theta - i_\alpha * \sin \theta & (20.b) \end{cases}$$

3.4.3. Inverse Park and Clarke Transformations

Now that is was given the whole process that will be used to transform the input data obtained from the system into the control signal reference, it is also important to keep in mind how to do the opposite process.

The inverse Park transformation, which consists on the opposite process of transforming rotating reference frame quantities into a two-axis orthogonal stationary reference frame, is expressed as (21).

$$\begin{cases} i_\alpha = i_d * \cos \theta - i_q * \sin \theta & (21.a) \\ i_\beta = i_q * \cos \theta + i_d * \sin \theta & (21.b) \end{cases}$$

And lastly, the inverse Clarke transformation, which consists on the opposite process of transforming a two-axis orthogonal stationary reference frame into a three-phase stationary reference frame, is expressed as displayed below in (22).

$$\begin{cases} i_a = i_\alpha & (22.a) \\ i_b = -\frac{1}{2}i_\alpha + \frac{\sqrt{3}}{2}i_\beta & (22.b) \\ i_c = -\frac{1}{2}i_\alpha - \frac{\sqrt{3}}{2}i_\beta & (22.c) \end{cases}$$

Both Clarke and Park transformations are important to take into consideration when doing the modelling of the generator used in this project.

3.5. Modelling of the system

In order to determine how to design the control of the system, it is needed the modelling procedures for both the converters, RSC and GSC, respectively, as well as the DC-link capacitor. The content in this part of the chapter is based in [15], [27], [29] and [30].

3.5.1. Modelling for the RSC

In order to determine the control algorithm for the RSC it is necessary to analyse the modelling of an asynchronous machine. Its concept representation is displayed in figure 30. To understand the behaviour of this type of machine, its model in dq coordinates will be calculated and presented.

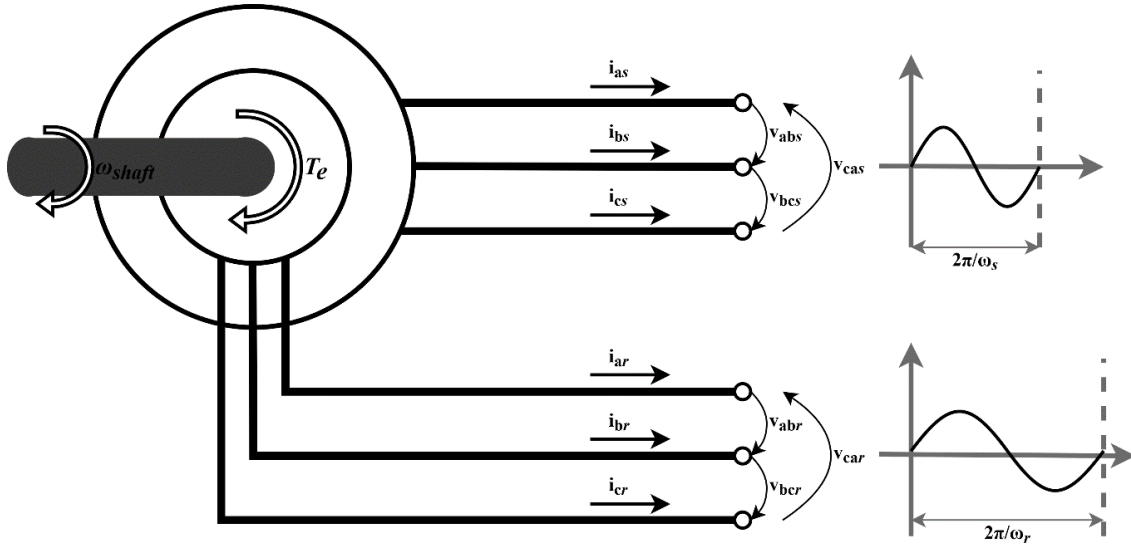


Figure 30 - Representation of concepts of the asynchronous machine (Adapted [29])

Having in mind both the Kirchhoff and Faraday laws, the phase voltages of the stator and the rotor are expressed by (23). When it comes to the flux linkage of both the stator and the rotor, they are represented by equations (26.1) and (26.2), respectively.

$$\begin{cases} u_{abcs} = R_s i_{abcs} + \frac{d}{dt} \phi_{abcs} \Leftrightarrow \begin{bmatrix} u_{as} \\ u_{bs} \\ u_{cs} \end{bmatrix} = R_s \begin{bmatrix} i_{as} \\ i_{bs} \\ i_{cs} \end{bmatrix} + \frac{d}{dt} \begin{bmatrix} \phi_{as} \\ \phi_{bs} \\ \phi_{cs} \end{bmatrix} & (23.a) \\ u_{abcr} = R_r i_{abcr} + \frac{d}{dt} \phi_{abcr} \Leftrightarrow \begin{bmatrix} u_{ar} \\ u_{br} \\ u_{cr} \end{bmatrix} = R_r \begin{bmatrix} i_{ar} \\ i_{br} \\ i_{cr} \end{bmatrix} + \frac{d}{dt} \begin{bmatrix} \phi_{ar} \\ \phi_{br} \\ \phi_{cr} \end{bmatrix} & (23.b) \end{cases}$$

$$\begin{cases} \phi_{abcs} = L_s i_{abcs} + L_m i_{abcr} \Leftrightarrow \begin{bmatrix} \phi_{as} \\ \phi_{bs} \\ \phi_{cs} \end{bmatrix} = L_s \begin{bmatrix} i_{as} \\ i_{bs} \\ i_{cs} \end{bmatrix} + L_m \begin{bmatrix} i_{ar} \\ i_{br} \\ i_{cr} \end{bmatrix} & (24.a) \\ \phi_{abcr} = L_r i_{abcr} + L_m^T i_{abcs} \Leftrightarrow \begin{bmatrix} \phi_{ar} \\ \phi_{br} \\ \phi_{cr} \end{bmatrix} = L_r \begin{bmatrix} i_{ar} \\ i_{br} \\ i_{cr} \end{bmatrix} + L_m^T \begin{bmatrix} i_{as} \\ i_{bs} \\ i_{cs} \end{bmatrix} & (24.b) \end{cases}$$

The relation between both the angular speed of the rotor and the stator, with the speed of the shaft can be given by the equation (25).

$$\omega_r = \omega_s + \omega_{shaft} \quad (25)$$

With (25) in mind, the slip in (13) can be rewritten as shown in the equation (26).

$$s = \frac{\omega_s + \omega_{shaft}}{\omega_s} \leftrightarrow s = \frac{\omega_r}{\omega_s} \quad (26)$$

As previewed shortly before in the section where the Clarke and Park transformations are analysed, the equations listed below are obtained after applying the transformations in both the three-phase voltage and current quantities of the system. The equations given by (27), represent the transformation applied from *abc* to *dq* coordinates of the voltages of the stator and rotor.

$$\begin{cases} u_{ds}(t) = u_{\alpha s}(t) \cos \theta_s(t) + u_{\beta s}(t) \sin \theta_s(t) & (27.a) \\ u_{qs}(t) = -u_{\alpha s}(t) \sin \theta_s(t) + u_{\beta s}(t) \cos \theta_s(t) & (27.b) \\ u_{dr}(t) = u_{\alpha r}(t) \cos \theta_r(t) + u_{\beta r}(t) \sin \theta_r(t) & (27.c) \\ u_{qr}(t) = -u_{\alpha r}(t) \sin \theta_r(t) + u_{\beta r}(t) \cos \theta_r(t) & (27.d) \end{cases}$$

In order to develop further, the values of the angular positions must be understood. $\theta_m(t)$ represents the angular position of the shaft and can be measured directly there, while $\theta_s(t)$ is the angular speed of the stator, given by the grid synchronizer. $\theta_r(t)$ is given by (28).

$$\theta_r(t) = \theta_s(t) - \frac{N_{poles} \theta_m(t)}{2} \quad (28)$$

One thing not mentioned so far in this analysis is the units that are used in the modelling of the DFIG. It is needed to work with the circuit quantities in either the rotor side or the stator side. It is very desirable to work with this procedure to avoid having to constantly use the turns ratio during the circuit calculation, so, for the purpose of this project, all rotor quantities will be referred to the stator to simplify the circuit analysis. This procedure is represented in equations (29).

$$\left\{ \begin{array}{l} i'_{dr}(t) = n_{rs} i_{dr}(t) \\ i'_{qr}(t) = n_{rs} i_{qr}(t) \\ u'_{dr}(t) = \frac{1}{n_{rs}} u_{dr}(t) \\ u'_{qr}(t) = \frac{1}{n_{rs}} u_{qr}(t) \\ \phi'_{dr}(t) = \frac{1}{n_{rs}} \phi_{dr}(t) \\ \phi'_{qr}(t) = \frac{1}{n_{rs}} \phi_{qr}(t) \\ R'_r = \frac{1}{n_{rs}^2} R_r \\ L'_r = \frac{1}{n_{rs}^2} L_r \end{array} \right. \quad \begin{array}{l} (29.a) \\ (29.b) \\ (29.c) \\ (29.d) \\ (29.e) \\ (29.f) \\ (29.g) \\ (29.h) \end{array}$$

Solving the equations represented on (27), both (30) and (31) are obtained. (30) represents the voltages of the stator in dq coordinates while (31) represents the rotor voltages referred to the stator. (32) represents the stator flux, while (33) represents the rotor flux referred to the stator. On (34) is displayed the electromagnetic torque. These equations represent the diagram of the model of the asynchronous machine in dq coordinates represented in figure 31.

$$\left\{ \begin{array}{l} u_{ds}(t) = R_s i_{ds}(t) - \omega_s \phi_{qs}(t) + \frac{d}{dt} \phi_{ds}(t) \\ u_{qs}(t) = R_s i_{qs}(t) + \omega_s \phi_{ds}(t) + \frac{d}{dt} \phi_{qs}(t) \end{array} \right. \quad \begin{array}{l} (30.a) \\ (30.b) \end{array}$$

$$\left\{ \begin{array}{l} u'_{dr}(t) = R'_r i'_{dr}(t) - (\omega_s - \omega_{shaft}) \phi'_{qr}(t) + \frac{d}{dt} \phi'_{dr}(t) \\ u'_{qr}(t) = R'_r i'_{qr}(t) + (\omega_s - \omega_{shaft}) \phi'_{dr}(t) + \frac{d}{dt} \phi'_{qr}(t) \end{array} \right. \quad \begin{array}{l} (31.a) \\ (31.b) \end{array}$$

$$\left\{ \begin{array}{l} \phi_{ds}(t) = (L_s + L_m) i_{ds}(t) + L_m i'_{dr}(t) \\ \phi_{qs}(t) = (L_s + L_m) i_{qs}(t) + L_m i'_{qr}(t) \end{array} \right. \quad \begin{array}{l} (32.a) \\ (32.b) \end{array}$$

$$\left\{ \begin{array}{l} \phi'_{dr}(t) = (L'_r + L_m) i'_{dr}(t) + L_m i_{ds}(t) \\ \phi'_{qr}(t) = (L'_r + L_m) i'_{qr}(t) + L_m i_{qs}(t) \end{array} \right. \quad \begin{array}{l} (33.a) \\ (33.b) \end{array}$$

$$T_e(t) = \frac{3}{2} N_p L_m (i_{qs}(t) i'_{dr}(t) - i_{ds}(t) i'_{qr}(t)) \quad (34)$$

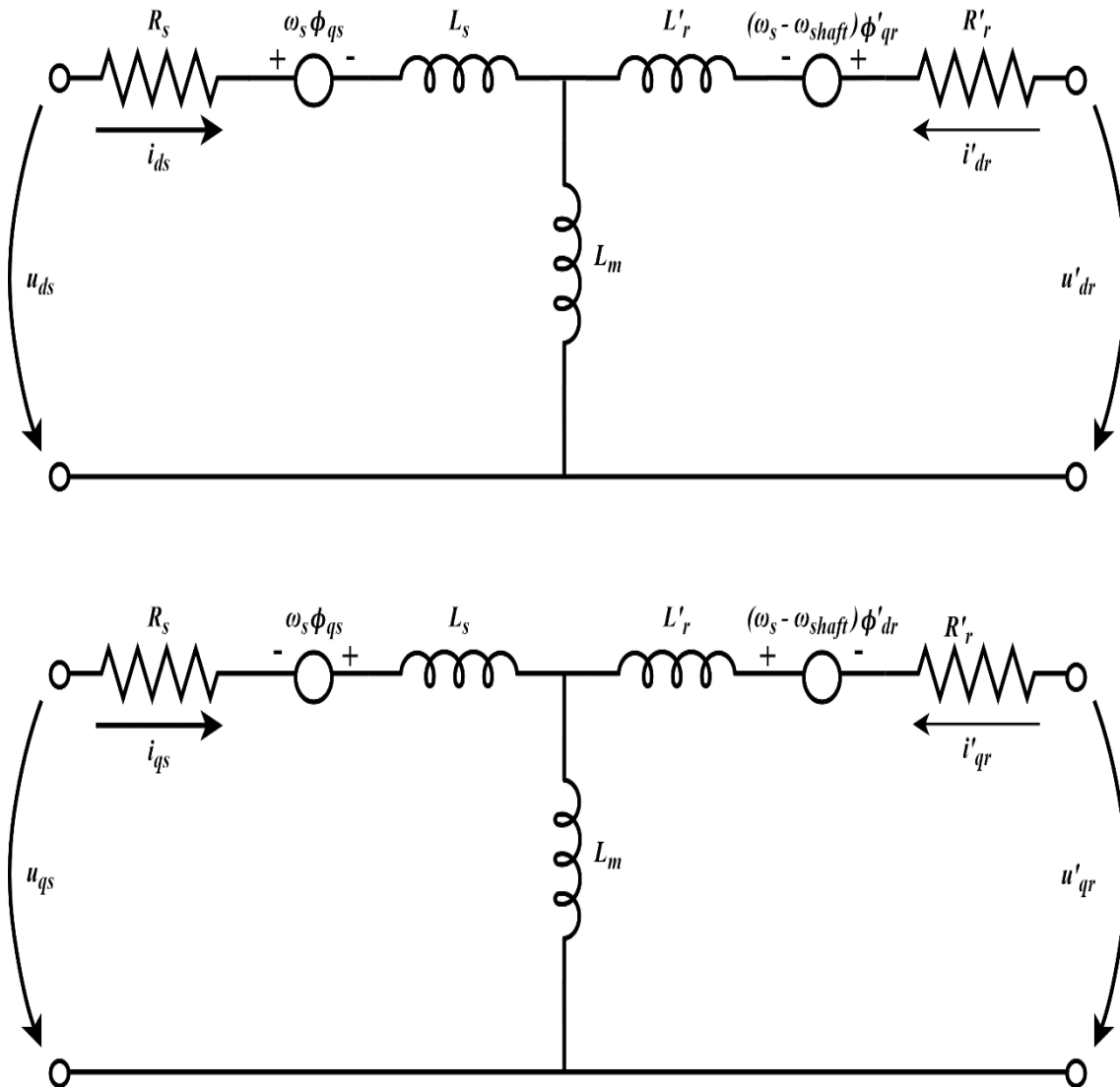


Figure 31 - Model of the asynchronous machine in dq coordinates referred to the stator (Adapted [27])

All of the equations mentioned throughout this section are important to develop and organize the control algorithm needed to generate the control signals that will be used for the RSC.

3.5.2. Modelling for the DC-link section

Normally the DC part of a back-to-back converter is called as DC-link. The display of the DC-link system can be displayed in figure 32. Equation (35) indicates how to calculate the u_{dc} voltage and equation (36) indicates how to calculate the i_{dc} current.

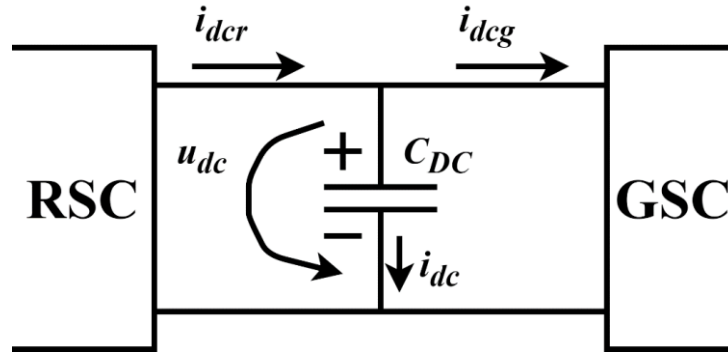


Figure 32 - Display of the DC-link system in the back-to-back converter (Adapted [15])

$$u_{dc}(t) = \frac{1}{C_{DC}} \int i_{dc} dt \quad (35)$$

$$i_{dc} = i_{dcr} - i_{dcg} \quad (36)$$

This DC-link modelling will be important when determining the control algorithm necessary for the GSC.

3.5.3. Modelling for the GSC

When it comes to the GSC, some other parts of the system to keep in mind when doing the modelling are both the grid and the RL filter used. Equations (37) represent how to calculate the output voltages of the RSC.

$$\begin{cases} u_{af}(t) = R_f i_{ag}(t) + L_f \frac{di_{ag}(t)}{dt} + u_{ag}(t) \end{cases} \quad (37.a)$$

$$\begin{cases} u_{bf}(t) = R_f i_{bg}(t) + L_f \frac{di_{bg}(t)}{dt} + u_{bg}(t) \end{cases} \quad (37.b)$$

$$\begin{cases} u_{cf}(t) = R_f i_{cg}(t) + L_f \frac{di_{cg}(t)}{dt} + u_{cg}(t) \end{cases} \quad (37.c)$$

Applying the transformations to (37), the voltages required by the grid are given by (38) in dq coordinates. Based on (38), figure 33 displays the model of the grid in dq coordinates.

$$\begin{cases} u_{df}(t) = R_f i_{dg}(t) + L_f \frac{di_{dg}(t)}{dt} + u_{dg} - \omega_a L_f i_{qg} & (38.a) \\ u_{qf}(t) = R_f i_{qg}(t) + L_f \frac{di_{qg}(t)}{dt} + u_{qg} + \omega_a L_f i_{dg} & (38.b) \end{cases}$$

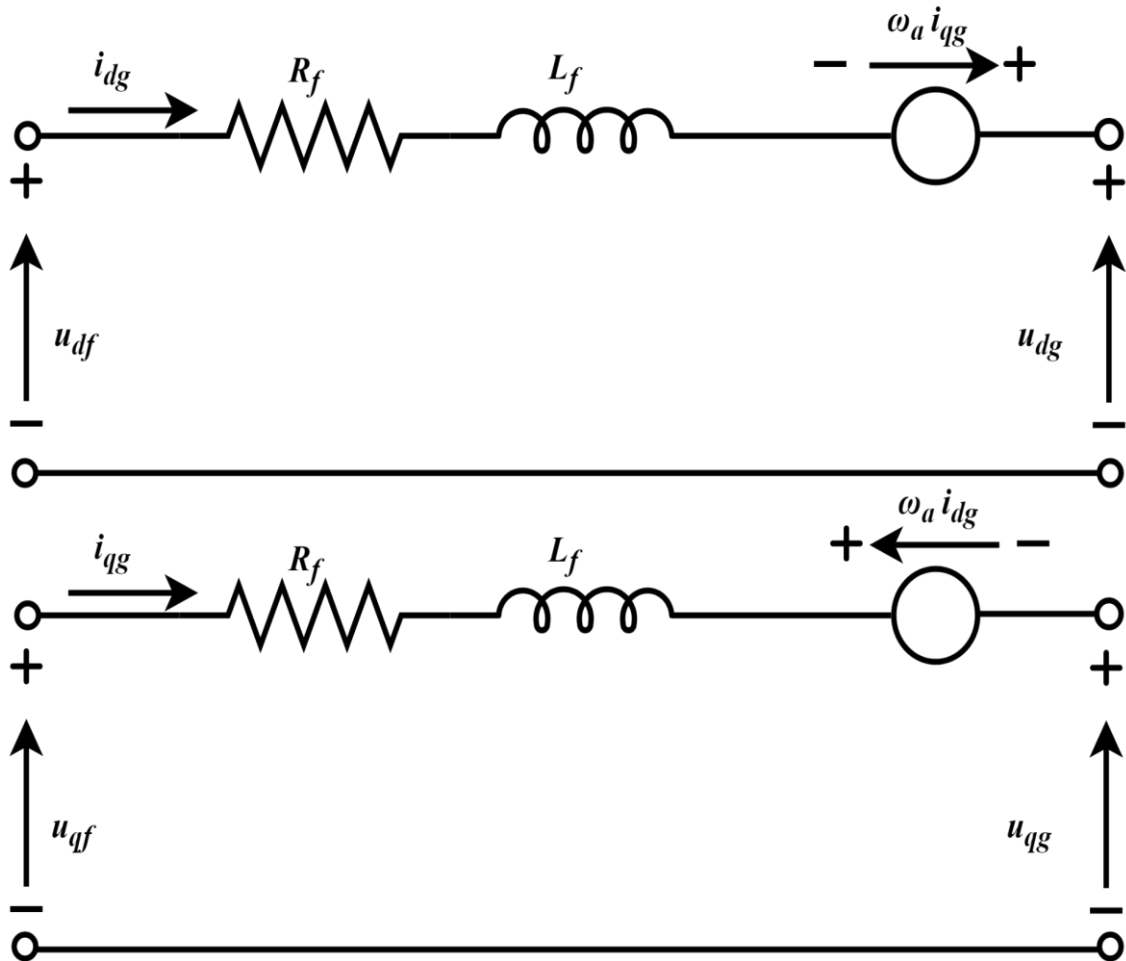


Figure 33 - Model of the grid in dq coordinates (Adapted [15])

With all of this needed theory previewed about the back-to-back converter, the control algorithms can be designed and implemented.

3.6. Control algorithms

Going into detail in regards to the control algorithm used in this project, its general overview is present below in figure 34 (without showing the transformer).

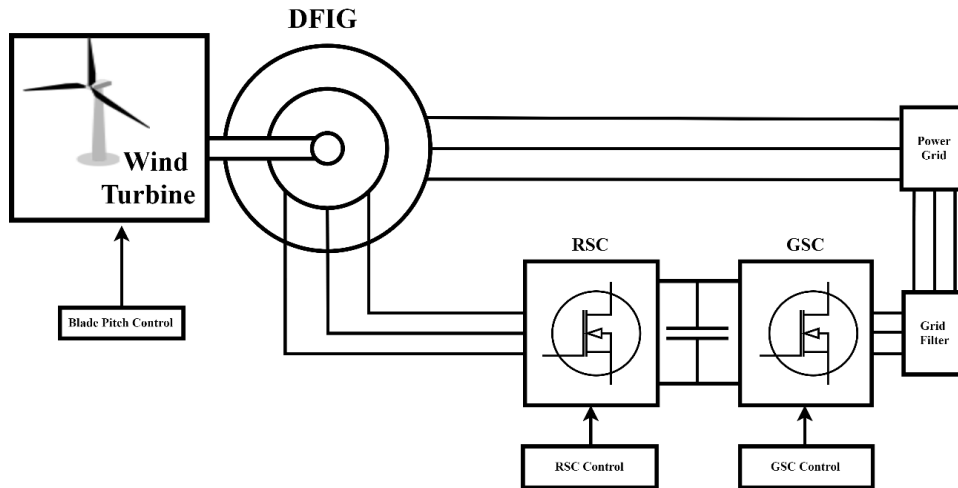


Figure 34 - Simple control schematic of a WTGS

In control systems involving the use of active and reactive power control in generators, it is important to understand the concept of coupling and decoupling of active and reactive powers. A form of coupling is the existence of interactions between the inputs and outputs of a MIMO system (multiple-input and multiple-output) which impacts the several control variables and affects the desired output of the given system. This leads to having difficulty in properly controlling a given system, that is why it is necessary to decouple it. Decoupling can be achieved by using different methods, but for the purpose of this project the strategy used was the use of vector control, using as well feed-forward controllers. A control system with a feed-forward type of control reacts to its predefined way without responding on how the load reacts. In this type of system, the control variables are not error-based. It is based instead on the knowledge from the mathematical model of the process as well as knowledge or measurements of the project disturbances. [31]

3.6.1. Control algorithm of the RSC

The first section analysed of the control algorithms will be the one used for the RSC. Figure 35 displays the control method used in regards to the RSC. It contains the representation of the machine used, as well the RSC and the power grid. For the purpose of this project and since it will be taken into consideration the fact that the power involved is relatively low and it is impossible to simulate the wind turbine module in the conditions taken, the generator used can be either supplied by another machine working as a motor or through the power grid, and its supply in the figure is considered as the power grid for simplicity purposes.

In order to determine the angle that represents the angular position of the rotor, $\theta_r(t)$, it is needed to measure the angular position of the rotor shaft, $\theta_m(t)$, and transform it as shown in the graphic displayed on the top right corner, which is also highlighted in the control schematic. Ideally, the better option would be to use a PLL instead for this part, but this method used, despite not being so efficient, works as well for its purpose. It is possible also to observe the abc to dq transformation and vice-versa, as well as the PI controllers and the respective gains used along the schematic, which will help to determine the several reference signals needed alongside the whole control process implemented for the RSC.

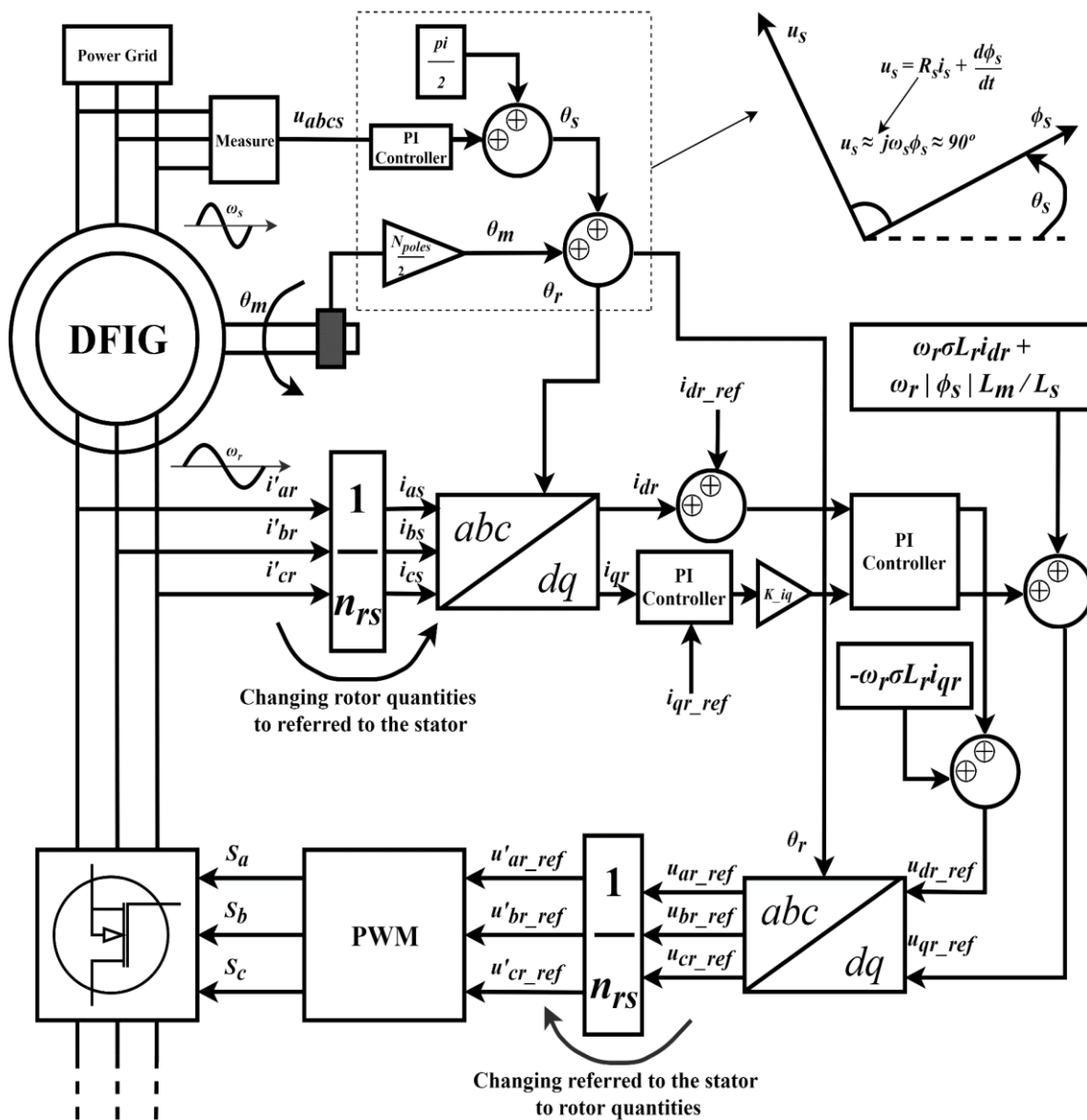


Figure 35 - Schematic of the RSC control algorithm (Adapted [29])

As mentioned before in this report about the coupling and decoupling of active and reactive powers, it is necessary to have the sum blocks before the dq to abc transformation in order to cancel this effect and to correctly generate the control signal. Also, in regards to the units of the control signal, it is very important to handle carefully the respective units in the circuit as it is desired to convert the quantities measured in the rotor as quantities as referred to the stator, so that during the control circuit it is not needed to convert every time a calculation is necessary. However, it is needed to convert them back to rotor quantities before generating the three PWM signals that will implement the control of the RSC.

This control schematic is based on the models presented previously, and also adapted from [24]. This decision is based on the principle that the main goal of this project is to have the system functioning correctly and not to do a deep analysis on all of the factors and equations relevant to the design of this control algorithm. The implementation of this algorithm as well as the gains used will be previewed in the next chapter of this report.

3.6.2. Control algorithm of the GSC

The control part regarding the GSC contains the DC-link and the GSC. Although not shown in the control figure, it also has a filter, which connect the grid with each phase of the GSC, and is composed of at three inductances and three resistors, but depending on the filter requirement, it can have more components such as capacitors or even higher values for the inductances used if it requires a higher filter. Also, the connection between the GSC and the grid is made by means of a transformer. For the purpose of this project it is not taken into consideration any effect the impedances from either the transformer or the grid. And also, it is assumed that the AC voltage from the transformer is under normal operation conditions. All of this is done in order to simplify the theory used in this already complex system.

Figure 36 gives a detailed explanation about the procedures for the GSC control. Measuring the voltage from the DC-link, U_{bus} , having the reference voltage from the DC-link from equations (35) and (36), and also by having both the voltages and the currents of the GSC, U_{abcg} and i_{abcg} , it is possible to generate the three PWM signals, s_{abcg} , that will control the converter. It is also included the PI controllers needed as well as the sum block necessary to cancel the coupling and decoupling

Chapter 4 – Simulations using Computer Programs

All of the simulations done with regards to this project will be previewed and documented in this chapter. Using MATLAB-Simulink program, all of the content of the previous chapter will be implemented in four different stages, each of which simulated and analysed in order to have a better understanding of each part that integrates the system.

The first simulation is done to test the working principles of the machine used, and it incorporates the DFIG with the RSC (composed of ideal MOSFETs and connected with a DC link capacitor on the other side) and its respective control, being the supply for the generator a three-phase voltage source. The second simulation comes in as a steady state analysis of the machine, being possible to better understand its behaviour. Third simulation brings to the system the implementation of the wind turbine module as well as showing the MPPT algorithm used. The fourth and last simulation incorporates the GSC and its respective control in the project of the previous simulation, providing an all-rounded analysis of the complete system.

These simulations are done in order to fully understand the behaviour of the whole system. Also, all of the protection procedures and circuits are ignored during the simulations as mentioned before, because the computer program used allows the system to be run at specific conditions, which would be impossible to have in a real system without any kind of protection. So, in order to simplify the system as much as possible, this was taken advantage of during these simulations.

Everything in this chapter, from the control algorithm implemented as well as the strategies used throughout the control schematics are based on the references [15], [30], [32] and [33].

4.1. Simulation of machine working principles

The goal of this simulation is to demonstrate the working principles of the machine. After implementing a system with the machine, its behaviour will be analysed for different values of the speed reference

In order to do the first simulation where the machine working principles are verified it is needed to develop the basic system with the DFIG machine and the RSC using MATLAB Simulink, along with other relevant blocks to help with measurements.

Taking a look at figure 37, it is possible to observe that the asynchronous machine has the mechanical input by means of electromagnetic torque. Also, its stator is directly connected to the grid, which is not how it should be in theory (and is also impractical to do), but since this simulation is very complex, it was chosen this way to make this machine start-up part simpler. As a result of this choice, there will be a lot of noise and perturbations in the start-up of the system, but once it reaches the steady-state it will work as intended, despite still having some perturbations. Lastly, there are also represented the RSC, the DC link capacitor, and several other blocks used for important measurements of several variables from the system.

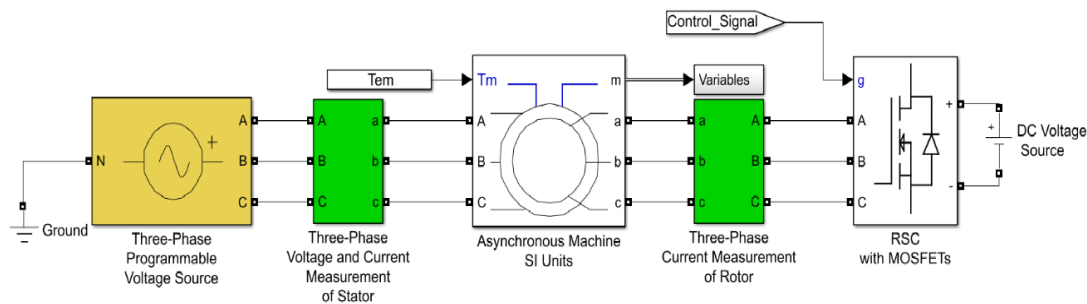


Figure 37 - System developed in MATLAB Simulink for testing the machine working principles

Table 1 identifies all the parameters of the Asynchronous Machine used for this project, as well as other relevant parameters, with their respective identification and values. Some attention was needed for the values of these parameters, since they could not just be created out of nothing, for fear of not being able to estimate or explain the results obtained, nor could they be straight up copied from the references, since the results would be the same thus turning this project rather useless, not to mention the copyright infringement. So, some the parameters used, like L_s and L_r , were set by default when creating the block in MatLab, while others, like L_s and L_r , were determined based on the strategies used in the references but with the values already established by default. Doing so, it was avoided having to calculate all the parameters necessary after estimating one or more of them.

Table 1 - Simulink program data parameters

Parameter (Program Variable name)	Value (Unit)
Frequency (f)	50 (Hz)
Rated Stator Power (Ps)	40000 (W)
Rated rotational speed (n)	1500 (rpm)
Rated Stator line-to-line Voltage (Us)	400 (V)
Rated Torque of the machine (Tem)	250 (N.m)
Pole Pairs of the machine (p)	2
Stator/Rotor turns ratio (ratio)	$\frac{1}{3}$
Rated Rotor Voltage (Ur)	1200 (V)
Maximum Slip (smax)	$\frac{1}{3}$
Rated Rotor Voltage referred to the stator (Ur_stator)	$U_r * s_{max} * ratio$ (V)
Stator Resistance (Rs)	0.5968 (Ω)
Leakage Inductance (Lsi)	0.00087 (H)
Magnetizing Inductance (Lm)	0.0354 (H)
Rotor Resistance referred to the stator (Rr)	0.6258 (Ω)
Stator Inductance (Ls)	$L_{si} + L_m$ (H)
Rotor Inductance (Lr)	$L_{si} + L_m$ (H)
DC Bus Voltage referred to the stator (Ubus)	$U_{r_stator} * \sqrt{2}$ (V)
Electrical Conductivity (sigma)	$\sigma = 1 - \left(\frac{L_m^2}{L_r L_s}\right)$ (S/m)
Stator Flux (Fs)	$\frac{U_s * \sqrt{3}}{2 * \pi * f}$ (Wb)
Inertia of the machine (J)	0.05 (kg.m ²)
Friction damping factor of the machine (D)	$1 * 10^{-3}$ (N.m.s)

PWM switching frequency (fswitch)	$4 * 10^4$ (s)
Sampling time (Ts)	$\frac{1}{f_{switch}} * 50$ (s)

Based on the references, table 2 indicates all of the variables used to determine the gains used in this respective simulation.

Table 2 - Gains used for the RSC system

Gain	Expression
tau_i	$\frac{\sigma * L_r}{R_r}$
tau_n	0.05
wni	$100 * \frac{1}{tau_i}$
wnn	$\frac{1}{tau_n}$
kp_id	$(2 * wni * \sigma * L_r) - R_r$
kp_iq	kp_{id}
ki_id	$wni^2 * \sigma * L_r$
ki_iq	ki_{id}
ki_n	$\frac{wnn^2 * J}{p}$
kp_n	$\frac{2 * wnn * J}{p}$
k_iq	$\frac{1}{-\frac{3}{2} * p * \frac{Lm}{Ls} * \phi_s}$
k_bus	$\frac{1}{U_{bus} * \frac{1}{2}}$

The control circuit developed in this simulation that is represented in Figure 38 was based on the control algorithm presented in Figure 35. There are two input variables, i_d_ref and $speed_ref$ which are initialized in the start-up parameter program with the values 0 and πf . The value of i_d_ref is chosen as this because the generator is being magnetized through the stator, which means that the value of i_d is always 0. The value of $speed_ref$ represents the synchronous speed of the asynchronous machine, and it is the main value to take into consideration to fully understand the working principles as intended in this simulation. Its value will be changed throughout the simulation and it will be explained in detail during the results analysis. The other input variables needed, $omega_m$, I_r , U_s , and $teta$ represent, the mechanical speed, the rotor current, the stator voltage measured, the $teta$ angle of the stator, respectively, being $teta$ measured in the system in Figure 39. The value of the stator voltage, rotor current are measured in the green blocks. The use of Zero-Order Holders for these variables is to make the system work as close to the reality as possible.

The Angle block displayed in Figure 39 is highlighted in the control algorithm of Figure 35, where it is possible to see as well the graphic for a better understanding of this calculation that was implemented. This value is after used to determine the real value of the i_{dr} and the i_{qr} .

In Figure 40, 41, 42 and 43 it is possible to see the implementation of the normal and inverse Park and Clarke transformations, having in mind the understanding and analysis done in the previous chapter.

The control block to convert the speed reference to the torque reference intended to perform the PI controller of the i_q variable is represented in Figure 44 as the typical PI controller block used in this project. The gains used for the controller are k_{p_n} and k_{i_n} , for $k1$ and $k2$, respectively. Following this block, it is necessary to convert the torque into the i_q_ref , so the following gain k_{i_q} must be applied.

The references and measurements of i_d and i_q currents are already obtained so it is applied PI controller blocks to them, being $k1$ and $k2$ in the two controllers taken as k_{p_id} and k_{i_id} for the i_d PI block, and k_{p_iq} and k_{i_iq} for the i_q PI block. After this, the cancelation of the coupling terms is added before taking the reverse transformations, and a gain is also added, k_{bus} in order to make the PWM signal generate signals between 0 and 1.

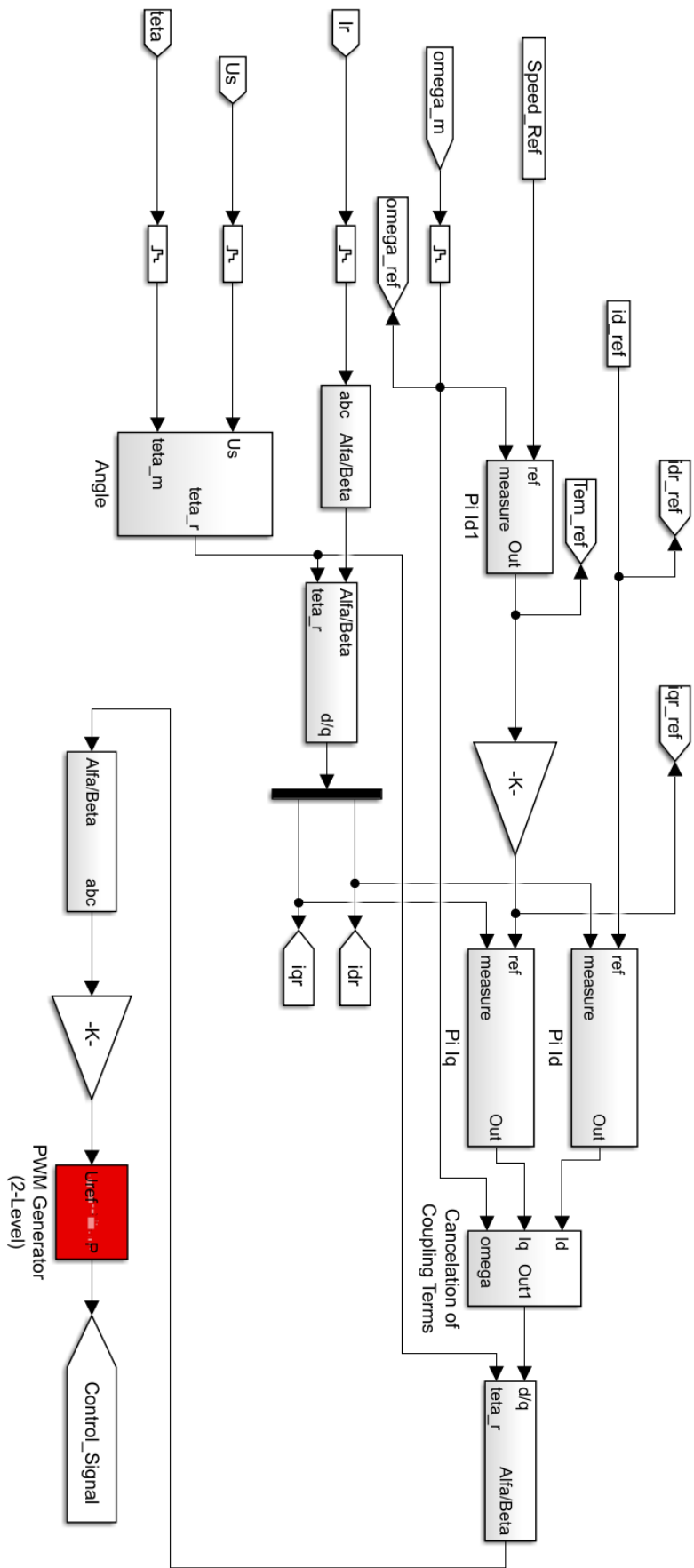


Figure 38 - Control circuit of the RSC

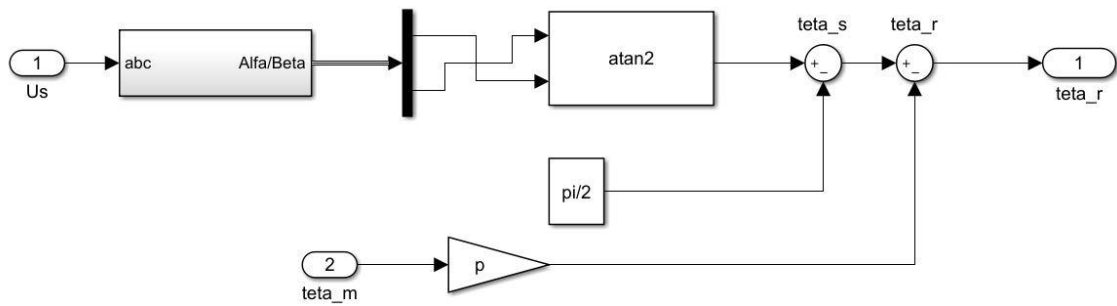


Figure 39 – Control block of the calculation of the teta angle of the rotor

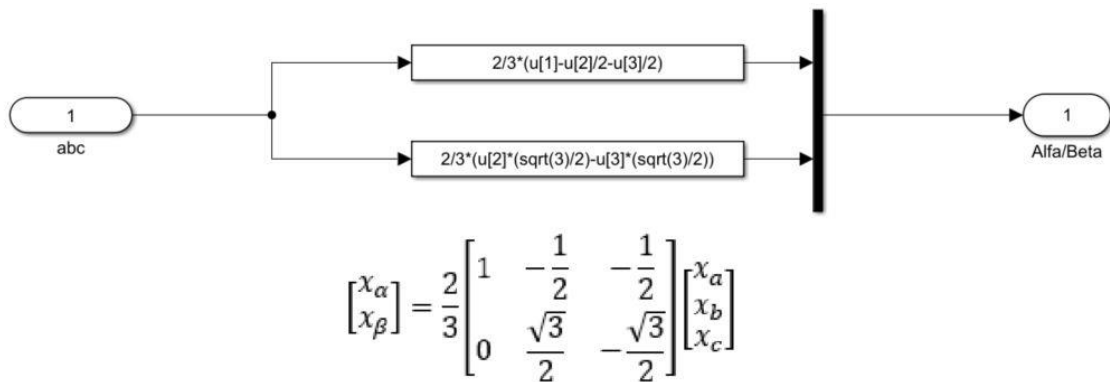


Figure 40 – Clarke transformation control block

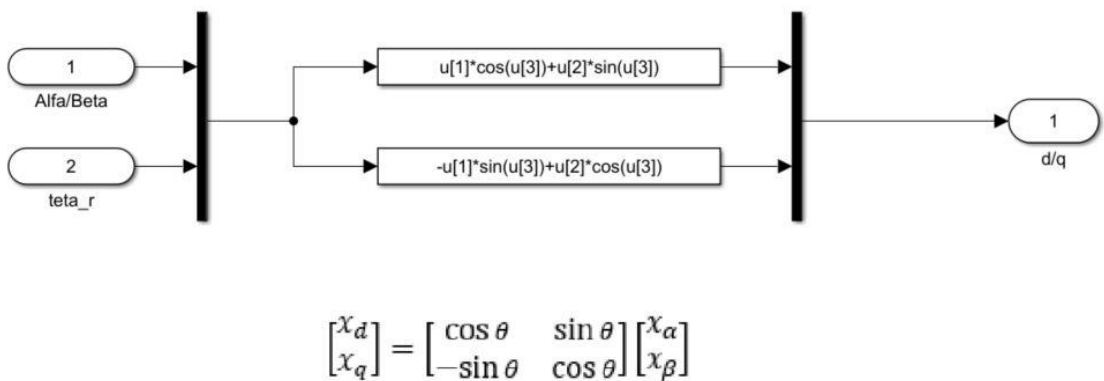
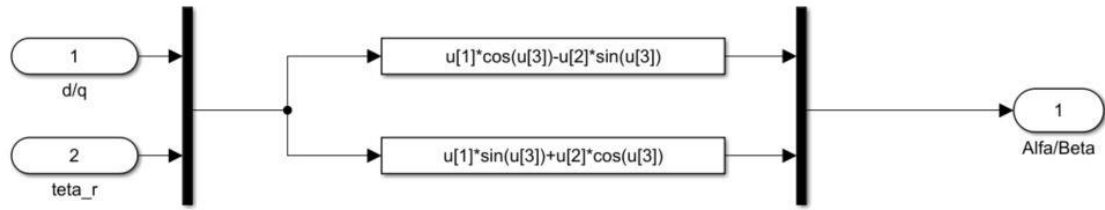
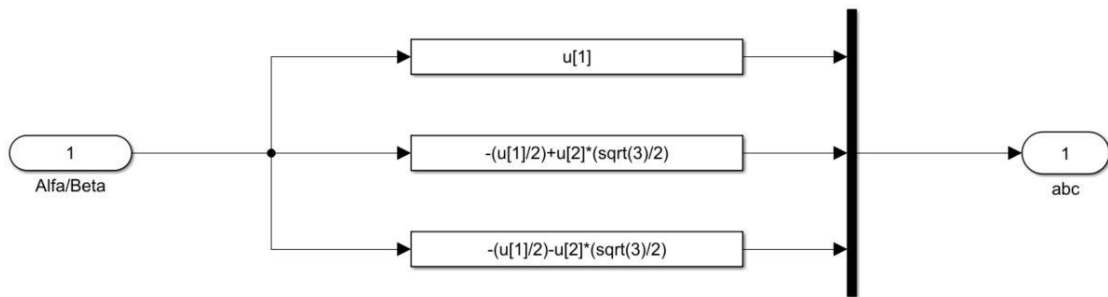


Figure 41 – Park transformation control block



$$\begin{bmatrix} x_\alpha \\ x_\beta \end{bmatrix} = \begin{bmatrix} \cos \theta & -\sin \theta \\ \sin \theta & \cos \theta \end{bmatrix} \begin{bmatrix} x_d \\ x_q \end{bmatrix}$$

Figure 42 - Inverse Park transformation control block



$$\begin{bmatrix} x_a \\ x_b \\ x_c \end{bmatrix} = \begin{bmatrix} 1 & -\frac{1}{2} & -\frac{1}{2} \\ 0 & \frac{\sqrt{3}}{2} & -\frac{\sqrt{3}}{2} \end{bmatrix} \begin{bmatrix} x_\alpha \\ x_\beta \end{bmatrix}$$

Figure 43 - Inverse Clarke transformation control block

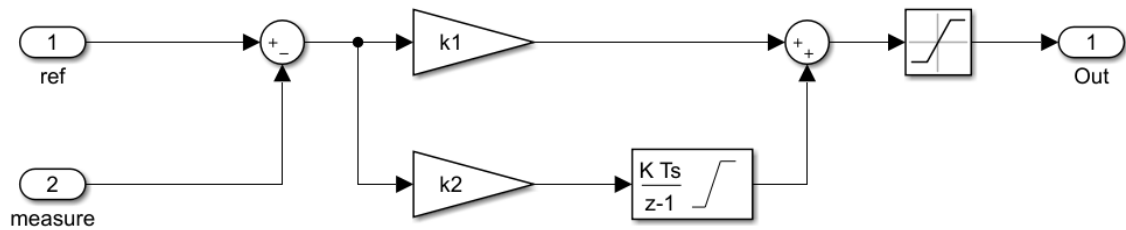


Figure 44 - Standard PI control block used in system

Figure 45 represents the active and reactive power decoupling, where it is made the vector control as shortly described in the previous chapter. It follows the control schematic of figure 35.

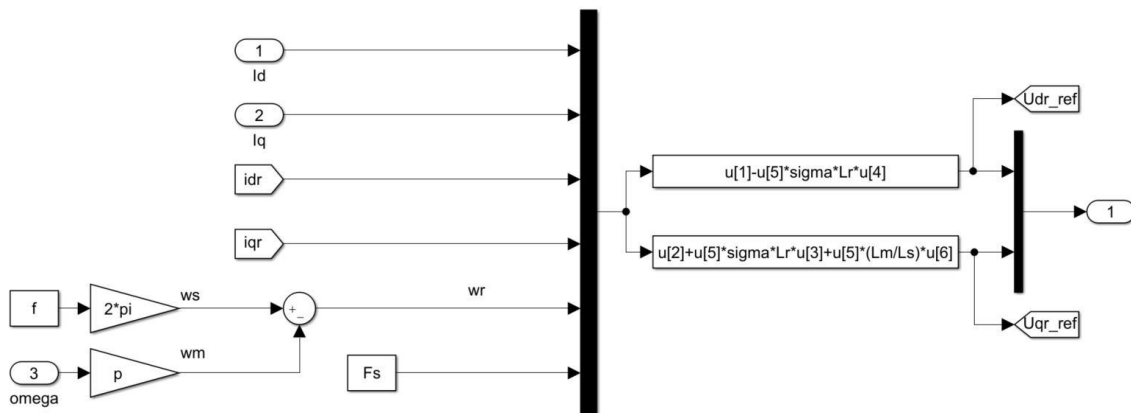


Figure 45 - Control block of active and reactive powers decoupling of the RSC

There are a couple of parameters measured in the machine that are needed for the control circuit, more specifically the rotor angle, the rotor speed and the electromagnetic torque, and they are represented in Figure 46 below.

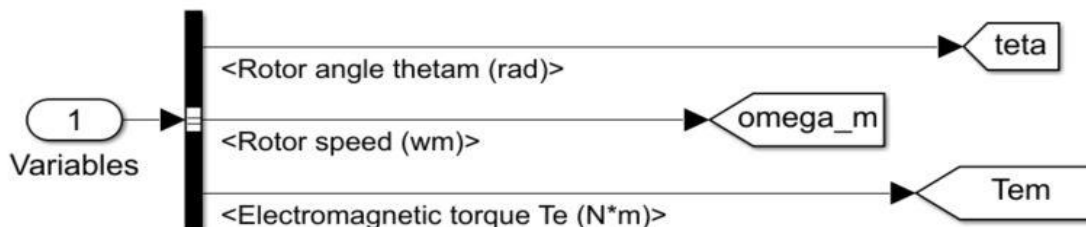


Figure 46 - Machine measured variables

With the help of a scope to monitor the variables necessary to understand this simulation, it is possible to test and observe how the machine behaves in sub-synchronous, synchronous and hyper-synchronous speeds for both motor and generator operations. For the graphics that were obtained in the section of this report, it was showcased the start-up of the system to be possible to understand what was mentioned before about why it is ignored throughout the experiment.

Figures 47 and 48 represent the machine working in sub-synchronous speed, as a motor and as a generator, respectively, with ninety per cent of synchronous speed and with twenty-five per cent of the rated torque as input. The beginning of this simulation is ignored for analysis purposes, as it will have strong perturbations due to the fact that all the start-up procedures have been ignored, so the values are analysed after the system reaches the steady state.

Since in this control method the reference value of the i_{dr} variable is 0, meaning its value will not vary, it was only considered for the scope the reference and real speed values, as well as both reference and real torque, the i_{dr} value, which changes with the input torque, and lastly the rotor currents, which change depending on the operation mode based on the speed of the machine. It is possible to observe each value in the figure below, in where the yellow line in both speed and torque graphic represent the reference value while the blue line represents the real value. In this operation mode, the stator is producing power but a part of it is fed back to the rotor. Also, one last thing to keep in mind about this figure is the rotor current phases (dark blue line followed by orange and light blue lines, respectively, which represent abc phases) to compare with the hyper-synchronous rotor current phases in the analysis.

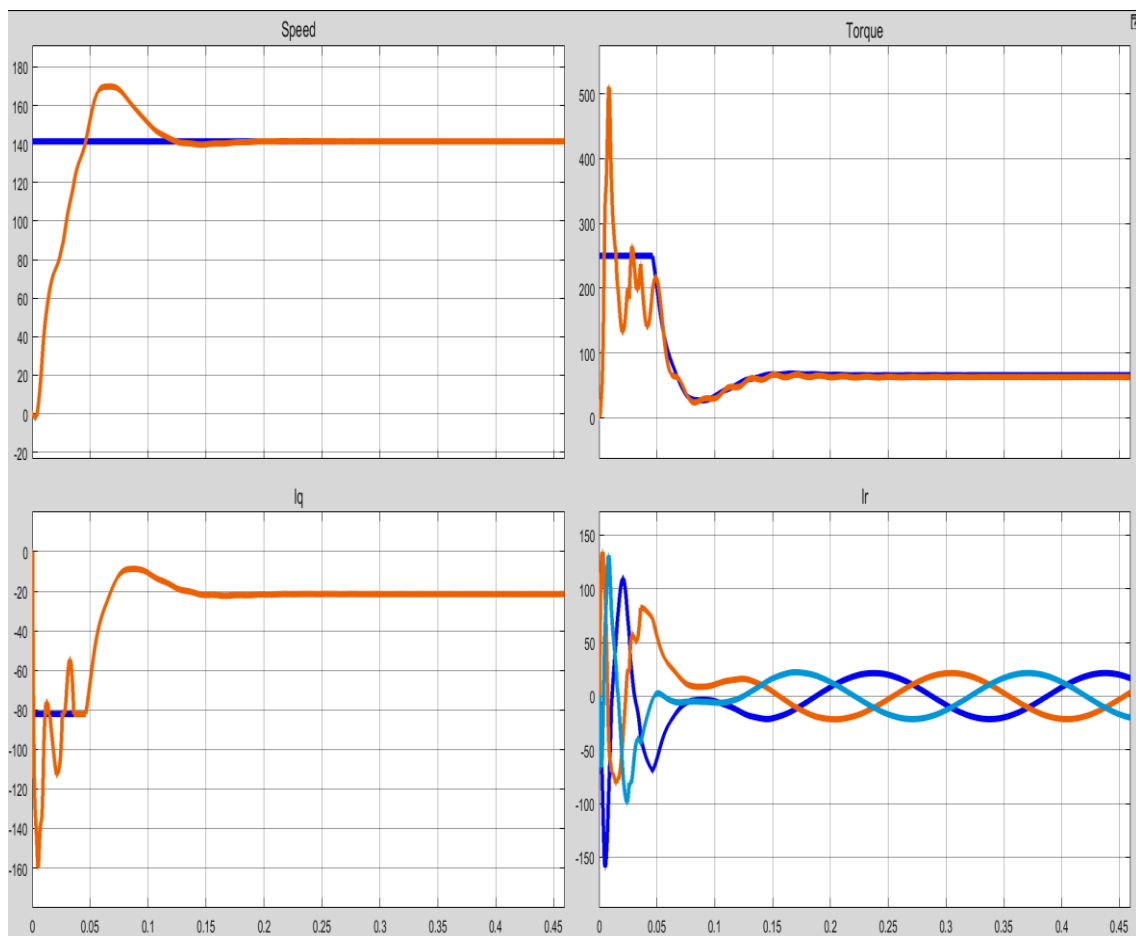


Figure 47 – Machine operating as a motor at sub-synchronous speed

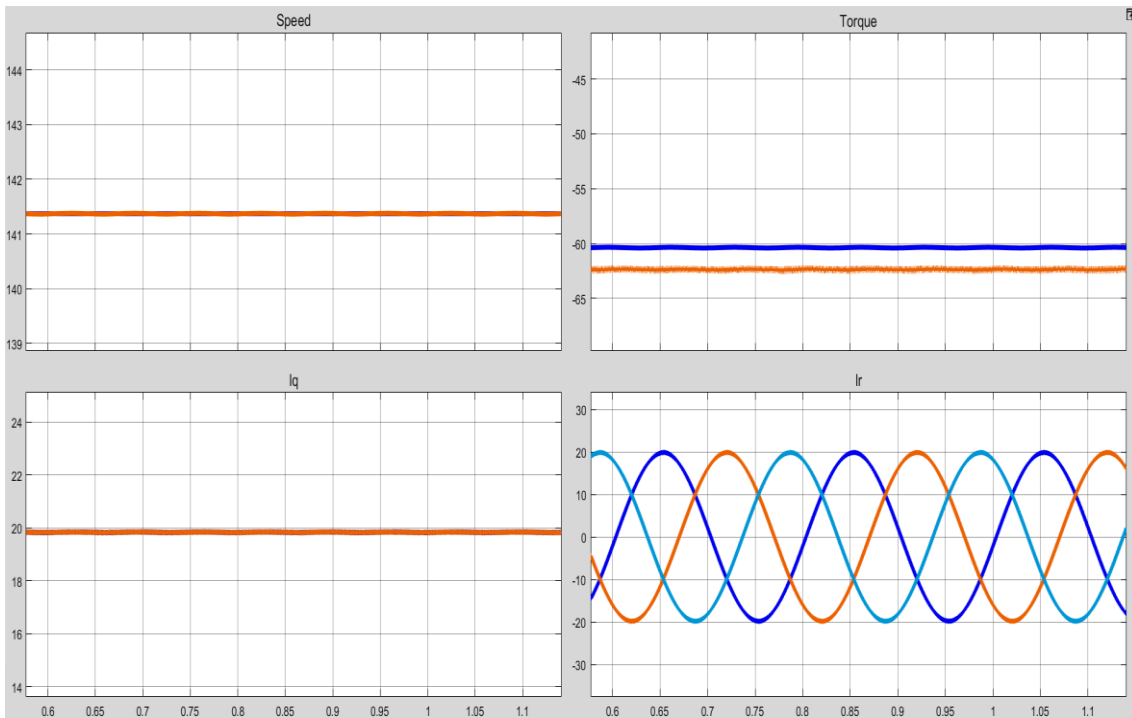


Figure 48 - Machine operating as a generator at sub-synchronous speed

In Figures 49 and 50, the machine is simulated running at the synchronous speed, as a motor and as a generator, respectively, with ten per cent of the rated torque as input. It is possible to understand that, at this specific speed, the machine is working as a synchronous machine with DC currents at the rotor.

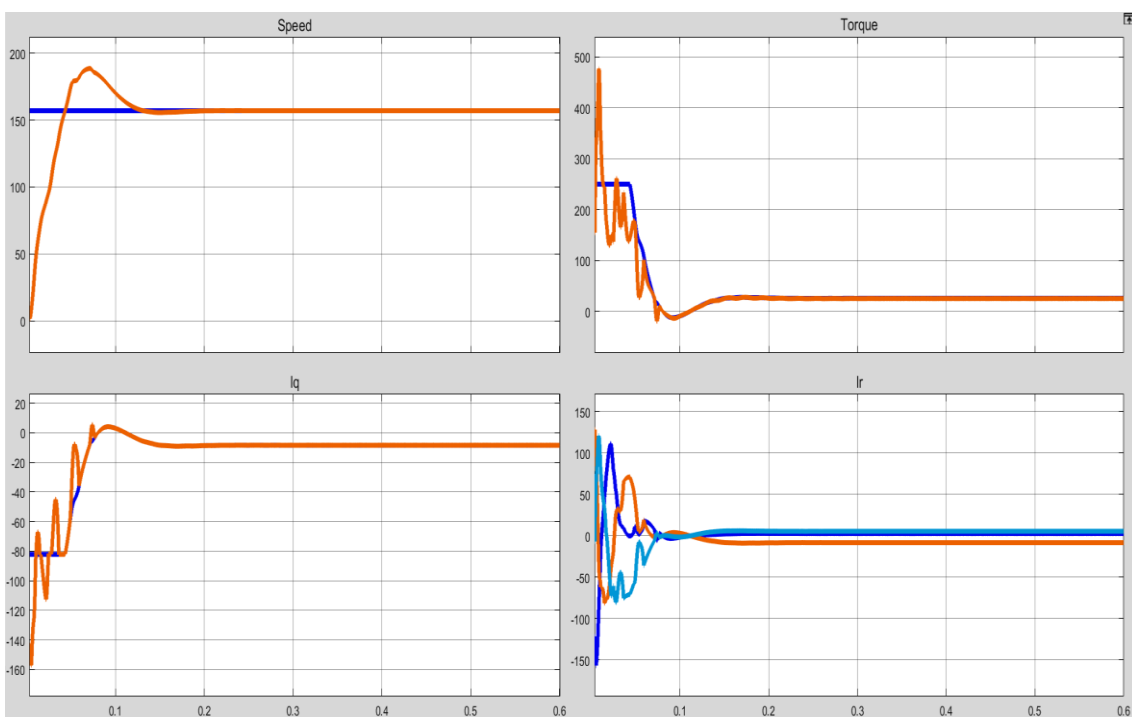


Figure 49 - Machine operating as a motor at synchronous speed

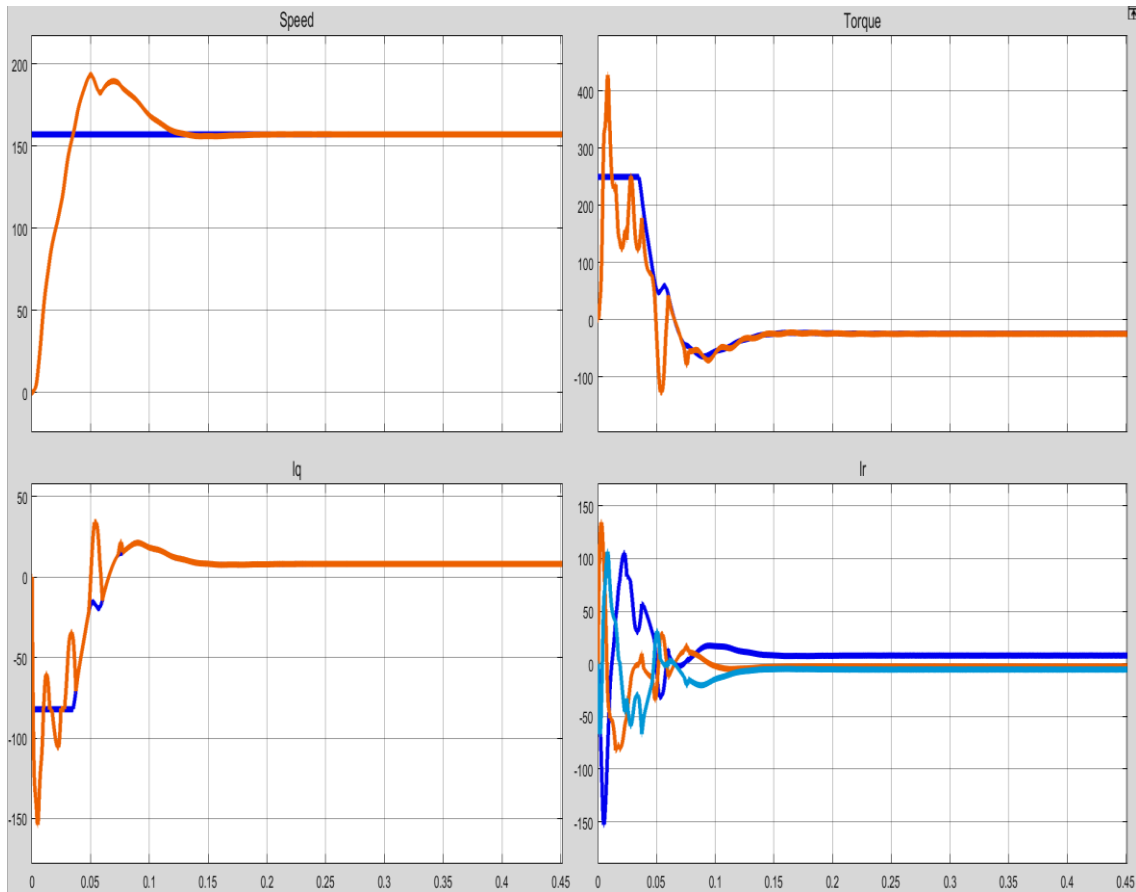


Figure 50 - Machine operating as a generator at synchronous speed

Figures 51 and 52 represent the machine simulated running at the hyper-synchronous speed, as a motor and as a generator, respectively, with one hundred and ten per cent of synchronous speed and with forty-five per cent of the rated torque as input. In this operation mode, both the stator and the rotor are producing power to the grid, and comparing the rotor currents produced with the results from the sub-synchronous speed operation, it is possible to distinguish the different flux of power in the rotor (dark blue line followed by light blue and orange lines, respectively, which represents *acb* phases, when compared with Figures 47 and 48).

Taking into consideration all the results obtained in this simulation, it can also be mentioned that the value of the i_{qr} takes either negative or positive value depending on if it is working as a motor or a generator, respectively.

Despite this analysis, it is needed a better understanding of the behaviour of this machine, so, the next step after this simulation is to analyse the steady state behaviour of this machine and relate it with the estimations created based on the theory behind it before moving on to implement the wind turbine module.

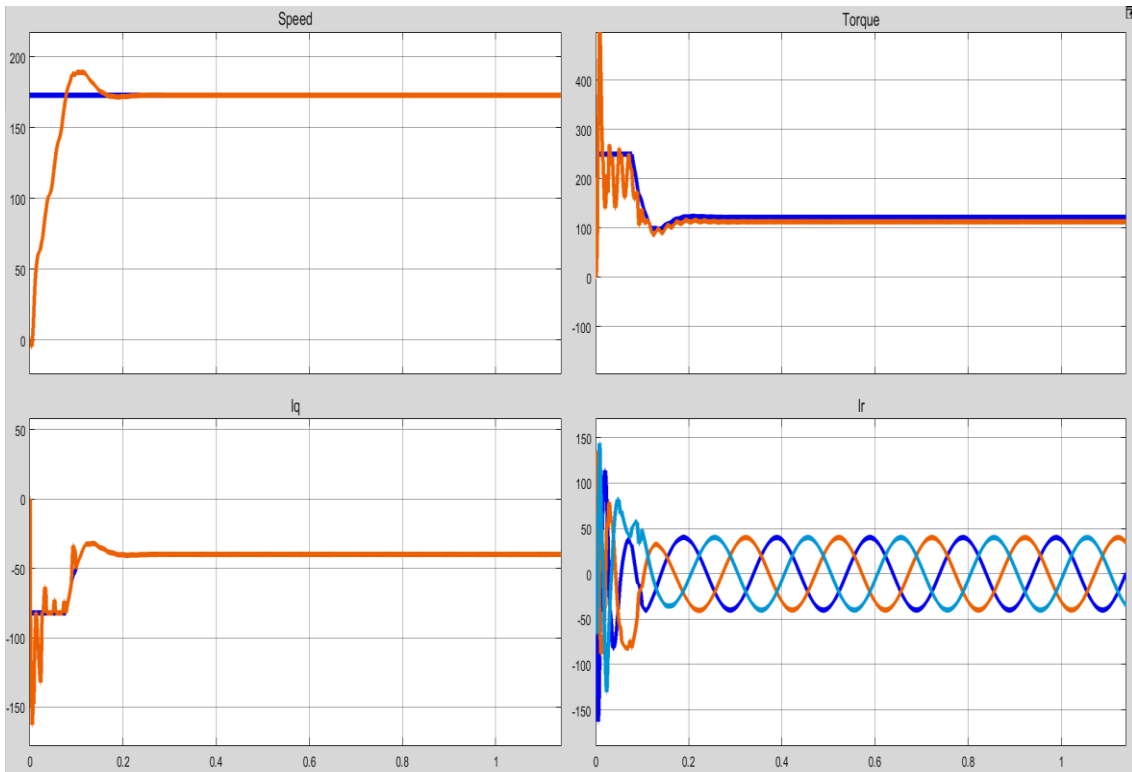


Figure 51 - Machine operating as a motor at hyper-synchronous speed

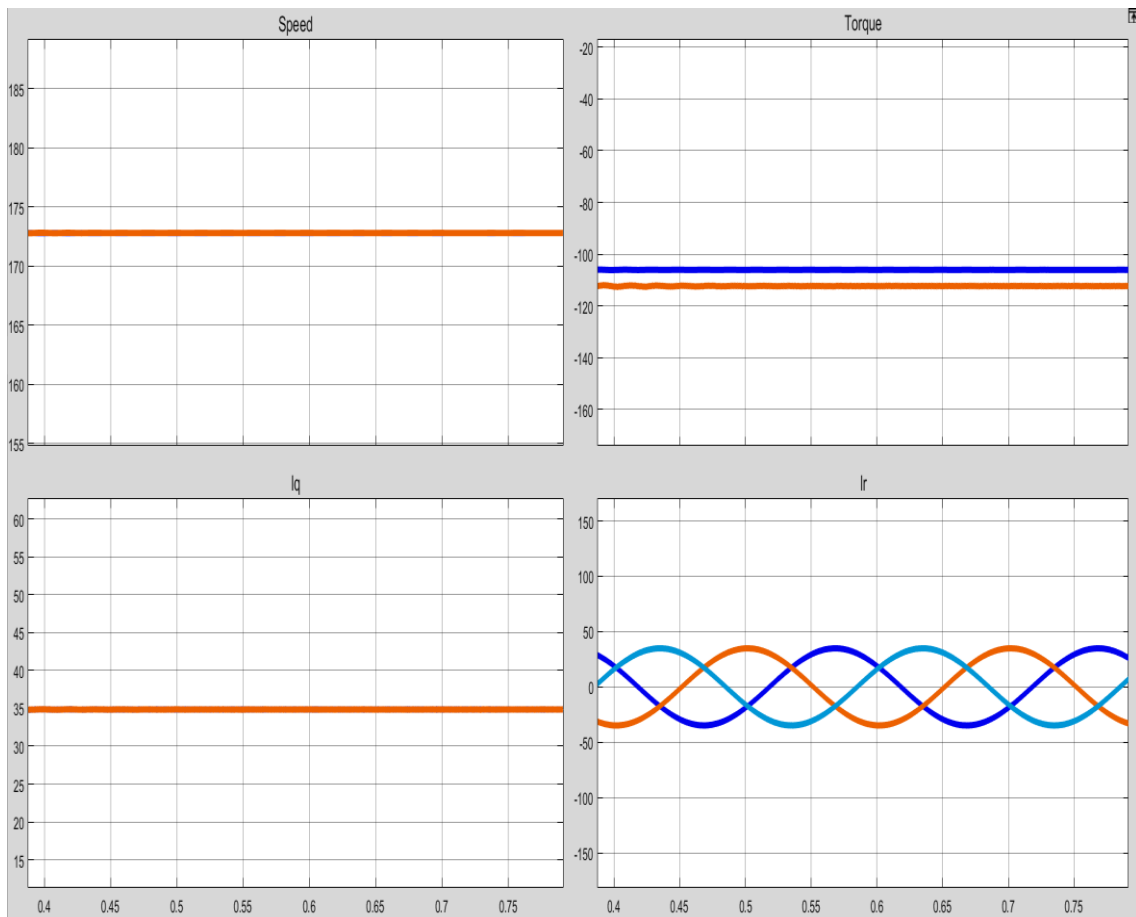


Figure 52 - Machine operating as a generator at hyper-synchronous speed

4.2. Simulation and analysis of the steady state of the machine

In order to understand how the estimated values were generated, a further read on the equations in the Attachment A is suggested. Using these equations for this simulation, the values generated from the previous simulation will be compared to the estimated ones. The estimated values of these equations are used to generate graphics, which are displayed below in figure 53.

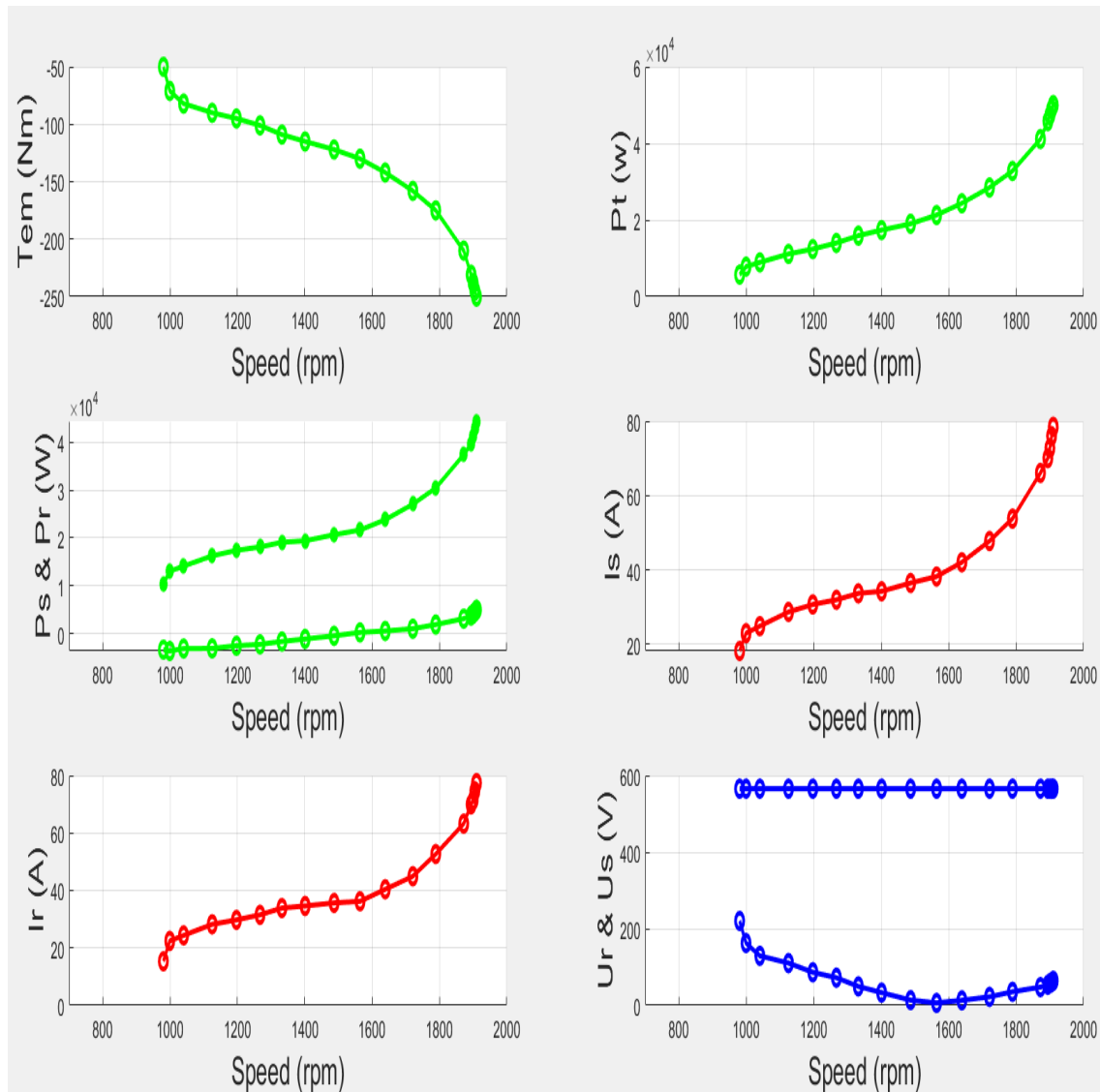


Figure 53 - Steady State Analysis of the system

It is possible to see the values of the electromagnetic torque, as well as the Power of the turbine, the Power of the Stator and the Rotor (taking into consideration when the Rotor is consuming or supplying energy), the currents of both Stator and Rotor, as well as their respective

voltages. The values of the reactive power of both Stator and Rotor were not taken into consideration as there is no control. To notice the rotor voltages are given as referred to the stator, hence not real voltages.

Taking these values into consideration and going back to the system simulated, it is possible to check points in the previous simulation to compare starting with a sub-synchronous speed point displayed in figure 54. Taking the values of the torque as -100 Nm, as well as the speed as 1267 rpm, both displayed in the graphics, as the inputs of the previous simulation, it is possible to compare all values represented. The value of I_r can be calculated as the square root of the sum of both i_d and i_q currents, or simply by looking at its graphic. In both cases, the value goes around 31/32 A which is in line with estimations. The rotor voltage is calculated as the square root of the sum of both u_{dr} and u_{qr} , and its value gives around 70 V, which is in line with estimated value. When it comes to the stator current, it is possible to observe the current obtained in the simulation, which is around 35 A. Since the Rotor values are more or less in line, the power estimated will correspond more or less to the obtained, and when it comes to the Stator values, the same can be said. And lastly, the value of the power of the wind turbine can be obtained using (7), so with this speed and torque as inputs, the value goes around 13.7 kW, which is similar to the estimated value.

Taking now another point in the graphics, but this time in hyper-synchronous operation mode of the generator, it is possible to compare the values in figure 55. Having the values of the torque as -210 Nm, as well as the speed as 1872 rpm, both displayed in the graphics, as the inputs of the previous simulation, it is possible to compare all values represented. The value of I_r can be calculated as the square root of the sum of both i_d and i_q currents, or simply by looking at its graphic. In both cases, the value goes around 62/63 A which is in line with estimations. The rotor voltage is calculated as the square root of the sum of both u_{dr} and u_{qr} , and its value gives around 51/52 V. When it comes to the stator current, it is possible to observe the current obtained in the simulation, is around 64/65 A. Having both Rotor and Stator values are more or less in line with the estimated values, the power estimated will correspond more or less to the obtained. And lastly, the value of the power of the wind turbine can be obtained using (7), so with this speed and torque as inputs, the value goes around 41 kW, which is similar to the estimated value.

The next simulation will incorporate the system already developed with a wind turbine model, and the results obtained will be analysed.

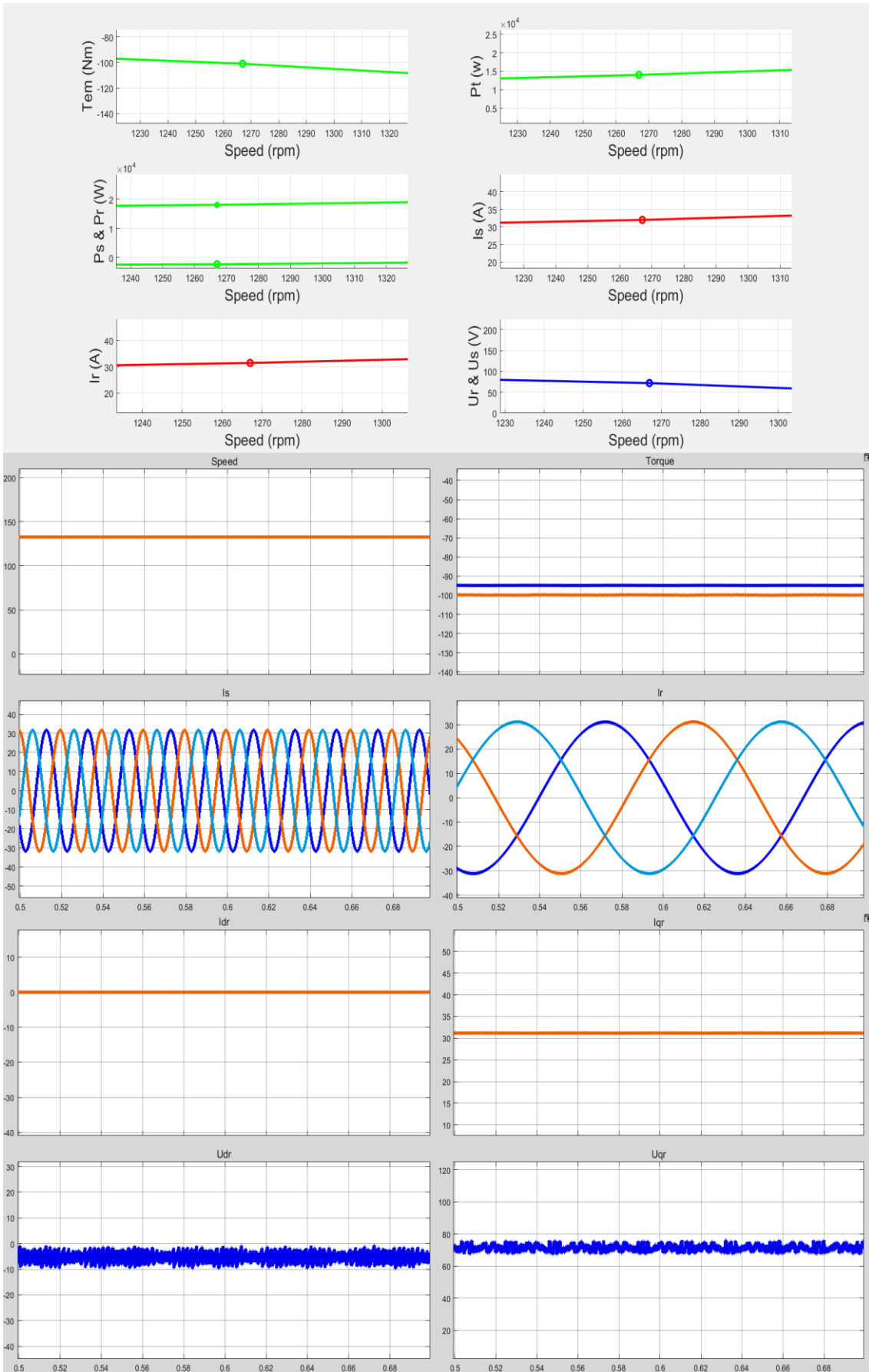


Figure 54 - Analysis of sub-synchronous operating point in steady state

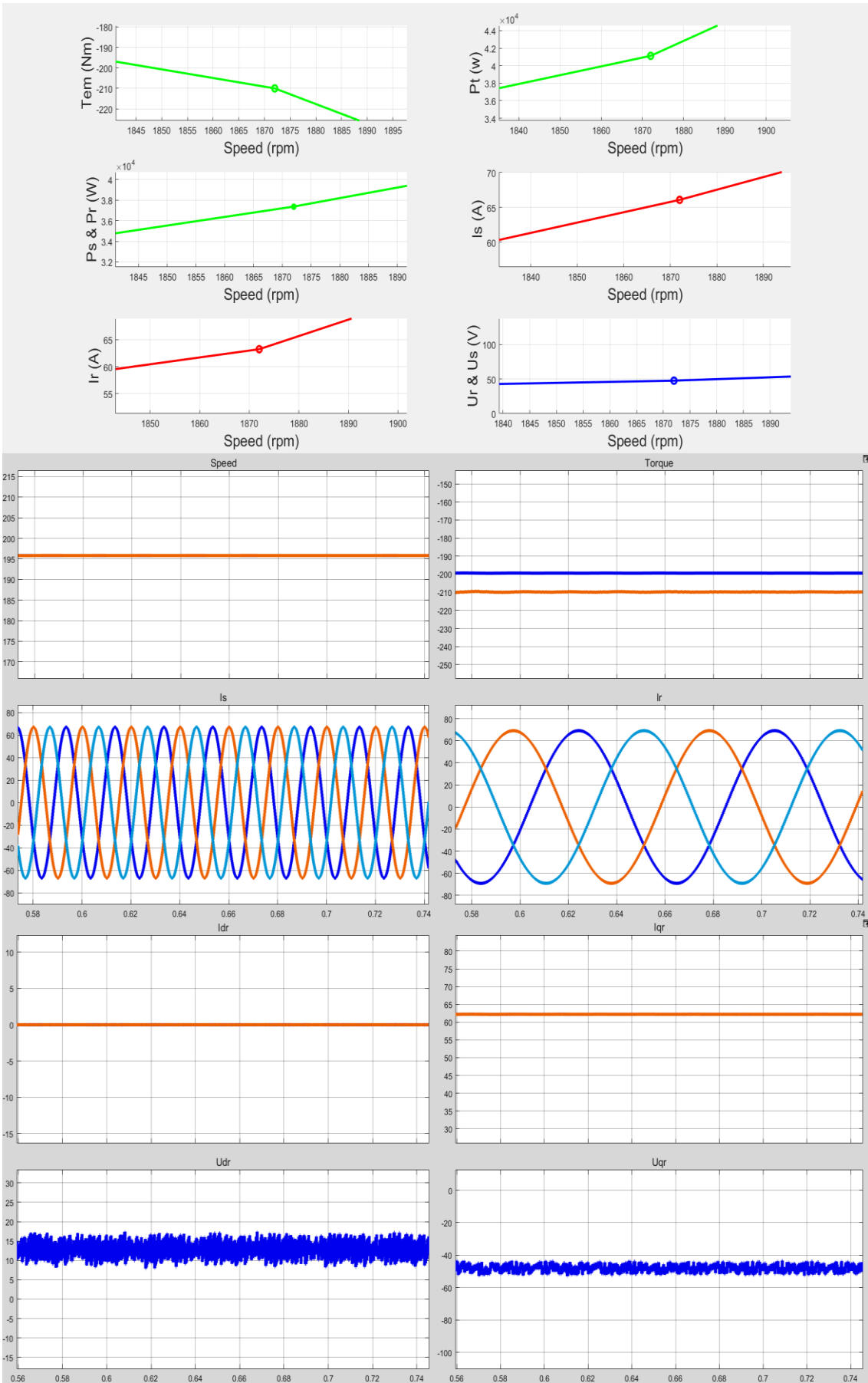


Figure 55 - Analysis of hyper-synchronous operating point in steady state

4.3. Simulation of the machine with the wind turbine model

For this simulation, it is implemented the module of the wind turbine in the already developed system in Simulink as well as a MPPT block in the control circuit to track the optimal power point for the system based in the figure 8 displayed in previous chapters.

Taking a look now at the Figure 56, it is possible to interpret that the first function block represents the equation (8), where it is made the calculation of λ . The mechanical speed, ω_m , is measured in the machine variables and then converted based on the gearbox ratio N . Then, λ can be calculated taking both the wind speed, this one inserted as an input, and the radius of the blade into consideration like represented in the equation mentioned. After this process, it is possible to calculate the wind turbine torque represented in (9), having the curve C generated in the one-dimensional look-up table block of Simulink. The variable is ready to connect to the system after converting again based on the gearbox ratio N , this one in negative instead, since the normal convention of the machine in Simulink is to work as a motor, but for the purpose of this project it will be working as a generator, so the output of this block, the wind turbine torque, must be negative. The output signal from this block will connect to the mechanical input of the machine.

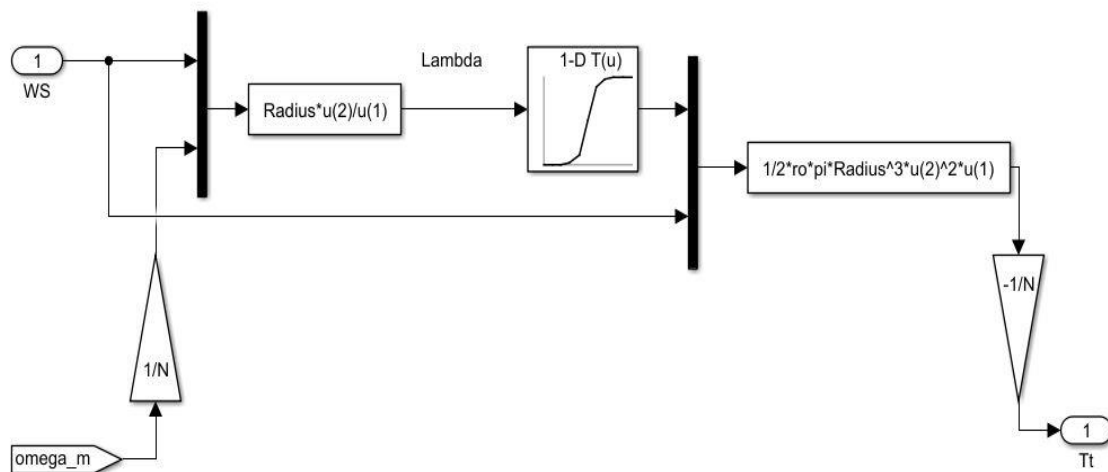


Figure 56 - Wind Turbine block

Taking into consideration the equations from (5) to (11), as well as figure 8 and table 4 in the Attachment A, it is possible to generate in Simulink a graphic about the values estimated for

both lambda and beta, that will go along with the implemented blocks. This graphic is represented in figure 57. Having those estimations in mind, the optimal values of the tip-speed ratio vary between 6 and 8, while beta is around 0, since with this value the wind the efficiency of the harnessing of the wind by the turbine is the maximum. For the purpose of this project, in order to design the both the coefficient and power curves, it was considered the characteristics from the Aeolos-H 50kW wind turbine, manufactured by the Aeolos Wind Turbine company, and also was considered the optimal tip-speed ratio. It was not possible to find a commercial model of a wind turbine using the generator used in this project, because it is not reliable when compared to synchronous generators for wind energy production at low power.

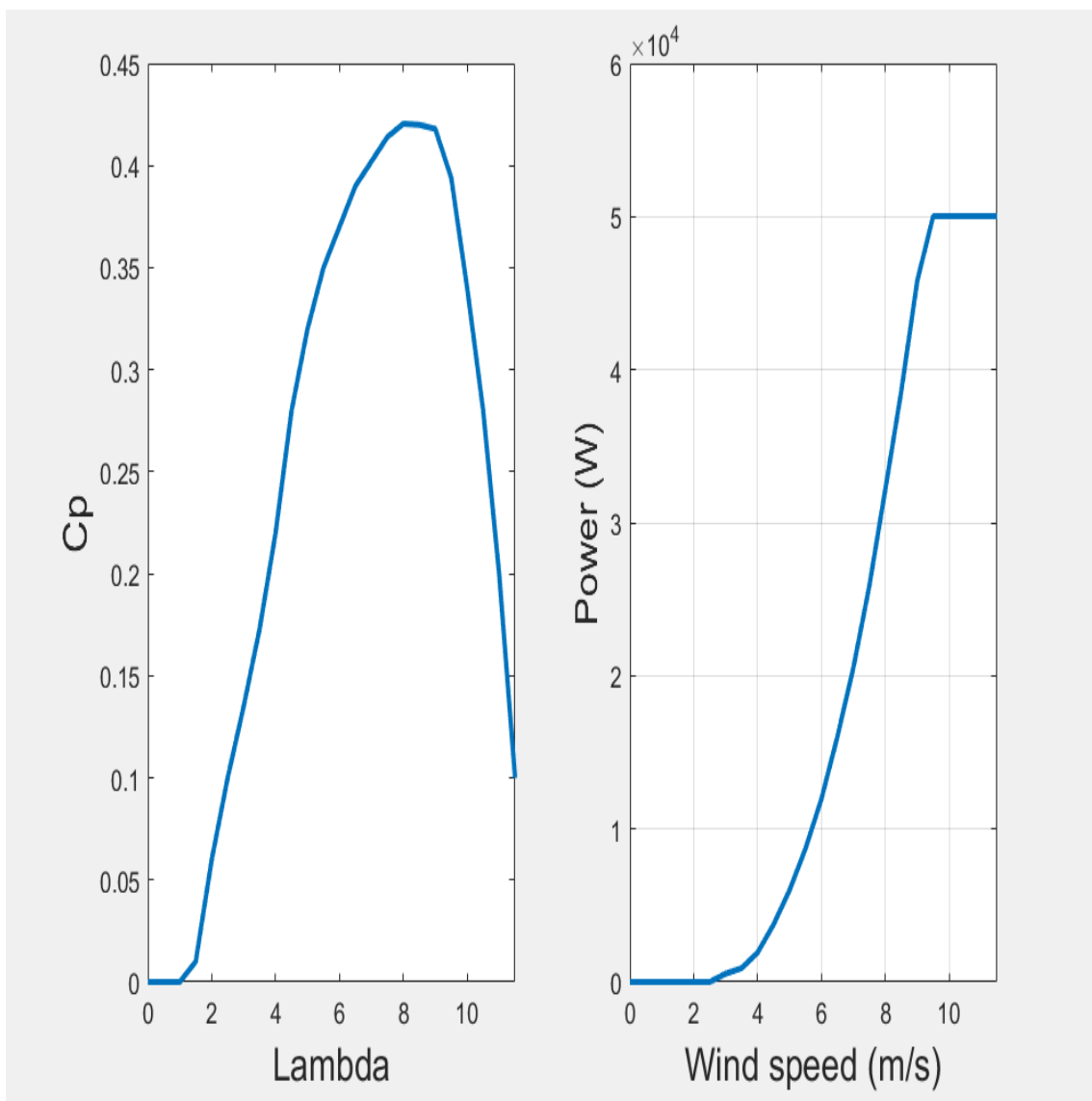


Figure 57 - Graphic of estimated wind power based on both the tip-speed ratio and the wind speed

Figure 56 represents a block that is going to replace the reference of the mechanical input previously developed. This algorithm generates but it is still needed to generate the estimated mechanical torque to implement the rest of the control algorithm. As a result of this, figure 58 represents the block that is needed to be added in order to convert the turbine input values, as it is called as the MPPT block of the system. The value of N is taken as 1, meaning there will not be considered a gearbox, and this value is chosen this way due to the fact that the turbine power output is really small to consider even using a gearbox, even more so when the data used from the Aeolos Turbine indicates no gearbox, but since the algorithm adapted to use in this project incorporates it, it was included as well.

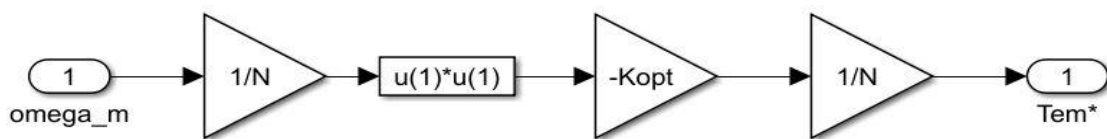


Figure 58 - MPPT control block

To test all of the things implement in this section, a random point in the power graphic is selected to compare the power value from graphic with the value obtained from the simulation, and it is illustrated in figures 59 and 60.

Looking at the point marked in graphic, for the wind speed of 8 meters per second, the turbine is supposed to produce more or less 32.2 kW of power, as where if the graphic from simulation is analysed, taking the speed as 187.35 and the torque as 169.5, it is possible to calculate the power using (7), and its value is 31.755 kW, which is relatively close to the estimated value obtained from the power estimation graph.

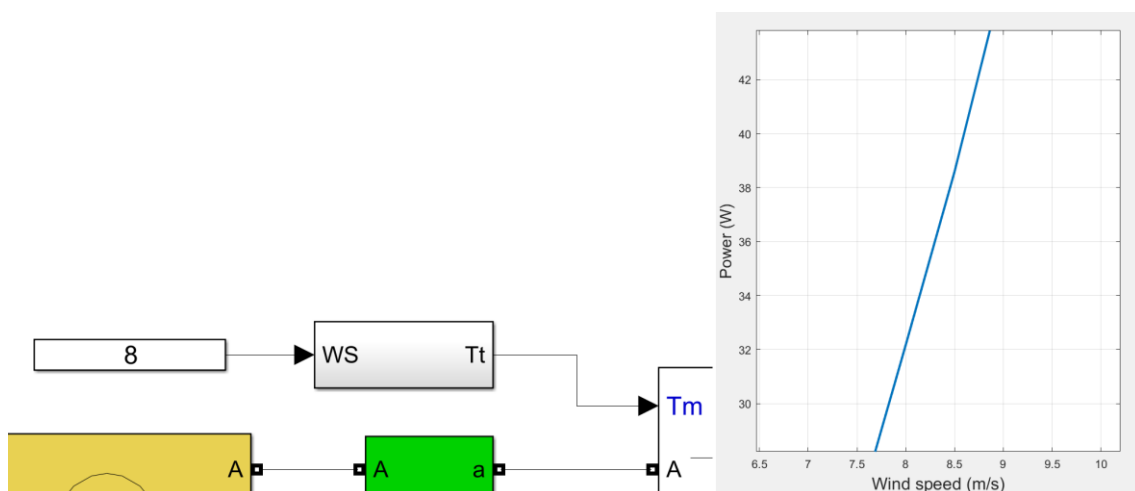


Figure 59 – Wind speed input and expected power to be obtained

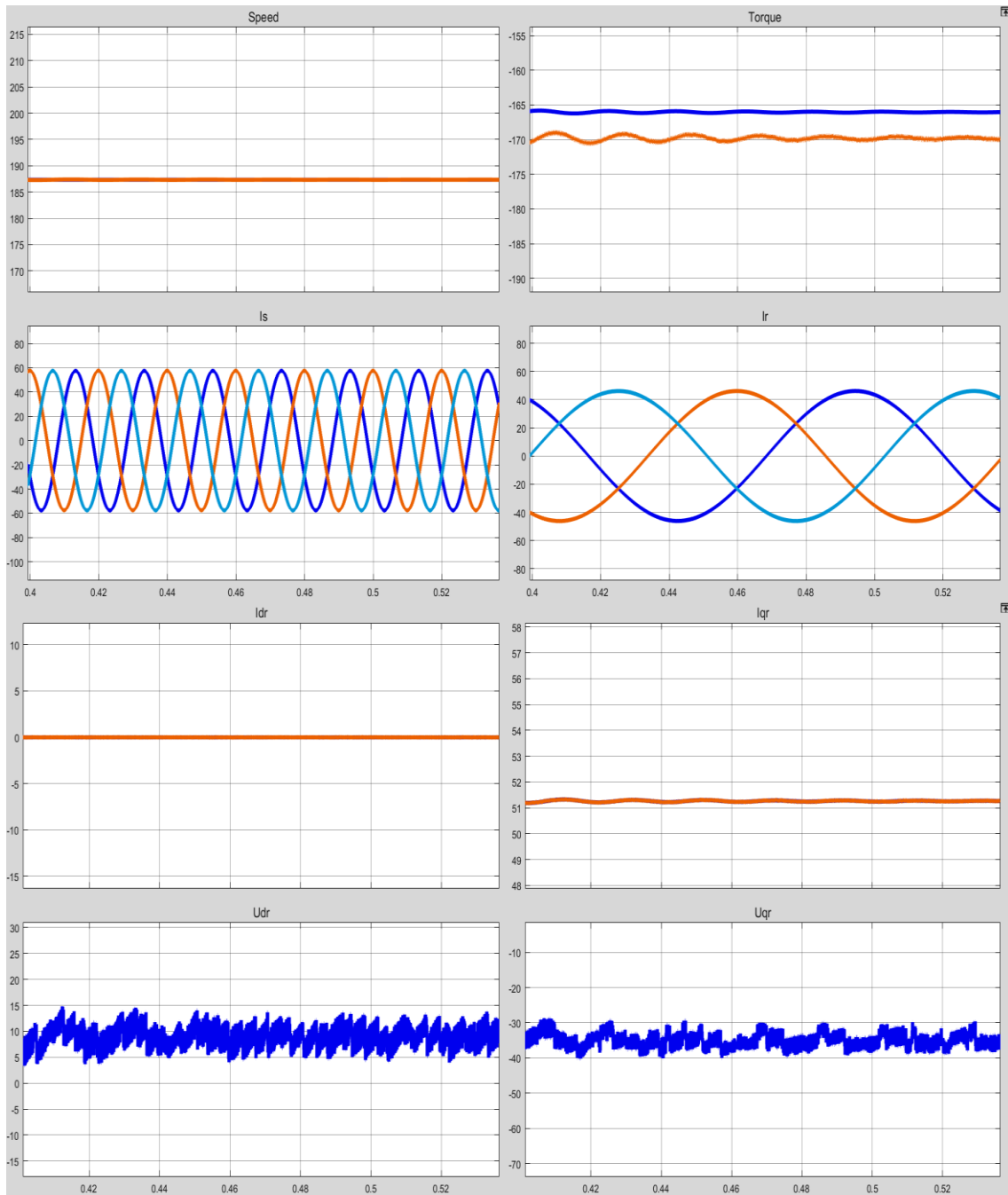


Figure 60 - Test of the MPPT block

4.4. Simulation of the implemented system

With everything developed so far, it is needed to implement now the GSC as well as its control, and put some RL filters as well as a transformer for galvanic isolation to simulate the whole circuit as intended.

Table 3 represents the variables added to the system for this simulation to run the GSC correctly, while table 4 represents the gains used for the control circuit.

Table 3 - Parameters added to the system

Parameter (Program Variable name)	Value (Unit)
Capacitance of DC-link capacitor	$4.2 * 10^{-6}$ (F)
Resistance of the Grid Side filter	$400 * 10^{-4}$ (Ω)
Inductance of the Grid Side filter	$20 * 10^{-6}$ (H)

Table 4 - Gains used for the GSC control

Gain	Expression
kpg	$\frac{1}{\frac{3}{2} * U_s * \sqrt{\frac{2}{3}}}$
tau_ig	$\frac{L_g}{R_g}$
wnig	$2 * \pi * 60$
kp_idg	$(2 * wnig * L_g) - R_g$
kp_iqg	kp_idg
ki_idg	$wni^2 * L_g$
ki_iqg	kp_idg
ki_u	-3600
kp_u	-30

In figure 61 is displayed the control block of the active and reactive power decoupling of the GSC, while the full system is displayed in figure 62, where it is possible to observe the addition of the GSC as well as a block to measure its currents, and the circuit of the control signal generated for it is displayed in figure 63.

In the control circuit there are three input variables, the voltage of the DC-link capacitor, U_{bus} , the grid side converter current, I_g , and the stator voltage, U_s . The stator voltage is needed in order to determine the angle of the grid, $teta_g$, and it is done as such because in this way it is possible to synch the GSC with the RSC. The voltage of the DC-link capacitor is required as well as its reference, to generate the reference for the id current by means of a PI controller, in which both kp_u and ki_u are taken as $k1$ and $k2$, respectively. The reference for the iq current used in the algorithm in which this control strategy is based on is taken as the reactive power, and since in this project the reactive power is not taken into consideration, it is taken as 0. The measured values of both id and iq currents are generated by the transformation of the currents from the GSC, and in the respective PI controllers, kp_{idg} and ki_{idg} are taken as $k1$ and $k2$ in the id controller while kp_{iqg} and ki_{iqg} are taken as $k1$ and $k2$ in the iq controller. After this, the cancelation of the coupling terms is added before taking the reverse transformations, and a gain is also added in order to make the PWM signal generate signals between 0 and 1.

The PI control blocks are the same as displayed in figure 44, and all of the control components and algorithm can be understood by taking a look at the schematic displayed at figure 36.

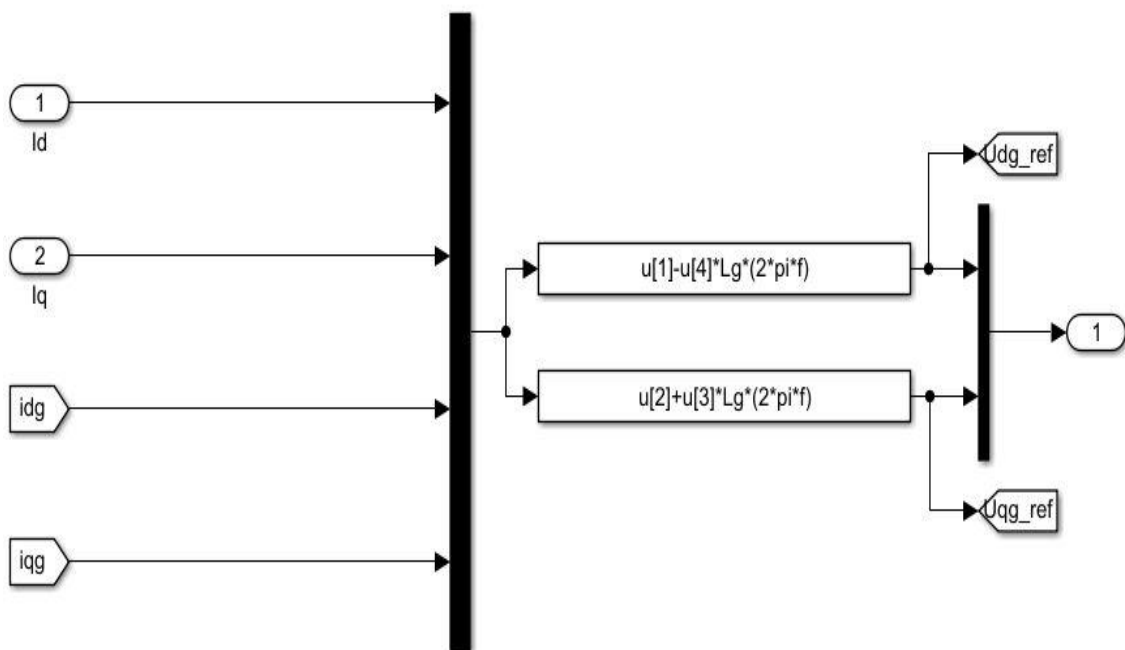


Figure 61 - Control block of active and reactive powers decoupling of the GSC

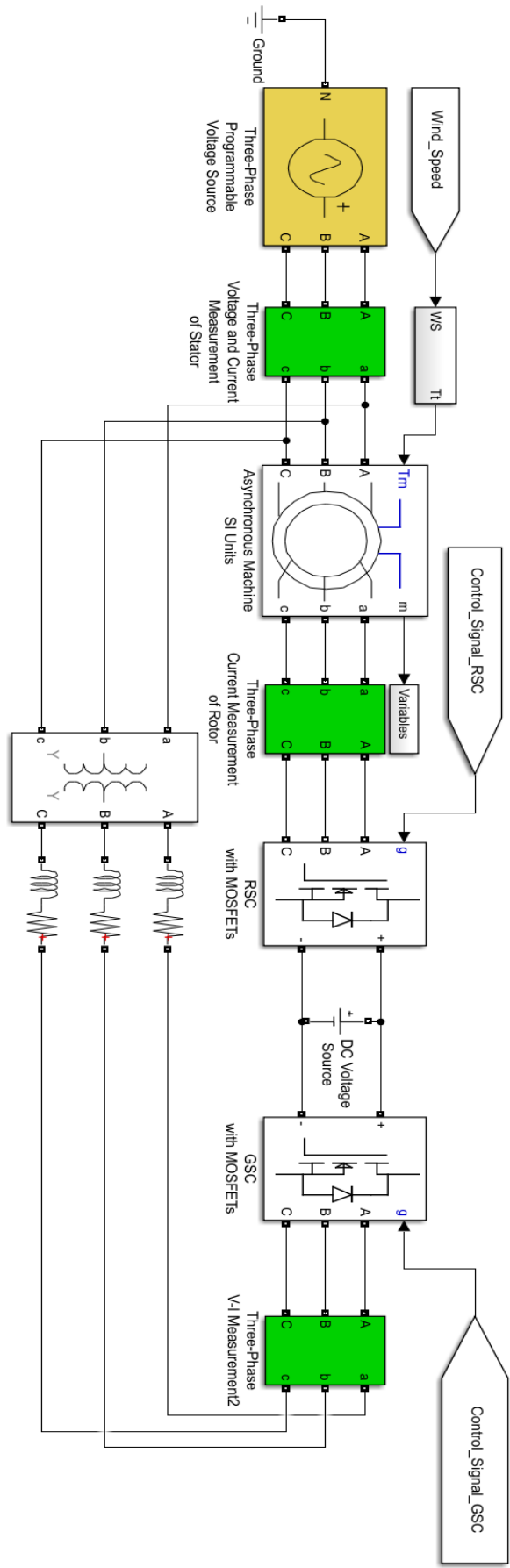


Figure 62 - Power electronics of the WTGS

Figure 64 and 65 display the simulation results of the system, in the RSC and the GSC, respectively, running at 9 metres per second of wind speed as the input after reaching the steady state.

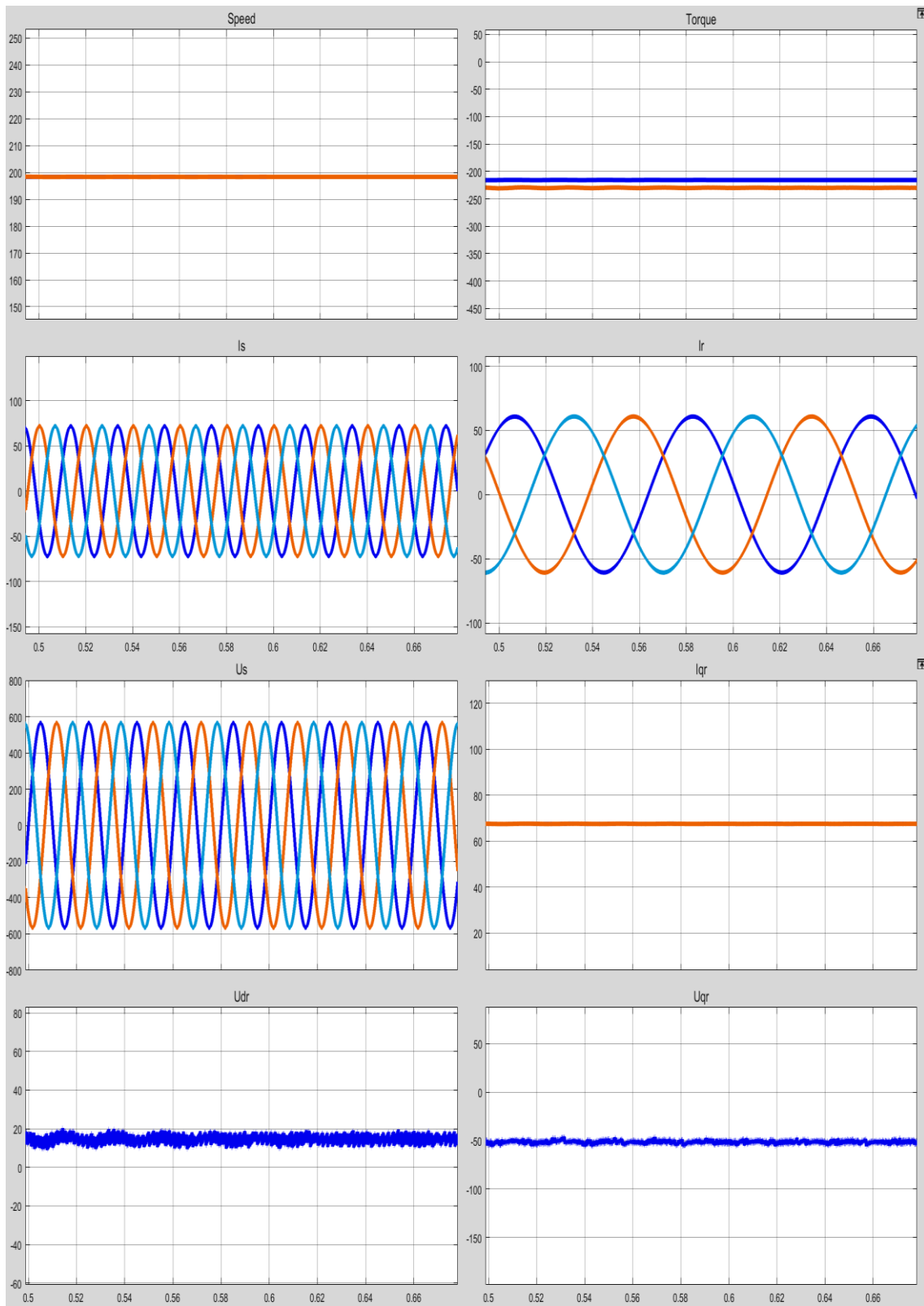


Figure 64 - GSC simulation results for 9 metres per second of wind speed

Looking at the RSC simulation results, the values obtained are pretty much in line with what was expected from all the previous simulations and analysis done previously, and the power output of the wind turbine is around 45 kW.

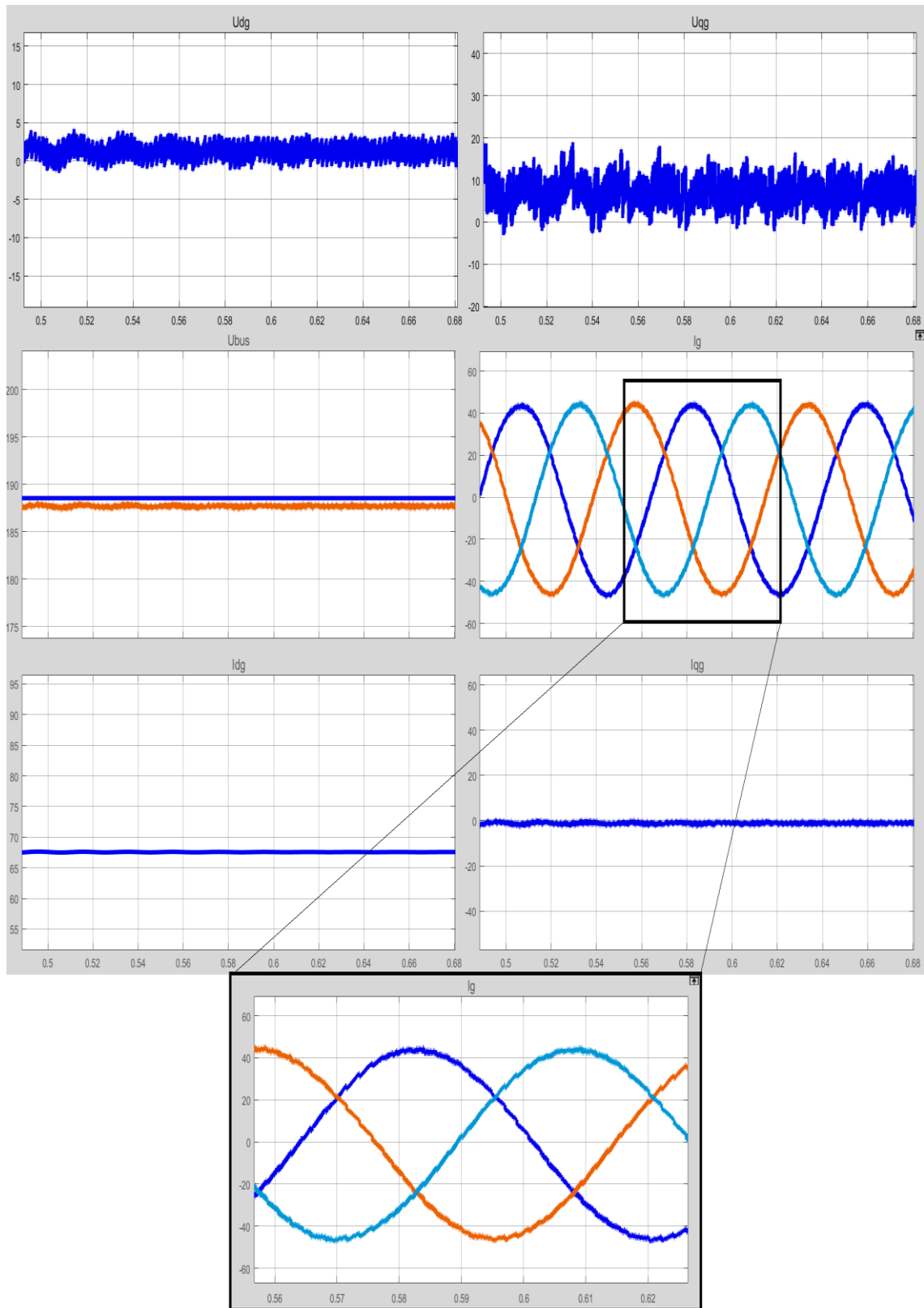


Figure 65 - RSC simulation results for 9 metres per second of wind speed

In the scope which represents the GSC control circuit, the value of the U_{bus} goes around the established reference value, and the voltage references are low values because, as displayed in figure 63, it is done a feedback of the grid voltage which justifies these low values. Last thing to observe is the GSC current, since it is perceptible that it has relevant perturbations despite having the sinusoidal waves. These perturbations were already expected due to several procedures skipped in order to make this implementation as simple as possible, but they can be immensely reduced mainly by considering the system startup procedures, as well as with the insertion of an active power filter, and also with a bit of improvement of the system. But despite this, the main objective intended in this project was to have this complex system working, so avoiding the control of the active and reactive powers was the best option moving towards the main goal. And with the simulation results displayed, it is possible to conclude this chapter and move on to the practical approach.

Chapter 5 – Laboratory experiment

In the current chapter, one laboratory experiment is attempted to prove concept. This is chosen this way due to the fact that this project is very complex, especially the control algorithm, and fully implementing it would go far beyond the expected work for this project, not to mention the amount of time required to do so. With this being said, the laboratory experiment attempted in order to prove the concept of this project is the implementation of a three-phase MOSFET converter in veroboard (which corresponds to the AC-DC converter from the back-to-back converter), which is connected to the rotor of the machine. The machine, working as a generator, is supplied by either the grid or by another machine working as a motor, and there is a DC link capacitor after the converter to generate a DC voltage source. This experiment contains a very high switching frequency in the MOSFETs, since the point is to use as much data from the simulation experiments as possible, so it is necessary the use of snubbers to protect from voltage peaks and store the energy released from the commutations of the semiconductors. It is also necessary to mention that the capacitors used in the snubbers must be polypropylene, which are the only type of capacitors with fast enough charge and discharge speed to withstand the high switching frequency used in this experiment. Also, the placement of the circuit components in the veroboard will have to be as close together to one another as possible, to have the fastest reaction as possible as well as to avoid any impedances from any wires that are to be used in the system.

In order to get into the practical experiment, it was necessary to develop a control algorithm for the microcontroller used based on the algorithm used to control the RSC in the simulations done in the previous chapter, and figure 66 represents its flowchart.

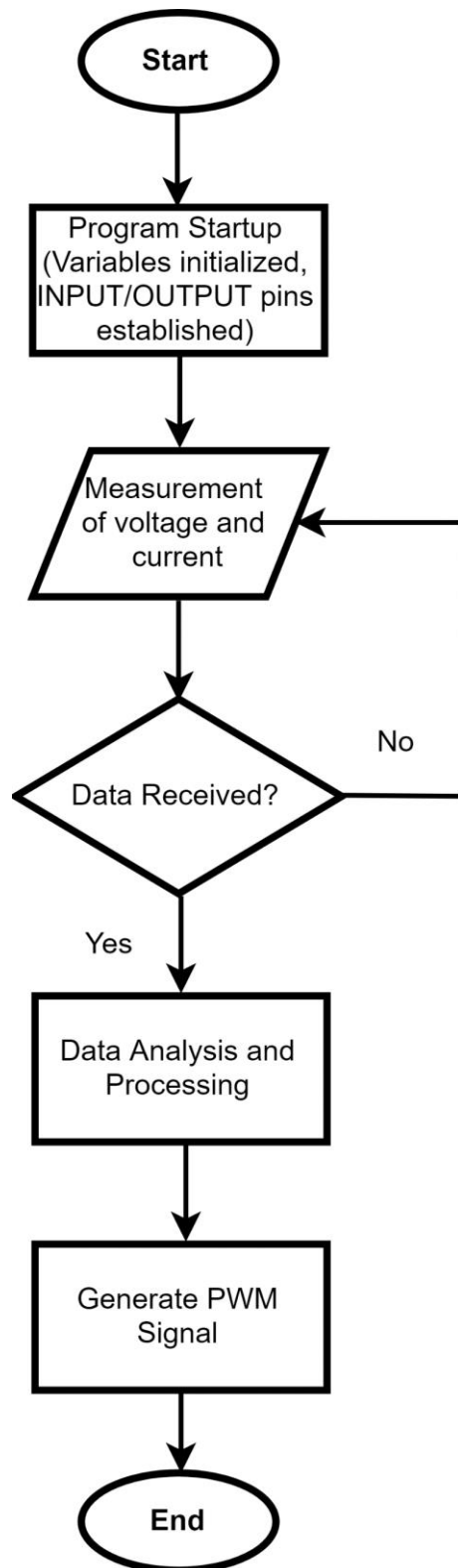


Figure 66 - Flow chart of the control design for the microcontroller

As it can be observed, in the start of the algorithm the program is initialised and the variables used as well at the INPUT/OUTPUT pins are established before moving on to the next step. By means of voltage and current sensors, the respective values of the rotor of the generator used are measured and passed onto the microcontroller. Then, it is checked if the values are received by the microcontroller before moving advancing any further. After, the transformations described in earlier chapter of this document will be applied to the values received, in order to have the measured values so it is possible to do the PI controllers before applying the inverse transformations and to generate the control signal, which will be converted to a PWM signal.

Figure 67 represents the partial implementation in veroboard of the circuit displayed in figure 68. This last figure represents the circuit design that was intended to be implemented for this practical test, where it can be observed the snubbers and its specifications used as well as the measurements block, which contains voltage and current sensors. Since the code developed for the Arduino wasn't working as intended, this circuit developed in veroboard could not be tested as initially planned (that is also the reason why figure 67 does not have any other components besides the snubbers that form the AC-DC converter, and since the sensors are components very limited to have, putting them onto the veroboard without certainty to do the test properly would be a big waste of utility for the department). The code developed for the Arduino can be found in appendix B, while all of the conclusions of this report will follow this chapter.



Figure 67 - Partial circuit design in veroboard

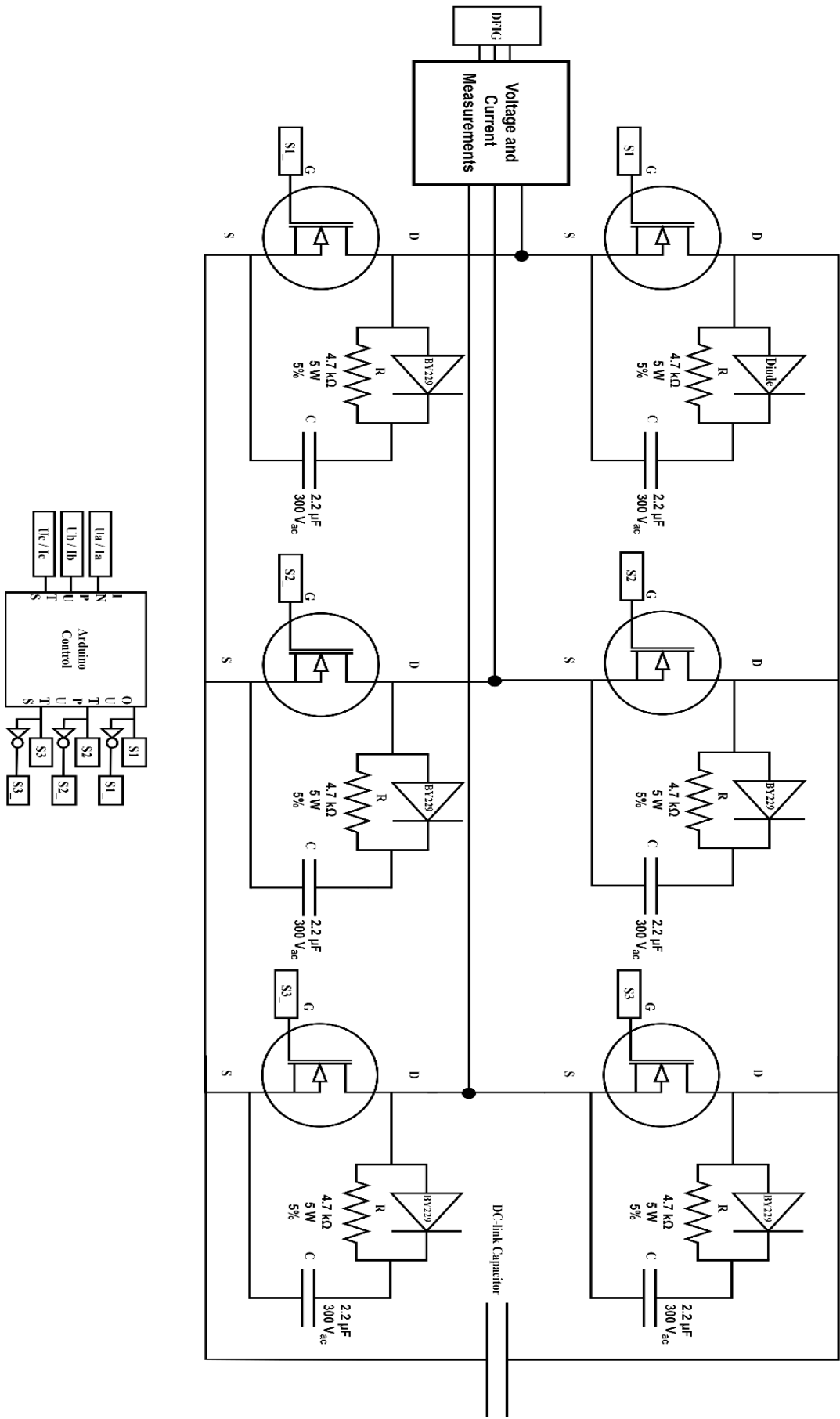


Figure 68 - Circuit design

Chapter 6 – Conclusions and future work

This project seemed way simpler than in reality. At first, this project was taken as a follow up from another project done within another subject, and little was the understanding and knowledge of what needed to be done in order to achieve the objectives intended for the full development of the system. During the time of this work, the more insight and specifications of the complexity of this project came to be known, the harder it seemed to achieve the initially proposed objectives properly and soon enough it looked already like too much work for the available time. As a result of this, several times the initial objectives had to be adjusted.

In regards to the references used, there are huge amounts of information related to the topic of this project, as well as every part of it available on the internet today. Having a lot of misleading information, it was really difficult to filter out the useful information from all of the sources and to gather it up in order to understand better the system and develop it alongside the making of this report. This took much more time than initially intended.

After spending much more time than expected for the system simulations and gaining a deeper understanding on the complexity of the desired system to be fully implemented for laboratory testing, it was thought that the amount of work was too much for what was intended for this project work and that it would not be possible to implement the full system with the amount of time available due to the several reasons mentioned a lot of times already in the several chapters that incorporate this report, so after the adjustment of the objectives, a simple laboratory experiment as a proof of concept was thought to be the best plan available for the remaining estimated time of this project for its practical component.

Moving on to the results part, after the adjustments were made to the initial objectives, it is fair to consider that, when it comes to simulation purposes, the project was successful as everything intended was done, being the results obtained pretty much in line with what was planned in the beginning, since a lot of procedures were ignored in order to save up time and the perturbations that exist were already expected.

In regards to the practical component, it was not possible to conclude successfully this experiment due to the complexity of the understanding and simulation of the system as described before. Too much time was invested into the research and control algorithm understanding, so that the simulations part would be successful and complete, which left this proof of concept test with

almost no time to be developed, as it can be understood by reading through chapter 5. The circuit that was developed in veroboard was not properly tested due to the fact that the code developed for the microcontroller was not complete nor fully functional as initially intended. However, due to the amount of time dedicated for planning it, even if it was unsuccessful, it was still included in this report. Regarding its unsuccessfulness, all of it came mainly as a result of bad planning as well as bad management regarding the procedures and the objectives at the start of this project, as well as a certain unconsciousness about the difficulty ahead of what was proposed as the project goals, and this happened multiple times during the making of this project, especially in the beginning as the knowledge about the topic and the understanding of the amount of work required in order to make this project successful was little to none.

As for future work, the control system of this project in these simulations needs still a bit of adjusting and improving, especially when it comes to the noise and perturbations and taking it further into the practical approach. The code developed for the microcontroller also needs more development and maybe an adjust at the algorithm used to make it more effective since at the time of writing it is still a bit confusing to have a clear idea on how to properly execute this task. And also, this report wishes to be of help to any student of this university that will go on to develop projects related to this topic, with hopes that it can be prove useful in terms of understanding the topic as well as gaining knowledge, while helping with the fulfilment of their respective project objectives.

Appendix A

In this appendix it is displayed the equations used to estimate the values to be obtained in the simulations based on the control strategy used during the implementation of the system. Firstly, it is displayed Table 5, which shows all equations needed for estimating both stator and rotor values.

Table 5 - Equations to estimate both stator and rotor values during simulations

	Stator	Rotor
Currents	$i_{ds} = \frac{\phi_s}{L_s} - i_{dr} \frac{L_m}{L_s}$ $i_{qs} = -i_{qr} \frac{L_m}{L_s}$ $i_s = \sqrt{i_{ds}^2 + i_{qs}^2}$	$i_{dr} = 0$ $i_{qr} = -\frac{2 T_{em} L_m}{3 p L_m \phi_s}$ $I_r = \sqrt{i_{dr}^2 + i_{qr}^2}$
Voltages	$u_{ds} = R_s i_{ds}$ $u_{qs} = R_s i_{qs} + w_s \phi_s$ $u_s = \sqrt{i_{ds}^2 + i_{qs}^2}$	$u_{dr} = R_r i_{dr} - L_r w_r i_{qr} - L_m w_r i_{qs}$ $u_{qr} = R_r i_{qr} - L_r w_r i_{dr} - L_m w_r i_{ds}$ $U_r = \sqrt{u_{dr}^2 + u_{qr}^2}$
Active Power	$P_s = \frac{3}{2} (R_s * i_{ds}^2 + R_s i_{qs}^2 + w_s \phi_s i_{qs})$	$P_r = \frac{3}{2} (u_{dr} * i_{dr} + u_{qr} * i_{qr})$
Flux	$\phi_{ds} = L_s i_{ds} + L_m i_{qr}$ $\phi_{qs} = L_s i_{qs} + L_m i_{dr}$ $\phi_s = \sqrt{\phi_{ds}^2 + \phi_{qs}^2}$	$\phi_{dr} = L_r i_{dr} + L_m i_{qs}$ $\phi_{qr} = L_s i_{qr} + L_m i_{ds}$ $\phi_r = \sqrt{\phi_{dr}^2 + \phi_{qr}^2}$

Table 6 contains other relevant equations for the rest of the simulations that are important to be mentioned.

Table 6 - Other relevant equations for the simulation analysis

Mechanical Power	$P_{mec} = T_{em} \frac{\omega_m}{p}$
Sigma	$\sigma = 1 - \left(\frac{L_m^2}{L_r L_s}\right)$
Rotor Hub Speed	$\omega_r = \omega_s - slip$

Appendix B

Here it is displayed all the code developed towards the microcontroller used in this project, the Arduino. The code is commented accordingly to enable a better understanding. This code at the time of this report was intended to only read the currents from the rotor and generate a control signal that would not take into consideration the angular position of the rotor neither the cancelation of the coupling terms, and this can be understood taking a look back at figure 36.

```
// libraries used
#include <avr/io.h>
#include <avr/interrupt.h>
#include <math.h>
// defining the input pins for the currents
int analogPin1 = A0;
int analogPin2 = A1;
int analogPin3 = A2;
int PWMs1 = 2;
int PWMs1n = 3;
int PWMs2 = 4;
int PWMs2n = 5;
int PWMs3 = 6;
int PWMs3n = 7;
// definition of the variables to hold current values
int ia = 0;
int ib = 0;
int ic = 0;
int ialfa = 0;
int ibeta = 0;
int id = 0;
int iq = 0;
int i1 = 0;
int i2 = 0;
int out1 = 0;
int out1n = 0;
int out2 = 0;
int out2n = 0;
int out3 = 0;
int out3n = 0;
// definition of machine variables
int Us = 400; // Table 1
int J = 0.05; // Table 1
int p = 2; // Table 1
int Lm = 0.0354; // Table 1
int Ls = 0.03627; // Table 1
int Lr = Ls; // Table 1
int FluxStator = Us*(sqrt(2/3)/(2*f*PI)); // Table 1
int busgain = (1200*sqrt(2))/9;
```

```

// definition of the variables related to the gains used
int sigma = 1 - ((Lm*Lm)/(Lr*Ls)); // Appendix A
int tau_i = sigma*Lr/Rr; // Table 2
int tau_n = 0.05; // Table 2
int wni = 100/tau_i; // Table 2
int wnn = 1/tau_n; // Table 2
int kp_id = (2*wni*sigma*Lr)-Rr; // Table 2
int kp_iq = kp_id; // Table 2
int ki_id = wni*wni*sigma*Lr; // Table 2
int ki_iq = ki_id; // Table 2
int k_iq = 1/(-1.5*p*(Lm/Ls)*FluxStator)); // Table 2
// Speed ref value altered based on the speed it is desired to perform, since
// the code for reading the machine rotations by means of an encoder were skipped
int speed_ref = 0;
const int f = 50; // frequency
const double w = 2*PI*f; // frequency as angular speed ( $\omega$ )

void setup()
{
  Serial.begin(9600); // setup serial
  pinMode(analogPin1, INPUT); // setup desired pins as inputs and outputs
  pinMode(analogPin2, INPUT);
  pinMode(analogPin3, INPUT);
  pinMode(PWMs1, OUTPUT);
  pinMode(PWMs1n, OUTPUT);
  pinMode(PWMs2, OUTPUT);
  pinMode(PWMs2n, OUTPUT);
  pinMode(PWMs3, OUTPUT);
  pinMode(PWMs3n, OUTPUT);
}

int main() // processes every value as it read, in order to make response fast
{
  setup();
  ia = analogRead(analogPin1); // read the input pins
  ib = analogRead(analogPin2);
  ic = analogRead(analogPin3);
  Serial.println(ia); // to debug the values
  Serial.println(ib);
  Serial.println(ic);

  convert_referred(&ia,&ib,&ic);
  abc_alfabeta_transformation(ia,ib,ic,&ialfa,&ibeta);
  alfabeta_dq_transformation(ialfa,ibeta,&id,&iq);

  Plcontroller(id,0,kp_id,ki_id,&i1);
  Plcontroller(iq,0,kp_iq,ki_iq,&i2);
}

```

```

dq_alfabeta_transformation(&ialfa,&ibeta,i1,i2);
alfabeta_abc_transformation(&ia,&ib,&ic,ialfa,ibeta);
convert_referred(&ia,&ib,&ic);

pwm_signal(ia,&out1,&out1n,ib,&out2,&out2n,ic,&out3,&out3n);

analogWrite(out1, PWMs1); // Output S1
analogWrite(out1n, PWMs1n); // Output S1_
analogWrite(out2, PWMs2); // Output S2
analogWrite(out2n, PWMs2n); // Output S2_
analogWrite(out3, PWMs3); // Output S3
analogWrite(out3n, PWMs3n); // Output S3_
}

void convert_referred(int *a, int *b, int *c) // conversion of the rotor quantities to quantities referred
to the stator
{
    int nrs=10;
    // can be understood taking a look at figure 36
    a=a/nrs;
    b=b/nrs;
    c=c/nrs;
}

void abc_alfabeta_transformation(int a,int b,int c, int *d, int *e) // Clarke transformation
{
    d=(2/3)*a-(1/3)*(b+c); // following equation (19.a)
    e=(2/sqrt(3))*(b+c); // following equation (19.b)
}

void alfabeta_dq_transformation(int a, int b, int *c, int *d) // Park transformation
{
    c=a*cos(w)+b*sin(w); // following equation (20.a)
    d=b*cos(w)-a*sin(w); // following equation (20.b)
}

void dq_alfabeta_transformation(int *a, int *b, int c, int d) // Reverse Park transformation
{
    a=c*cos(w)-d*sin(w); // following equation (21.a)
    b=d*cos(w)+c*sin(w); // following equation (21.b)
}

void alfabeta_abc_transformation(int *a, int *b, int *c, int d, int e) // Reverse Clarke transformation
{
    a=d; // following equation (22.a)
    b=(-1/2)*d+(sqrt(3)/2)*e; // following equation (22.b)
    c=(-1/2)*d-(sqrt(3)/2)*e; // following equation (22.c)
}

```

```

void Plcontroller(int *a, int *b, int *c, int *d, int *e)
{
    int error = (a - b); // Error calculation, being a the measured value and b the reference
    int proportional = error*c; // Proportional control
    int integral = integral + error*d; // Integral control
    e = proportional + integral; // Output of controller
}

```

```

void pwm_signal(int a, int *b, int *c, int d, int *e, int *f, int g, int *h, int *i)
{
    // Generate PWM for S1/S1_ like displayed in figure 69
    a=a*busgain;
    b = a*255;
    c = (1-a)*255;
    // Generate PWM for S2/S2_ like displayed in figure 69
    d=d*busgain;
    e = d*255;
    f = (1-d)*255;
    // Generate PWM for S3/S3_ like displayed in figure 69
    g=g*busgain;
    h = g*255;
    i = (1-g)*255;
}

```

References

- [1] International Energy Agency. “World Energy Investment 2018”. [Online] accessed on 16-12-2019.
<https://www.iea.org/reports/world-energy-investment-2018>
- [2] Jonathan Watts, The Guardian. “Global atmospheric CO₂ levels hit record high”. [Online] accessed on 30-10-2019.
<https://www.theguardian.com/environment/2017/oct/30/global-atmospheric-co2-levels-hit-record-high>
- [3] International Institute for Sustainable Development. “Renewable Energy Investments Increased Five-fold Globally Over Past 15 Years”. [Online] accessed on 16-12-2019.
<https://sdg.iisd.org/news/investment-in-renewable-energy-is-clean-but-in-transmission-and-distribution-technologies-not-necessarily/>
- [4] United Nations Environment Programme. “Renewable energy investment in 2018 hit USD 288.9 billion, far exceeding fossil fuel investment”. [Online] accessed on 16-12-2019.
<https://www.unenvironment.org/news-and-stories/press-release/renewable-energy-investment-2018-hit-usd-2889-billion-far-exceeding>
- [5] O Jornal Económico. “Renováveis em Portugal valem investimento superior a 650 milhões de euros e criam 4 mil empregos diretos”. [Online] accessed on 16-12-2019.
<https://jornaleconomico.sapo.pt/noticias/renovaveis-em-portugal-valem-investimento-superior-a-650-milhoes-de-euros-e-criam-4-mil-empregos-diretos-459745>
- [6] Jornal Expresso. “Portugal deverá investir pelo menos 17 mil milhões para cumprir metas de renováveis para 2030”. [Online] accessed on 16-12-2019.
<https://expresso.pt/economia/2019-01-28-Portugal-devera-investir-pelo-menos-17-mil-milhoes-para-cumprir-metas-de-renovaveis-para-2030>
- [7] Wind Europe organization. “Wind in Power 2016 European Statistics”. [Online] accessed on 30-10-2019.
<https://windeurope.org/wp-content/uploads/files/about-wind/statistics/WindEurope-Annual-Statistics-2016.pdf>
- [8] APREN Associação Portuguesa de Energias Renováveis. “Evolução da Potência Instalada nos Centros Electroprodutores de Portugal Continental”. [Online] accessed on 30-10-2019.
<http://www.apren.pt/pt/energias-renovaveis/potencia>
- [9] ANJE – Energy Meeting Coimbra 2013, Celso Costa, Megajoule. “Desenvolvimento da região centro e o potencial eólico”. [Online] accessed on 30-10-2019.
https://pt.slideshare.net/ANJE_SS/frum-29326987?from_action=save
- [10] Wikipedia, The Free Encyclopaedia. “History of wind power” [Online] accessed on 30-10-2019.
https://en.wikipedia.org/wiki/History_of_wind_power
- [11] Ahmad Hemami, CENGAGE Learning 2001. “Wind Turbine Technology”.
- [12] Marcelo Molina, “Modelling and Control Design of Pitch-controlled Variable Speed Wind Turbines”. [Online] accessed on 30-10-2019.
<https://www.researchgate.net/publication/221911675>
- [13] Tony Burton, David Sharpe, Nick Jenkins, Ervin Bossanyi, WILEY 2001. “Wind Energy Handbook”.
- [14] João Luiz Afonso, Maria de Fátima Rodrigues, GEP - Departamento de Eletrónica Industrial da Universidade do Minho. “Tecnologia Eólica”.

- [15] Gonzalo Abad, Jesús López, Miguel A. Rodríguez, Luis Marroyo, Grzegorz Iwanski, WILEY. “Doubly Fed Induction Machine Modeling and Control for Wind Energy Generation”.
- [16] Office of Energy Efficiency & Renewable Energy, Government of the United States of America. “The Inside of a Wind Turbine”.
- [17] Andreas Petersson, Department of Electric Power Engineering of the Chalmers University of Technology. “Analysis, Modelling and Control of Doubly-fed Induction Generators for Wind Turbines”.
- [18] Wei Qiao, Department of Electrical and Computer Engineering of the University of Nebraska-Lincoln. “Dynamic Modeling and Control of Doubly-fed Induction Generators Driven by Wind Turbines”.
- [19] Vítor José Lavrador Sousa, Faculdade de Engenharia da Universidade do Porto. “Ligação à rede eléctrica de micro-geração eólica”.
- [20] Md. Rabiul Islam, Youngang Guo, Jian Guo Zhu, Faculty of Engineering and Information Technology, University of Technology Sydney, Australia. “Steady State Characteristic Simulation of DFIG for Wind Power System”.
- [21] Wikipedia, The Free Encyclopaedia. “Rotating Magnetic Field”. [Online] accessed on 30-10-2019.
https://en.wikipedia.org/wiki/Rotating_magnetic_field
- [22] Festo Didatic, Quebec, Canada. “Courseware Sample - Principles of Doubly-Fed Induction Generators (DFIG)”.
- [23] Ned Mohan, Tore M. Undeland, William P. Robbins, WILEY. “Power Electronics Converters, Applications and Design”.
- [24] Wikipedia, The Free Encyclopaedia. “Transformer”. [Online] accessed on 30-10-2019.
<https://en.wikipedia.org/wiki/Transformer>
- [25] Arduino. “Arduino Mega”. [Online] accessed on 30-10-2019.
<https://www.arduino.cc/en/Main/arduinoBoardMega>
- [26] Broadcom. “HCPL-3120”. [Online] accessed on 30-10-2019.
<https://docs.broadcom.com/docs/AV02-0161EN>
- [27] Microsemi Corporation. “Park, inverse Park and Clarke, inverse Clarke Transformations MSS Software Implementation – User Guide”. [Online] accessed on 30-10-2019.
https://www.microsemi.com/document-portal/doc_view/132799-park-inverse-park-and-clarke-inverse-clarke-transformations-mss-software-implementation-user-guide
- [28] C&P Texas Instruments. “Clarke & Park Transforms on the TMS320C2xx”. [Online] accessed on 30-10-2019.
<http://www.ti.com/lit/an/bpra048/bpra048.pdf>
- [29] Carlos João Costa Ramos, Dissertação Doutoramento em Engenharia Electrotécnica e de Computadores pela Faculdade de Engenharia da Universidade do Porto. “Modelação e Controlo de Conversores de Tensão Aplicados à Máquina Assíncrona Duplamente Alimentada”.
- [30] Edited by Haitham Abu-Rub, Mariusz Malinowski & Kamal Al-Haddad, WILEY. “Power Electronics for Renewable Energy Systems and Industrial Applications”.
- [31] Research Gate. “What is Coupling and Decoupling in Control System Engineering?”. [Online] accessed on 30-10-2019.
https://www.researchgate.net/post/What_is_Coupling_and_Decoupling_in_Control_system_engineering
- [32] DFIM Tutorials by Gonzalo Abad, Mondragon Unibertsitatea, Youtube. [Online] accessed on 30-10-2019.
https://www.youtube.com/channel/UCXIYk0v_RLOldeR3wacNUjw

[33] Aeolos Wind Turbine Company. [Online] accessed on 30-10-2019.
<https://www.windturbinestar.com/>